Lipid-based nanocarriers for the delivery of biotherapeutics

Maria Betânia Carreira de Matos

Lipid-based nanocarriers for the delivery of biotherapeutics | 2019

M
B C
M
2019

Lipid-based nanocarriers for delivery of biotherapeutics

Maria Betânia Carreira de Matos
2019

The printing of this thesis was financially supported by
Utrecht Institute for Pharmaceutical Sciences (UIPS), Utrecht, the Netherlands
Lipoid GmbH, Ludwigshafen, Germany

Lipid-based nanocarriers for delivery of biotherapeutics
Maria Betânia Carreira de Matos
Department of Pharmaceutics, Utrecht Institute for Pharmaceutical Sciences (UIPS), Faculty of Sciences, University of Utrecht, the Netherlands

ISBN: 978-94-6380-286-4
Cover: Eric Guevremont Photography, USA
Printed by: ProefschriftMaken || www.proefschriftmaken.nl

Dit proefschrift werd (mede) mogelijk gemaakt met financiële steun van Phospholipid Research Centre en People Program (Marie Curie Actions) of the European Union's Seventh Framework Program FP7.

Lipid-based nanocarriers for delivery of biotherapeutics

Lipide-gebaseerde nanocarriers voor aflevering van biotherapeutica
(met een samenvatting in het Nederlands)
Nanopartículas lipídicas para entrega de biofármacos
(com resumo em Português)

Proefschrift

ter verkrijging van de graad van doctor aan de Universiteit Utrecht op gezag van de rector magnificus, prof.dr. H.R.B.M. Kummeling, ingevolge het besluit van het college voor promoties in het openbaar te verdedigen op maandag 8 April 2019 des middags te 12.45 uur.

door

Maria Betânia Carreira de Matos
geboren op 9 Mei 1984
te Coimbra, Portugal

Promotor
Prof. Dr. Raymond M. Schiffelers

Copromotor
Dr. Robbert Jan Kok

Endast den som sover gör inga fel.
Ingvar Kamprad

Table of contents

Part I | General considerations

Chapter 1 - Introduction and outline

Chapter 1 – Introduction and Outline

Improved medicines are needed for cancer treatment. The objective of this thesis was to rationally explore novel tumor targeted nanotherapeutics and develop technologies for their manufacture.

Over the last decades the continuous incremental improvements in chemotherapy, radiotherapy and surgical techniques have had a significant positive impact on life expectancy of cancer patients. Still, cancer burden is expected to increase and millions of new cases are diagnosed annually worldwide [1]. The associated morbidity and mortality demand better therapeutic options.
Conventionally, cancer patients are treated with chemotherapeutic drugs, radiotherapy, surgical resection or combination of these. A forth cancer treatment pillar has emerged and refers to cancer immunotherapy [2]. Classical chemotherapeutic drugs are, however, still used in most patients diagnosed with cancer. The major problem of chemotherapeutic drugs are the severe side-effects that mainly relate to the dosing regimen used for such cytotoxic agents. In order to maximize tumor cell killing, chemotherapeutic drugs are dosed at the maximum tolerated dose. This high dosage often causes undesired (side-) effects in healthy tissues. These adverse effects eventually limit the dose and duration of drug administration. In addition, low stability of the drug, poor pharmacokinetic properties or development of (multi-)drug resistance of tumor cells may infer that the highest possible drug dose is not capable of overcoming drug resistance in antitumor pharmacotherapy [3,4].
In contrast, encapsulation of drugs in nanocarriers offers the opportunity to improve the therapeutic potential of anticancer drugs, both by protecting these compounds against degradation in the physiological environment, and by improving tumor versus whole body distribution. The net result of the altered in vivo fate of the drug is an increase in the therapeutic index: this is achieved both by more efficient delivery to the target site (improved therapeutic effects) and by a reduced distribution to many normal tissue sites (and hence a diminished toxicity) [5–9].

Although the application of nanotechnology in medicine has been presented often as the panacea for effective cancer treatment, its translation in clinical therapeutics is still in its infancy and true successes are yet limited [10–14]. Proven clinical successes are still limited, and so far, liposomes are the golden standard for nanomedicine cancer therapy. Redesigning or producing incremental improvements in existing nanocarrier systems together with careful

matching of active payload to nanocarrier system may provide viable nanomedicines.

Liposomes

Liposomes are unilamellar or multilamellar vesicles, which were first described in the 1960s by Bangham[15]. Liposomes consist mainly of phospholipids, which spontaneously form lipid bilayers surrounding an aqueous core, by non-covalent interactions, when dispersed in water. Hydrophilic drugs can be encapsulated in the aqueous core of the liposomes while hydrophobic drugs can be solubilized in the lipid bilayer [15–17].

The versatility of these systems allows surface decoration and functionalization, according to the intended application. The targeting mechanisms of these colloidal systems are schematically represented in **Figure 1** and detailed in **Chapter 2**. Although the targeting mechanisms are conceptually different, they rely on the enhanced permeability and retention (EPR) effect for accumulation at the tumor site.

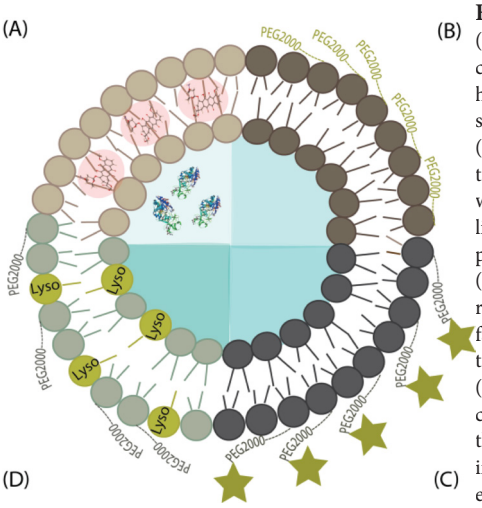

Figure 1 – Evolution and versatility of liposomes. Panel (A) represents simple 1st generation liposomes. A liposome can entrap hydrophobic molecules (red shading) within the hydrophobic bilayer, while hydrophilic cargos (green-blue shading) can be encapsulated in the aqueous core. In panel (B) 'stealth' liposomes are represented. The lipid bilayer contains a small percentage of poly(ethylene glycol (PEG)-lipids which create a hydrophilic corona at the outer surface of the liposomes. This "stealth layer" prevents clearance of the liposomes and hence increases blood circulation times. Panel (C) represents actively targeted liposomes. The star symbol represents a ligand attached to the PEG-polymers that can facilitate the interaction with target (tumor) cells. Actively targeted liposomes are out of the scope of this thesis. Panel (D) represents stimuli responsive liposomes. The bilayer has components (in this case depicted as golden "Lyso" lipids) that can change the physicochemical stability of the bilayer in response to certain stimuli like heat, ultrasound or other external pulses. The altered behavior of the bilayer will favor release of the payload cargo.

The EPR effect was first observed 40 years ago [18] and has been extensively explored for the development and improvement of drug nanocarriers for tumor targeting [19–21]. The EPR effect refers to the preferential localization of nanotherapeutics in pathological tissues due to increased permeability of the vasculature that supplies these tissues, allowing passage of nanosized carriers [22,23]. The lack of functional lymphatic drainage of solid tumors limits the removal of extravasated nanocarriers from the target site [19,20], therefore contributing for the accumulation at the tumor site. The enhanced extravasation and accumulation at pathological sites is commonly referred to as *passive targeting*.

In **Figure 1** we show panel (C) representing actively targeted liposomes. *Active targeting* involves the use of ligands conjugated onto the surface of nanocarriers to facilitate localization to and/or uptake by target cells [19,24]. This class of nanocarriers offers potential for site-specific delivery of drugs to designated cell types in organs *in vivo*, which selectively express or over-express specific receptors at the site of disease [25,26]. The therapeutic advantages offered by ligand-targeted liposomes is still subject of debate [24,27–29].

The EPR is a very heterogeneous phenomenon as it depends on the type of tumor and can vary significantly within the same tumor type [30,31], but in some cases the degree of tumor vascularization and passive targeting of nanocarriers are correlated [32]. The most successful example is the first FDA-approved nanomedicine Doxil® (pegylated liposomal doxorubicin). It demonstrated superior efficacy in ovarian cancer and AIDS-related Kaposi's sarcoma compared to standard conventional therapies [33] by prolonging the circulation half-life and enhancing accumulation at the target tissues, rather than in non-target healthy tissues [34]. Furthermore, the use of Doxil® inhibits high plasma peak levels of free drug [35] and ensures that doxorubicin can pass through the heart vasculature without being released, strongly reducing the risk of cardiotoxicity [34].
Conventional liposomes are robust systems and are designed to display high stability in the bloodstream, preventing premature release of the drug before arrival to the tumor site. The high stability impairs the release of the drug from liposomes, which results in a relatively low free drug concentration in the tumor. Consequently, free drug concentrations at the target site are often sub-optimal [3,17,36,37].

In this context, *stimuli-responsive nanocarriers* offer great opportunities to increase and control the drug concentration in the tumor: they are designed to release their payload cargo in the tumor cells or their local microenvironment upon endogenous or exogenous stimuli. Several methods of triggered release have been described in literature (e.g. enzymes, pH, light and ultrasound) but so far heat is the most intensively studied external trigger for drug release. Thermosensitive liposomes are typically prepared by incorporation of temperature-sensitive molecules (lipids or polymers) in the bilayer of the liposome; upon heating, the altered properties of the bilayer will favor drug release, while the carrier system is still stable at physiological temperature [38–46]. The potentialities of these temperature sensitive systems have been demonstrated in murine in vivo model of cancer, where ThermoDox® (i.e. thermosensitive liposomal Doxil®) was shown to be superior to its coun-

terpart Doxil®[47–49]. Currently, ThermoDox® is under clinical evaluation in multiple countries.

The ongoing rise of biotherapeutics

The use of biopharmaceutical drugs as therapeutic agents became popular in the past decades. The biotherapeutics drug class is rather broad and includes therapeutic peptides and proteins, nucleic acids, enzymes and antibodies. In general, biotherapeutic drugs display higher specificity and potency as compared to small molecules. These two key features arise from their macromolecular nature which allows complex interactions between drug and molecular drug target. [50,51].

However, their inherent complexity also makes biotherapeutic drugs challenging molecules for formulation and delivery. Loss of activity can already occur at relatively mild conditions because their structure is held together by weak non-covalent forces. This offers a substantial challenge on formulation technologies. There is also the added risk of immunogenic reactions and usually, for intracellularly active macromolecular drugs like nucleic acids, uptake into target cells does not occur spontaneously. From a drug formulation perspective, macromolecular biotherapeutics can be even considered as unattractive drug candidates. To be clinically viable, the stability shelf-life, immunogenicity, efficacy and toxicity are important criteria for evaluation [50,52,53].

The above listed problems of biotherapeutics are compensated by other qualities like higher specificity and potency. Toxins, venoms and pro-apoptotic factors from diverse sources have been identified as highly potent drugs. In addition to the intrinsic cytotoxicity , some of them possess (or can be engineered to possess) diverse functions such as specific cell-surface receptor binding, with potential applicability in cell-targeted oncotherapy and theragnosis [54]. In this thesis, cytotoxic lectins are studied as biotherapeutic drugs. To be more precisely, mistletoe lectin-1 (ML1) was investigated. ML1 belongs to the class of ribosome inactivating proteins type 2 (RIP-II) proteins, like ricin, cholera and shiga toxins. Cytotoxins typically are very potent and hence are attractive drug candidates in cancer therapy. An interesting feature of these RIP-II cytotoxins is their ability to bind to the cell membrane and their subsequent uptake via receptor mediated endocytosis [55,56]. Hence, the cellular targeting and internalization of the biotherapeutic is already part of the bioactivity of plant-derived cytotoxins. However, the translation into safe therapeutics is difficult due to their high cytotoxic potency and low specificity to tumor cells [57].

Even in this case, where the internalization of the therapeutic no longer constitutes a constraint for efficient cellular delivery, the challenges to ML1 drug delivery are complex. Given the potency and the intrinsic features of ML1, the development of triggerable nanocarriers could bring considerable benefits when release of the cytotoxic drug is set off in the tumor environment, the benefit/risk ratio can be greatly improved.

Challenges

Triggerable nanocarriers are relatively new additions to the nanomedicine field, especially for macromolecular payloads. A few studies performed in the 1990s and early 2000s studied the use of thermosensitive liposomes for the release of cytokines [58] and dextrans [59], formulated in hyperosmotic media. Although the release results *in vitro* showed tremendous potential, the in vivo results [58] did not convincingly demonstrate efficacy and safety. Therefore, it is necessary to re-address these concepts and adapt research strategies.

Moreover, efficient methods for the encapsulation of macromolecules in liposomes are not well developed. Standard protocols for small molecule encapsulation are not suitable for macromolecules as they are often based on passive encapsulation, leading to very low encapsulation. High encapsulation can be achieved for small molecules by remote loading but this also out of reach for macromolecules. The most efficient way of macromolecular drug loading is based on electrostatic interactions. Although this principle has been extensively studied for encapsulation of nucleic acids, the knowledge can be transferred to charged proteinaceous drugs. The electrostatic combination of negatively charged macromolecular drugs with cationic components of the carrier is common practice and is very efficient. However, the in vivo toxicity profiles associated with the cationic components, makes it difficult to put it into practice [57]. Investing on the technological development for asymmetric liposomes formation, can lead to major advances, by forcing the cationic components in the inner leaflet of the liposomal bilayer, preventing their exposure to the body.

Aim and outline of the thesis

Taking the above insights into account, the present thesis summarizes strategies to efficiently deliver potent therapeutic macromolecular drugs to tumors and suggests strategies to develop lipid nanoparticles for optimized therapeutic effects. In particular, the following challenges were experimentally addressed and discussed:

- encapsulation of protein-based therapeutics in lipid nanocarriers
- stability of the encapsulated cargo during the encapsulation process
- release of the protein cargo from the nanocarrier
- stability of the nanocarrier: colloidal stability and premature leakage
- alternative strategies for the preparation of lipid nanocapsules

Following this general introduction, **Chapter 2** provides an overview on nanomedicines and their clinical translation. We included a description of nanomedicines, in particular liposomes, and overall design features. The basic concepts of EPR effect, passive and active targeting and triggered release systems are additionally described. The discussion proceeds with the challenges related to biology, large-scale manufacturing, biocompatibility and safety, finalizing with the hurdles from intellectual property, government regulations and overall cost-effectiveness.

Chapter 3 focuses on the biological characterization of ML1 as an interesting candidate for targeted cytotoxic therapy in cancer. High content analysis of live cell imaging was used to describe the cell binding and uptake mechanisms by cancer cells, as well as to reveal information on the internalization pathway and intracellular mode of action.

Using this information, ML1 was used as high-molecular weight anticancer drug for formulation into thermosensitive liposomes (**Chapter 4a**). A comprehensive study on release properties was performed using model compounds with different molecular weights. The most promising composition was used for ML1 encapsulation, release and in vitro cytotoxicity studies. The Additional study (**Chapter 4b**) refers to complementary experimental studies in which cationic lipids were used to increase encapsulation of ML1.

Chapter 5 focuses on trigger-sensitive liposomes that respond to high-focused ultrasound (HIFU). Different liposomal formulations loaded with perfluorocarbon nanodroplets were tested for their response to HIFU and the final ul-

trasound-sensitive liposomes were loaded with ML1. The loading efficiency and release of bioactive ML1 were studied in a comparable manner to the results of **Chapter 4**.

Chapter 6 describes the use of an innovative method for preparation of asymmetrical liposomes, i.e. liposomes with a different composition of the inner and outer bilayer lipids. Asymmetrical liposomes are attractive nanocarriers as the inner leaflet can be optimized for loading and complexing of the payload cargo, while the outer leaflet is optimized for long-circulating purposes. We explored whether the water-in-oil centrifugation method is feasible for the loading of macromolecule biotherapeutics in asymmetrical lipid-based nanocarriers.

Finally, **Chapter 7** summarizes and this thesis, discusses the described findings and provides future perspectives.

References

[1] L. A. Torre, R. L. Siegel, E. M. Ward, A. Jemal, Cancer Epidemiol. Biomarkers Prev. 2016, 25, 16.

[2] L. A. Emens, P. A. Ascierto, P. K. Darcy, S. Demaria, A. M. M. Eggermont, W. L. Redmond, B. Seliger, F. M. Marincola, Eur. J. Cancer 2017, 81, 116.

[3] E. Blanco, H. Shen, M. Ferrari, Nat. Biotechnol. 2015, 33, 941.

[4] J. A. Kemp, M. S. Shim, C. Y. Heo, Y. J. Kwon, Adv. Drug Deliv. Rev. 2016, 98, 3.

[5] H. J. Kim, A. Kim, K. Miyata, K. Kataoka, Adv. Drug Deliv. Rev. 2016, 104, 61.

[6] M. Larsson, W.-T. Huang, D.-M. Liu, D. Losic, Cancer Treat. Rev. 2017, 55, 128.

[7] D. K. Mishra, N. Balekar, P. K. Mishra, Drug Deliv. Transl. Res. 2017, 7, 346.

[8] N. Shajari, B. Mansoori, S. Davudian, A. Mohammadi, B. Baradaran, Curr. Drug Deliv. 2017, 14, 36.

[9] M. Talekar, T.-H. Tran, M. Amiji, AAPS J. 2015, 17, 813.

[10] Y. H. Bae, K. Park, J Control Release 2012, 153, 198.

[11] K. Park, J. Control. Release 2014, 190, 3.

[12] K. Park, J. Control. Release 2017, 267, 2.

[13] V. J. Venditto, F. C. Szoka, Adv. Drug Deliv. Rev. 2013, 65, 80.

[14] S. Wilhelm, A. J. Tavares, Q. Dai, S. Ohta, J. Audet, H. F. Dvorak, W. C. W. Chan, Nat. Rev. Mater. 2016, 1, 1.

[15] D. W. Deamer, FASEB J. 2010, 24, 1308.

[16] T. M. Allen, P. R. Cullis, Adv. Drug Deliv. Rev. 2013, 65, 36.

[17] T. Ta, T. M. Porter, J. Control. Release 2013, 169, 112.

[18] Y. Matsumura, H. Maeda, Cancer Res. 1986, 46, 6387.

[19] F. Danhier, O. Feron, V. Préat, J. Control. Release 2010, 148, 135.

[20] H. Maeda, H. Nakamura, J. Fang, Adv. Drug Deliv. Rev. 2013, 65, 71.

[21] H. Nakamura, F. Jun, H. Maeda, Expert Opin. Drug Deliv. 2015, 12, 53.

[22] K. Greish, H. Nehoff, N. Parayath, L. Domanovitch, S. Taurin, Int. J. Nanomedicine 2014, 2539.

[23] H. Hashizume, P. Baluk, S. Morikawa, J. W. McLean, G. Thurston, S. Roberge, R. K. Jain, D. M. McDonald, Am. J. Pathol. 2000, 156, 1363.

[24] R. van der Meel, L. J. C. Vehmeijer, R. J. Kok, G. Storm, E. V. B. van Gaal, Adv. Drug Deliv. Rev. 2013, 65, 1284.

[25] S. Hua, Front. Pharmacol. 2013, 4, DOI 10.3389/fphar.2013.00127.

[26] Willis, Forssen, Adv. Drug Deliv. Rev. 1998, 29, 249.

[27] M. Puri, I. Kaur, M. a. Perugini, R. C. Gupta, Drug Discov. Today 2012, 17, 774.

[28] M. Ferrari, Curr. Opin. Chem. Biol. 2005, 9, 343.

[29] K. Riehemann, S. W. Schneider, T. A. Luger, B. Godin, M. Ferrari, H. Fuchs, Angew. Chemie Int. Ed. 2009, 48, 872.

[30] T. Lammers, F. Kiessling, W. E. Hennink, G. Storm, J. Control. Release 2012, 161, 175.

[31] T. Ojha, V. Pathak, Y. Shi, W. E. Hennink, C. T. W. Moonen, G. Storm, F. Kiessling, T. Lammers, Adv. Drug Deliv. Rev. 2017, 119, 44.

[32] B. Theek, F. Gremse, S. Kunjachan, S. Fokong, R. Pola, M. Pechar, R. Deckers, G. Storm, J.

Ehling, F. Kiessling, T. Lammers, J. Control. Release 2014, 182, 83.

[33] J. W. Nichols, Y. H. Bae, J. Control. Release 2014, 190, 451.

[34] A. M. Rahman, S. W. Yusuf, M. S. Ewer, Int. J. Nanomedicine 2007, 2, 567.

[35] O. Lyass, B. Uziely, R. Ben-Yosef, D. Tzemach, N. I. Heshing, M. Lotem, G. Brufman, A. Gabizon, Cancer 2000, 89, 1037.

[36] a Gabizon, H. Shmeeda, Y. Barenholz, Clin.Pharmacokinet. 2003, 42, 419.

[37] T. J. Evjen, E. Hagtvet, A. Moussatov, S. Røgnvaldsson, J. L. Mestas, R. A. Fowler, C. Lafon, E. A. Nilssen, Eur. J. Pharm. Biopharm. 2013, 84, 526.

[38] D. Needham, G. Anyarambhatla, G. Kong, 2000, 1197.

[39] N. Bertrand, J. Wu, X. Xu, N. Kamaly, O. C. Farokhzad, Adv. Drug Deliv. Rev. 2014, 66, 2.

[40] B. Jang, H. Kwon, P. Katila, S. J. Lee, H. Lee, Adv. Drug Deliv. Rev. 2016, 98, 113.

[41] Y. Min, J. M. Caster, M. J. Eblan, A. Z. Wang, Chem. Rev. 2015, 115, 11147.

[42] E. Oude Blenke, E. Mastrobattista, R. M. Schiffelers, Expert Opin. Drug Deliv. 2013, 10, 1399.

[43] R. R. Sawant, V. P. Torchilin, AAPS J. 2012, 14, 303.

[44] J. Shi, P. W. Kantoff, R. Wooster, O. C. Farokhzad, Nat. Rev. Cancer 2017, 17, 20.

[45] V. P. Torchilin, Adv. Drug Deliv. Rev. 2012, 64, 302.

[46] K. Kono, Adv. Drug Deliv. Rev. 2001, 53, 307.

[47] S. Dromi, V. Frenkel, A. Luk, B. Traughber, M. Angstadt, M. Bur, J. Poff, J. Xie, S. K. Libutti, K. C. P. Li, B. J. Wood, Clin. Cancer Res. 2007, 13, 2722.

[48] G. Kong, G. Anyarambhatla, W. P. Petros, R. D. Braun, O. M. Colvin, D. Needham, M. W. Dewhirst, Cancer Res. 2000, 60, 6950.

[49] L. Li, T. L. M. Ten Hagen, M. Hossann, R. Süss, G. C. Van Rhoon, A. M. M. Eggermont, D. Haemmerich, G. a. Koning, J. Control. Release 2013, 168, 142.

[50] S. Mitragotri, P. A. Burke, R. Langer, Nat. Rev. Drug Discov. 2014, 13, 655.

[51] R. Juliano, Biochem. Soc. Trans. 2007, 35, 41.

[52] D. Ding, Q. Zhu, Mater. Sci. Eng. C 2018, 92, 1041.

[53] N. Osman, K. Kaneko, V. Carini, I. Saleem, Expert Opin. Drug Deliv. 2018, 15, 821.

[54] N. Serna, L. Sánchez-García, U. Unzueta, R. Díaz, E. Vázquez, R. Mangues, A. Villaverde, Trends Biotechnol. 2018, 36, 318.

[55] L.-L. Fu, C.-C. Zhou, S. Yao, J.-Y. Yu, B. Liu, J.-K. Bao, Int. J. Biochem. Cell Biol. 2011, 43, 1442.

[56] N. Beztsinna, M. B. C. de Matos, J. Walther, C. Heyder, E. Hildebrandt, G. Leneweit, E. Mastrobattista, R. J. Kok, Sci. Rep. 2018, 8, 2768.

[57] H. Ghazarian, B. Idoni, S. B. Oppenheimer, Acta Histochem. 2011, 113, 236.

[58] Y. Yuyama, M. Tsujimoto, Y. Fujimoto, N. Oku, Cancer Lett. 2000, 155, 71.

[59] N. Oku, R. Naruse, K. Doi, S. Okada, 1994, 1191, 389.

[60] A. A. Mokhtarieh, S. Cheong, S. Kim, B. H. Chung, M. K. Lee, Biochim. Biophys. Acta - Biomembr. 2012, 1818, 1633.

Chapter 2 - Current Trends and Challenges in the Clinical Translation of Nanomedicines - Pathways for Translational Development and Commercialization

Susan Hua, Maria B.C. De Matos, Josbert M. Metselaar and Gert Storm

Frontiers in Pharmacology (2018)
DOI: 10.3389/fphar.2018.00790

Abstract

The use of nanotechnology in medicine has the potential to have a major impact on human health for the prevention, diagnosis, and treatment of diseases. One particular aspect of the nanomedicine field which has received a great deal of attention is the design and development of nanoparticulate nanomedicines (NNMs) for drug delivery (i.e. drug-containing nanoparticles). NNMs are intended to deliver drugs via various mechanisms: solubilization, passive targeting, active targeting, and triggered release. The NNM approach aims to increase therapeutic efficacy, decrease the therapeutically effective dose, and/or reduce the risk of systemic side effects. In order to move a NNM from the bench to the bedside, quite some experimental challenges need to be addressed. This review will discuss the current trends and challenges in the clinical translation of NNMs as well as the potential pathways for translational development and commercialization. Key issues related to the clinical development of NNMs will be covered, including biological challenges, large scale manufacturing, biocompatibility and safety, intellectual property (IP), government regulations, and overall cost-effectiveness in comparison to current therapies. These factors can impose significant hurdles limiting the appearance of NNMs on the market, irrelevant of whether they are therapeutically beneficial or not.

Introduction

Nanomedicine applies nanotechnology to highly specific medical interventions for the prevention, diagnosis, and treatment of diseases [1]. In the last several decades, the application of nanotechnology for medical purposes has received significant attention from researchers, academia, funding agencies, government and regulatory bodies [2-4].

One particular aspect of the nanomedicine field which has received a great deal of attention is the design and development of nanoparticulate nanomedicines (NNMs) for drug delivery (i.e. drug-containing nanoparticles), which are most often given by parenteral (particularly intravenous) administration. NNMs are intended to increase the therapeutic index of drugs (i.e. increase efficacy and/or reduce toxicity) by delivering them via various mechanisms: solubilization, passive targeting, active targeting, and triggered release (**Figure 1**).

Nanoencapsulation gives the opportunity to protect fragile compounds that degrade easily in biological environments and to provide solubilization, i.e. to deliver compounds which have physicochemical properties that strongly limit their aqueous solubility and therefore systemic bioavailability [5-9]. Targeted drug delivery and triggered release of NNMs have been shown to be beneficial for increasing the therapeutic index of compounds, by improving the in vivo fate of drug molecules such that more efficient delivery to the target site is achieved (to yield improved therapeutic effects) with less accumulation in many healthy body sites (to reduce toxicity). Also, NNMs have been studied for their ability to stimulate target cell uptake and improve intracellular trafficking, processes sometimes required when they have localized in target tissues [10-12].

Although NNMs have demonstrated significant therapeutic advantages for a multitude of biomedical applications, their clinical translation has not progressed as rapidly as the plethora of positive preclinical results would have suggested [13]. In order to move a NNM from the bench to the bedside, quite some experimental challenges need to be addressed. From a biological perspective, these include studies focused on understanding the in vivo fate and interactions of NNMs with the blood, tissue, cellular and intracellular com-

partments in the host in healthy and diseased states [3,4,14]. For NNMs to have clinical translation potential, the complexity in their design and development also needs to be minimized as much as possible to create systems that are able to be reproducibly prepared and characterized [15,16]. This review will address the current trends and challenges in the clinical translation of NNMs as well as the potential pathways for translational development and commercialization.

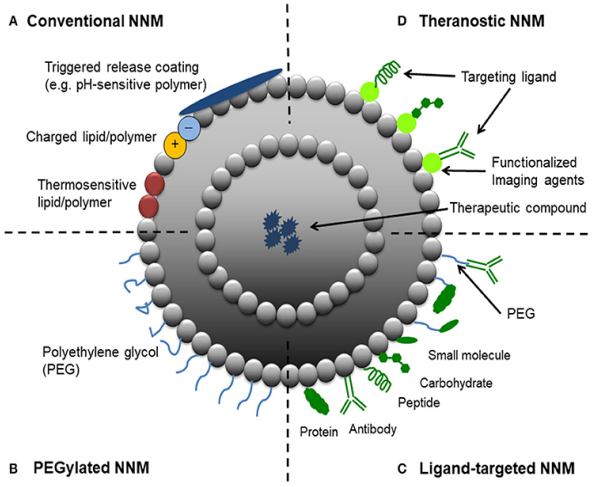

Figure 1 - Schematic representation of different strategic designs for nanoparticulate nanomedicines (NNMs). (A) Conventional NNM—These NNMs can be modified with charged lipids/polymers, thermosensitive lipids/polymers and/or components for triggered release (e.g., pH-sensitive coating). (B) PEGylated NNM—Nanoparticle characteristics and behavior in vivo can be modified by the addition of a hydrophilic polymer coating, polyethylene glycol (PEG), to the NNM surface to confer steric stabilization. (C) Ligand-targeted NNM—Nanoparticles can be used for active targeting by attaching ligands (e.g., antibodies, peptides and carbohydrates) to its surface or to the terminal end of the attached PEG chains. (D) Theranostic NNM – These NNM systems consist of an imaging component and a therapeutic component, and may include a targeting element.

Current trends in the clinical translation of nanomedicines

NNMs are often studied to improve drug targeting to specific sites of disease (i.e. site-specific drug delivery) and/or attenuate localization in healthy non-target tissues (i.e. site-avoidance drug delivery) [17]. The vast majority of NNMs in preclinical and clinical development as well in clinical use are for targeting a wide variety of cancers and tumors [3]. The application of NNM-based therapies for drug targeting to non-cancer conditions has increased in recent years. In particular, NNMs have been developed to address the clinical challenge of effectively managing inflammatory diseases by exploiting the underlying biology of these conditions. Non-cancerous inflammatory diseases

that have been explored with NNM therapy include rheumatoid arthritis, inflammatory bowel disease, asthma, multiple sclerosis, diabetes, and neurodegenerative diseases [18].

Enhanced permeability and retention (EPR) effect and passive accumulation of NNMs

The EPR effect refers to the preferential localization of NNMs in pathological tissues by virtue of an increased permeability of the vasculature that supplies such tissues (e.g. tumours and conditions involving inflammation). At these sites, deregulations in angiogenesis and/or the increased expression and activation of vascular permeability factors predominates, which can lead to fenestrations allowing passage of NNMs [14,19]. In addition to the enhanced leakiness of tumorous and inflamed blood vessels, the EPR effect also relates to the observation that solid tumors tend to lack functional lymphatic drainage, which limits the removal of extravasated NNMs from the target site [20,21]. These pathological properties allow NNMs to accumulate at pathological sites and is referred to as passive targeting. To achieve this, it is important that NNMs with drug cargo circulate long enough in the bloodstream (i.e., show prolonged circulation kinetics). This can be achieved by conjugating polyethylene glycol (PEG) to the surface of NNMs (**Figure 1**). Thus, the EPR effect is expected to increase the therapeutic efficacy of NNMs in comparison to small molecules, which often show inferior pharmacokinetic properties [22-24]. The EPR effect was first observed in 1986 [23] and has since been exploited particularly for the development of NNMs for passive tumor targeting, leading to NNMs with adequate physicochemical properties and prolonged circulation half-life that accumulate in tumors over time [20,21,25]. The EPR effect and thus extent of passive targeting is highly dependent on the tumor pathophysiology. Currently, it is recognized that EPR is a very heterogeneous phenomenon as it depends on the type of tumor and can vary significantly within the same tumor type [26,27]. The degree of tumor vascularization and passive targeting of NNMs has been observed to be positively correlated [28]. For example, Doxil® (pegylated liposomal doxorubicin) is the first FDA-approved NNM and has demonstrated superior efficacy in ovarian cancer and AIDS-related Kaposi's sarcoma compared to standard conventional therapies [29]. When doxorubicin is incorporated in PEGylated liposomes, it delays and minimizes the uptake and clearance by the reticuloendothelial system (RES), which results in the prolonged circulation half-life. This allows the NNM to accumulate in the tumor tissue exploiting the locally increased permeability of the tumor blood vessels, rather than in non-target healthy tissues which do

not have such leaky vessels [30]. Furthermore, the use of pegylated liposomal doxorubicin avoids high plasma peak levels of free drug [31] and ensures that doxorubicin can pass through the heart vasculature without being released, which strongly reduces the risk of cardiotoxicity [30].

NNMs and active targeting

Active targeting, also termed ligand-targeting or receptor-mediated targeting, involves the use of ligands (e.g. antibodies, peptides or sugar moieties) which are physically or chemically conjugated onto the surface of NNMs to facilitate localization to and/or uptake by target cells (**Figure 1**) [20,24]. Ligand-targeted NNMs offer a vast potential for site-specific delivery of drugs to designated cell types in organs in vivo, which selectively express or over-express specific receptors (e.g. cellular receptors or cell adhesion molecules) at the site of disease [10,32]. For example, three sets of cellular targets are generally considered for active targeting in cancer – (i) targeting of cancer cells, which present overexpression of receptors for transferrin, folate, epidermal growth factor or glycoproteins; (ii) targeting of the tumor endothelium overexpressing vascular endothelial growth factors, integrins, vascular cell adhesion molecule-1 or matrix metalloproteinases; and (iii) targeting of stroma cells (e.g. macrophages, fibroblasts) that can acquire a tumor survival-promoting phenotype in response to cytokines in the tumor microenvironment [20,33-35]. The notion that ligand-targeted liposomes have a therapeutic advantage over non-targeted liposomes by further enhancing NNM accumulation at the site of disease is still subject to debate, with conflicting results in the literature [24,36-38]. There are studies that have shown no difference in the biodistribution and target tissue accumulation of ligand-targeted NNMs compared with non-targeted NNMs, despite still demonstrating an enhanced therapeutic effect. For example, conjugation of HER2 monoclonal antibody fragments to liposomes did not increase the tumour localization of the nanoparticles, with both targeted and non-targeted liposomes achieving similarly high levels of tumor tissue accumulation (7-8% injected dose/g tumor tissue) in HER2-overexpressing breast cancer xenografts models [39,40]. However, doxorubicin-loaded anti-HER2 immunoliposomes produced significantly superior therapeutic results in comparison to all other control groups, including free doxorubicin, non-targeted liposomal doxorubicin and recombinant anti-HER2 Mab trastuzumab [41]. The mechanism of this enhanced anti-tumor efficacy was likely the result of the marked difference in pharmacodynamics of the targeted NNM formulation in vivo, by enhancing intracellular drug delivery to HER2-overexpressing cancer cells [40].

NNMs for triggered release

A third targeting strategy based on stimuli-responsive NNMs, referred to as triggered drug release, is currently receiving much attention from academia and industry. This class of NNMs is designed with the goal of enhancing drug release in tumors by means of endogenous or exogenous stimuli. Endogenous stimuli-responsive NNMs exploit factors associated with the local environment at the site of disease (**Figure 1**). For example, low pH, presence of redox gradients or certain enzymes in the tumor microenvironment. Exogenous-responsive NNMs respond to external stimuli to trigger drug release, such as temperature, light, magnetic field or ultrasound. Of these strategies, the use of an external hyperthermic trigger to release therapeutic compounds from NNMs (e.g. thermosensitive liposomal doxorubicin, ThermoDox®) appears to be the most promising to date [42]. ThermoDox® was shown to be superior to its counterpart Doxil® in an in vivo model of non-resectable hepatocellular carcinoma [43-49]. Thermosensitive liposomes are typically modified with temperature-sensitive lipids (e.g. distearoyl phosphocholine, DSPC) and/or polymers (e.g. poly(N isopropylacrylamide)), which enables the nanocarrier to remain stable and retain their contents at physiologic temperatures. Upon heating, these NNMs undergo a phase change that makes them more permeable, causing the release of their cargo [50]. The advantages of these NNMs can be further extended with the incorporation of imaging moieties (**Figure 1**) to enable monitoring of biodistribution, target accumulation and efficacy.

NNMs approved and in clinical trials

A number of NNM products are on the market with more in clinical development. The majority of NNMs in clinical development incorporate already approved drugs and are based on a variety of drug delivery platforms, including polymeric micelles, liposomes, dendrimers, and inorganic nanoparticles [4,49,51]. Despite the arsenal of nanoparticulate targeted systems currently under pre-clinical development or in clinical trials, it is indisputable that liposomes are dominant on the NNM market (**Table 1**) and were the first FDA-approved NNM [48,52]. In fact, liposomes have all the necessary features to allow formulation of highly toxic and/or poorly soluble drugs, such as paclitaxel and amphotericin B [45,52]. Soon after their discovery in 1965 [53,54], liposomes were proposed as drug delivery vehicles for both small molecules as well as macromolecular drugs [55,56]. Years of research led to the development of the first FDA-approved NNM (Doxyl®/Caelyx®) as well as additional therapeutics [57]. Expectedly, many more NNMs are progressing to clinical

Table 1. NNM formulations currently approved for marketing. (Ref: ema.europa.eu; drugs.com; fda.gov)

Type	Name	Targeting modality	Drug	Indication
Liposomal NNMs	Doxil/Caelyx	passive	Doxorubicin	HIV-related Kaposi's Sarcoma, metastatic breast cancer, advanced ovarian cancer, multiple myeloma
	AmBisome	passive	Amphotericin B	Fungal Infections
	DaunoXome	passive	Daunorubicin	HIV-related Kaposi sarcoma
	Myocet	passive	Doxorubicin	Metastatic breast cancer
	Abelcet	passive	Amphotericin B	Fungal Infections
	Lipo-Dox	passive	Doxorubicin	HIV-related Kaposi's Sarcoma, ovarian cancer, multiple myeloma
	Marqibo (Onco-TCS)	passive	Vincristine	Adult AML
	Onivyde	passive	Irinotecan	Pancreatic cancer
	Vyxeos (CPX-351)	passive	Cytarabine and daunorubicin	AML
	Visudyne	passive	Verteporfin	Wet AMD, myopia, ocular histoplasmosis
	DepoDur	passive	Morphine	Postoperative analgesia
	DepoCyt	passive	Cytarabine	Lymphomatous meningitis
Micellar NNMs	Genexol PM	passive	Paclitaxel	Metastatic breast cancer, advanced lung cancer
	Nanoxel M	passive	Paclitaxel	Advanced NSCLC, breast cancer, pancreatic cancer, ovarian cancer
Protein NNMs	Abraxane	passive	Paclitaxel	Breast cancer, NSCLC, pancreatic cancer

investigation every year (**Table 2**), and again liposomal formulations represent the biggest share of the NNMs under clinical evaluation. The most frequently observed clinical benefit so far has been a reduction in toxicity with little evidence of improved efficacy. However, recently approved liposomal NNM, Vyxeos® (daunorubicin/cytarabine liposomal formulation), demonstrated improved survival and response rates, with tolerable toxicity in phase III clinical trials in older patients with therapy-related acute myeloid leukemia (t-AML) or AML with myelodysplasia-related changes (AML-MRC) [58].

Challenges in the clinical translation of nanomedicines

The clinical translation of NNMs is an expensive and time-consuming process. NNM technology is usually far more complex in comparison to conventional formulation technology containing free drug dispersed in a base (e.g. tablets, capsules and injections) [1,59,60]. Key issues related to the clinical development of NNMs are listed in **Table 3**, and include biological challenges, large-scale manufacturing, biocompatibility and safety, intellectual property (IP), government regulations, and overall cost-effectiveness in comparison to current therapies [2,47,57,61,62]. These factors can impose significant hurdles limiting the appearance of NNMs on the market, irrelevant of whether they are therapeutically efficacious or not.

Biological challenges

Traditionally, NNM development has been based on a formulation-driven approach, whereby novel delivery systems are firstly engineered and characterized from a physicochemical perspective. It is only when attempting to align the NNM with a pathological application that limitations in the clinical translation of the system have been identified. Understanding the relationship between biology and technology, including understanding the influence of disease pathophysiology on nanomedicine accumulation, distribution, retention and efficacy, as well as the biopharmaceutical correlation between delivery system properties and in vivo behavior in animals versus humans are important determinants for the successful translation of NNMs. Therefore, applying a disease-driven approach by designing and developing NNMs that are able to exploit pathophysiological changes in disease biology has been suggested to improve clinical translation [3].

From the outset in NNM development, it is essential to consider the relationship between disease pathophysiology and the heterogeneity of the disease in humans, and the importance of physicochemical characteristics of different NNMs to overcoming biological barriers to enable improved targeting to dis-

Table 2 - NNM formulations in clinical trials. (*Ref: clinicaltrials.gov*)

Type	Name	Drug	Indication	Status
Lipid NNMs	LiPlaCis	Cisplatin	Advanced or refractory solid tumours, Metastatic breast cancer and skin cancer	Phase I/II
	ThermoDox	Doxorubicin	Hepatocellular carcinoma, breast cancer	Phase I/IIII
	9NC-LP	9-Nitro-20 (S)-Camptothecin	Ewing's sarcoma and other solid tumors with lung involvement, endometrial cancer	Phase I/II completed
	SPI-077	Cisplatin	Ovarian cancer, relapsed/progressive osteosarcoma metastatic to the lung	Phase I/ II/ III
	Lipoxal	Oxaliplatin	Colorectal cancer; Glioma	Phase II
	EndoTAG-1	Paclitaxel	Pancreatic cancer, liver metastases, HER-2 and triple negative breast cancer	Phase II completed
	OSI-211	Lurtotecan	SCLC	Phase I/II completed
	LE-DT	Docetaxel	Solid tumors, pancreatic cancer	Phase I/II completed
	LEP-ETU	Paclitaxel	Breast cancer, Neoplasm, Gastric carcinoma	Phase I/II/IV
	TKM-080301	siRNA against PLK1	Advanced hepatocellular carcinoma, solid tumors or lymphomas that are refractory to conventional therapies. Colorectal, gastric, breast and ovarian cancers with hepatic metastases.	Phase I/II completed
	Atu027	siRNA against PKN3	Advanced solid tumors, pancreatic cancer	Phase I/II completed
	2B3-101	Doxorubicin	Advanced solid tumors, brain metastases, lung, and breast cancers, melanoma, malignant glioma.	Phase I/II completed
	MTL-CEBPA	saRNA	Liver cancer	Phase I
	TLI	Topotecan	Small cell lung and ovarian cancers. Solid tumors	Phase I
	MM-398 Onivyde	Irinotecan	Solid tumors, ER/PR positive and triple negative breast cancer. Metastatic breast cancer with active brain metastasis, SCLC, metastatic pancreatic cancer	Phase I/II/III

Lipid NNMs (*Cont.*)	MM-302	doxorubicin	Breast cancer	Phase I
	ATI-1123	Docetaxel	Advanced solid tumors.	Phase I completed
	SGT-53	p53 pDNA	Solid tumors and recurrent glioblastoma	Phase I/II
	SGT-94	RB94 pDNA	Solid tumors and recurrent glioblastoma	Phase I, Phase II
	Anti-EGFR-IL-DOX	doxorubicin	Solid tumors	Phase II
	RNL	Rhenium-186	Glioblastoma and astrocytoma (treatment and imaging)	Phase I/II
	Patisiran	siRNA	TTR-mediated Amyloidosis	Phase I/II/III
Polymeric NNMs	Paclical	paclitaxel	Ovarian cancer	Phase III complete
	NK105	paclitaxel	Gastric cancer	Phase III complete
	BIND-014	Docetaxel	NSCLC. Solid tumors	Phase II completed
	CALAA-01	RRM2 siRNA	Solid tumors	Phase II terminated
	CRLX101	Camptothecin	NSCLC	Phase II completed

eased tissue and/or reduced accumulation in non-target organs. Considerably less research effort has been dedicated to comprehensively understanding the correlations between NNM behavior and patient biology in specific clinical applications as well as disease heterogeneity in patients – which are likely the major reasons for the failure seen in the translation of promising NNMs in clinical trials [3]. These biological challenges can be a significant deterrent for pharmaceutical industry investment into nanomedicines. In order to reduce investment risk for NNMs, the preclinical data sets need to comprehensively evaluate therapeutic efficacy, safety, biodistribution and pharmacokinetics in appropriate animal models of the disease that are relevant to human disease. Evaluation of NNMs in multiple preclinical animal models that represent aspects of the clinical disease is preferred to achieve reproducibility of results for the specific disease and not for a specific animal model. In addition, animal models that reflect only a narrow spectrum of the clinical disease may provide useful data that can predict their suitability for treating a specific patient sub-group [3]. Differences in the anatomy or physiology of the animal species compared to humans should be taken into account based on different routes of administration. Preclinical studies of NNMs should also be conducted under appropriate randomization and blinding to reduce bias, as well be evaluated against proper controls, including the gold standard treatment and not just free drug solution. These factors are currently lacking in many published studies, which makes it difficult to assess clinical applicability and translatability. Other considerations include designing preclinical studies to optimize NNM performance in vivo, dosing schedules, and treatment combinations based on the specific clinical disease, as well as understanding the influence of disease progression and severity on nanomedicine performance. This will determine whether specific patient sub-groups may respond more favorably to NNM-based treatment.

Interestingly, the majority of the NNM formulations in development and clinical trials are focused on cancer targeting, including more than 80% of the publications on nanomedicine in the last two decades alone [63]. Despite the large number of publications, the translation of the published studies to clinical applications has been disappointing. Cancer targeting of NNMs has generally been universally based on the EPR effect, despite the fact that EPR-mediated accumulation has only been reported for some tumor types [64]. Tumors, like other clinical diseases, can be highly heterogenous and can show inter-patient and intra-patient variability as the disease progresses. Hence a one-size-fits-all approach when designing NNM-based treatment is unlikely to translate to clinically beneficial outcomes. The EPR effect has increasingly been exploited

Table 3. Considerations in the translational development of nanomedicines

NANOPHARMACEUTICAL DESIGN
KEY CONSIDERATIONS
Route of administration
Reduce complexity in formulation design
Final dosage form for human use
Biocompatibility and biodegradability
Pharmaceutical stability (physical and chemical)
CURRENT OBSTACLES
Large-scale production according to GMP standards
E.g. Reproducibility, infrastructure, techniques, expertise and cost
Quality control assays for characterization
E.g. Size and polydispersity, morphology, charge, encapsulation, surface modifications, purity and stability
PRECLINICAL EVALUATION
KEY CONSIDERATIONS
Need for validated and standardized assays for early detection of toxicity
Evaluation in appropriate animal models of disease
Adequate understanding of in vivo behavior, incl. cellular and molecular interactions
Pharmacokinetics (absorption, distribution, metabolism and excretion)
Pharmacodynamics (intracellular trafficking, functionality, toxicity and clearance)
CURRENT OBSTACLES
Development of more specialized toxicology studies for nanomedicines
Adequate understanding of the interaction of NNM with tissues and cells
Adequate structural stability of NNM following in vivo administration
Limited degree of accumulation of nanomedicines in target organs/tissues/cells
CLINICAL EVALUATION FOR COMMERCIALIZATION
KEY CONSIDERATIONS
Simplification of development pathways from invention to commercialization to minimize time and expense
Evaluation of safety/toxicity in humans (acute and chronic)
Evaluation of therapeutic efficacy in patients
Optimal clinical trial design
CURRENT OBSTACLES
Lack of clear regulatory guidelines specific for NNM
Complexity of NNM patents and IP
Limited understanding of the biological interaction of NNM with the biological environment (incl. target site) in the body of patients

for NNM targeting in other non-cancer conditions, especially those involving an inflammatory component that causes leakiness of inflamed blood vessels (e.g. rheumatoid arthritis, atherosclerosis and inflammatory bowel disease) [11,18,65-69]. It should be appreciated that not all diseases can be accessed with NNMs due to biological barriers and that the EPR effect is unlikely to be present in all clinical diseases. EPR is also not the only determinant of NNM efficacy. NNM activity is also influenced by the extent of cellular uptake and kinetics of drug release within target tissues [3].

Furthermore, despite the improved biodistribution and therapeutic outcomes of ligand-targeted NNMs in a number of preclinical studies, the advantages have so far been negligible in the clinical research phase [4]. Possible reasons for this discrepancy have previously been reviewed [47,57], and include factors such as disease-dependent anatomical and physiological barriers, target accessibility and expression, and formulation stability. The optimal targeting ligand density on the surface of each NNM still remains to be resolved, and will likely depend on characteristics of the molecular target (e.g. location, expression, internalization rate and immunogenicity) [37,70,71]. In addition, detailed analysis of the degree of NNM accumulation, cellular internalization, intracellular functionality and intracellular degradation will be important parameters for clinical validation and translation [37]. Through extensive experimentation, we are gaining a better understanding of the more appropriate clinical indications for ligand-targeted liposomal formulations. Therefore, by taking a disease-driven approach to NNM development, it will be possible to build comprehensive preclinical data sets that best predicts efficacy for patient sub-groups and supports translatable clinical development.

Large-scale manufacturing

One of the important factors contributing to the slow pace in the clinical translation of NNMs is the structural and physicochemical complexity of the formulation itself. Platforms that require complex and/or laborious synthesis procedures generally have limited clinical translation potential, as they can be quite problematic to pharmaceutically manufacture on a large-scale [1,15,59,60]. Pharmaceutical manufacturing development is centered on quality and cost. Quality includes the manufacturing process and stability of the formulation, with NNM manufacturing being challenged by potential issues related to: (i) poor quality control; (ii) scalability complexities; (iii) incomplete purification from contaminants (e.g. by-products and starting materials); (iv) high material and/or manufacturing costs; (v) low production yield; (vi) insufficient batch-to-batch reproducibility, consistency and storage stability of

the final product (e.g. regarding size distribution, porosity, charge and mass); (vii) lack of infrastructure and/or in-house expertise; (viii) chemical instability or denaturation of the encapsulated compound during the manufacturing process; and (ix) scarcity of venture funds and pharmaceutical industry investment [1,60,61,72].

An essential requirement for clinical translation is to have access to a preparation method that allows the production of large scalable quantities of NNMs, which is also consistently manufactured at the same high level of quality and reproducibility [15,16,73]. Suitable methods for the industrial scale production of several basic nanomedicine platforms, such as liposomes, have been successfully developed without the need for numerous manufacturing steps or the use of organic solvents [70,74]. The challenges arise when the NNM system becomes more complex. For example, with the addition of surface modification with coatings and/or ligands, inclusion of multiple targeting components, or by encapsulating more than one therapeutic agent. Integration of multiple components into a single nanosized carrier requires multiple steps in the production process, which inevitably poses problems for large scale good manufacturing (cGMP) production, increases the cost of production, and makes the quality assurance and quality control (QA and QC) evaluation of such products more difficult [1,60,75].

Characteristics of the manufactured NNM need to be well-defined and reproducibly generated to allow initiation of clinical translation. Chemistry, Manufacturing, and Controls (CMC) information is required for investigational new drugs (IND) at each phase of investigation to ensure the proper identity, strength or potency, quality, and purity of the drug substance and drug product. The type of information submitted will depend on the phase of the investigation, the extent of the human study, the duration of the investigation, the nature and source of the drug substance, and the drug product dosage form. The characterization and validation of more complex NNMs can be particularly challenging due to the sheer number of parameters to address (e.g. size distribution, morphology, charge, purity, drug encapsulation efficiency, coating efficiency, and density of conjugated ligand/s) [1]. Batch-to-batch variation of NNMs can potentially lead to significant changes to their physicochemical properties (e.g. polarity and size), pharmacokinetic parameters (i.e. absorption, distribution, metabolism and excretion), and/or pharmacodynamic interactions (e.g. cellular interaction and activity) [1,15,60]. In addition, NNMs need to be stable after the manufacturing process, during long-term storage, and upon clinical administration (i.e. to avoid massive drug release or aggregation in the bloodstream and route to the site of action).

Biocompatibility and safety

Detailed toxicology is essential for the clinical translation of NNMs to determine the overall safety for human use [76]. Pharmaceutical regulatory authorities generally recommend that the sponsor carefully assess for any changes in the drug substance and drug product manufacturing process or drug product formulation at any phase of clinical development, in order to determine if the changes can directly or indirectly affect the safety of the product. CMC modifications throughout the IND process that can affect safety include: (i) changes in the synthetic pathway or reagents used to manufacture the drug substance, product or formulation; (ii) changes resulting in a different impurity profile; (iii) changes in the actual manufacturing method (e.g. chemical synthesis, fermentation, or derivation from a natural source); (iv) changes in the source material; (v) changes in the method of sterilization of the drug substance or drug product; (vi) changes in the route of administration; (vii) changes in the composition and/or dosage form of the drug product; (viii) changes in the drug product manufacturing process that can affect product quality; and (ix) changes in the drug product container closure system that can affect product quality (e.g. dose delivery). If any changes are identified, stringent procedures are in place to ensure appropriate comparison testing of the drug substance and/or drug product produced from the previous manufacturing process and the changed manufacturing process to evaluate product equivalency, quality, and safety. When analytical data demonstrate that the materials manufactured before and after are not comparable, sponsors should perform additional qualification and/or bridging studies to support the safety and bioavailability of the material to be used in the proposed trials.

Knowledge of the activity and toxicities of the free drug, the behaviour of different NNM delivery systems and their interaction with biological components, and the influence of drug release rate on target and off-target concentrations of bioavailable drug allow the ability to predict potential side effects or toxicities in vivo [3]. In particular, the rational design of NNMs from the early phase of material selection, production method optimization, and product purification is of fundamental importance to increase their clinical translation potential [77]. Although the safety of some common materials such as phospholipids and biodegradable polymers have been studied previously [78], increasing the complexity of NNMs, such as the use of different synthetic compositions, coatings and ligands, can have a significant effect on the biocompatibility, biodistribution and toxicology profile of nanomedicines following in vivo administration [2,47,57,60-62]. For example, complement ac-

tivation-related pseudoallergy (CARPA) is an acute adverse immune reaction caused by many NNMs [4,79-81. The complement system is part of the innate immune response and is involved in a range of immunological and inflammatory processes [82]. CARPA is an immediate, non-IgE-mediated hypersensitivity reaction that involves symptoms such as anaphylaxis, facial flushing, facial swelling, headache, chills and cardiopulmonary distress [81]. General clinical management involves slowing the infusion rate or ceasing therapy, as well as the use of standard allergy medications (e.g. antihistamines, epinephrine and corticosteroids) [4,80]. The development of immunogenic reactions to NNM-based therapies may lead to altered pharmacokinetics, loss of efficacy, and the rise of potentially serious toxicities (e.g. anaphylaxis) [80,83].

There is a regulatory need for validated, sensitive and standardizable assays incorporating in vitro, ex vivo and in vivo protocols to appropriately assess the nanotoxicology of NNMs during the early stages of clinical development [77,79,84]. Comprehensive in vitro or ex vivo assays for nanosafety testing are essential to screen for potential hazards prior to preclinical evaluation in animal models [85]. For example, standardized in vitro protocols using different cell culture models (i.e., blood, lung, placenta, brain, liver, gastrointestinal system) to assess potential risk of cytotoxicity, immunotoxicity, and genotoxicity of NNMs [77]. This is particularly important with the development of NNMs incorporating many new materials with the goal for use in the clinical setting. In order to do this effectively across the board, standardized reference materials would need to be established and the testing would also need to be relevant for the intended route of administration [60]. Although current testing approaches are limited and insufficient for nanotoxicology evaluations for clinical translation, a number of techniques that are more specific for nanomedicines are under development. This includes alternative test strategies, high-throughput screening techniques, high-content screening, and computational modelling [77,86-88]. These techniques have the potential to analyze in a comparative way many NNMs simultaneously.

There is also a need to perform specialized toxicology studies in animal models to assess both short-term and long-term toxicity, as circulation half-lives and drug retention times are generally significantly increased with nanoencapsulation. A thorough understanding of the absorption, distribution, metabolism, and excretion of emerging nanomaterials in vivo is important to predict the toxicological responses to NNMs [60,84]. Adequate assessment protocols are needed to monitor various aspects of the NNM drug delivery process, including pharmacokinetics, biodistribution, target site accumulation, local distribution at the target site, localization in healthy tissues, kinet-

ics of drug release, and therapeutic efficacy [89]. Incorporation of real-time imaging techniques have enabled better understanding of the interaction of NNMs with biological organs and tissues following in vivo administration [76,84,85,89].

In addition, biocompatibility, immunotoxicological and inflammatory potential should be assessed, with functional outcomes correlated with mechanisms of tissue uptake and clearance [85]. These parameters need to be well-investigated based on dose, dosage form and route of administration to establish safe limits prior to clinical trials [76,85]. This is of particular importance for NNMs composed of materials that have never been used before in clinical applications. Even in the clinical trial phase, regulatory protocols should be in place to detect any toxicity caused by not only the encapsulated therapeutic compounds, but also novel mechanisms unique to nanotechnology [76,85]. For example, the short-term and long-term effects of accumulation of NNMs in organs of the RES [83,90], especially the liver, spleen, kidneys, lungs, bone marrow and lymph nodes [91]. The RES is the main site of NNM accumulation following their systemic administration [91,92]. The cells of the RES are also part of the innate immune system, which has raised the question of whether macrophage saturation by NNMs leads to immunosuppression and increases the risk of infections [4]. Addressing these issues are necessary to safeguard the application of emerging NNMs in the clinical setting.

Intellectual property (IP)

Given the complexities of incorporating nanotechnology into biomedical applications, there needs to be more precise definitions on what constitutes novel IP of a nanomedicine [93]. Nanomedicines are complex as they have a number of variable components, and bridge between the field of medicine and medical device [94]. Generally, the control of a NNM product requires an IP position on: (i) the encapsulated cargo; (ii) the carrier technology; and (iii) the characteristics of the drug and carrier together. Although this definition is straightforward, it does open up a number of problems with the issuing of patents to date [95,96]. For example, NNMs that incorporate existing drugs with novel carrier technology, or those that incorporate existing drugs with existing carrier technology for a new biomedical or disease application. The IP situation becomes even more confusing with more complex drug delivery systems, such as those which incorporate commercially available targeting ligands (e.g. antibodies) or coatings (e.g. Eudragit®) that are owned by other companies. IP strategies may likely involve multiple patents associated with any given technology and the need for cross-licensing arrangements [97]. Therefore, it is im-

portant to simplify the pathway from invention to commercialization through new IP practices and protocols, so as to reduce the time and expense required for negotiating collaboration and licensing agreements [97].

With the significant increase in the number of nanotechnology patent applications over the last few decades, other key issues that need to be addressed include patent review delays, patent thickets, and issuance of invalid patents [95,98,99]. There needs to be a universal nano-nomenclature on identical or similar nanostructures or nanomaterials, and more refined search tools and commercial databases to avoid the issuing of multiple nanopatents on the same invention [95,99]. Databases used by the Patent and Trademark Office (PTO) need to be able to search through nanotech-related prior art that resided in scientific publications world-wide, including earlier publications that preceded the emergence of online publication databases [60]. Patent examiners also require expertise and training with respect to the emerging fields of nanotechnology and nanomedicine. The complexities with nanotechnology have led to the so called "patent thickets", which can lead to costly litigation and halt commercialization efforts [60]. Therefore, improved clarity on IP and patenting surrounding nanotechnology in health and medicine is required, and will need to involve implementation of universal regulations and policies that are tailored towards this niche commercialization field.

Government regulation

Nanomedicines have significant potential to increase the growth of the pharmaceutical market and improve health benefits, however the current scientific and regulatory gap for nanomedicines is large and challenging. Commercialization of nanomedicines is highly dependent on a number of regulatory factors based on government policies in the area of manufacturing practice, quality control, safety, and patent protection [59,60,85]. The lack of clear regulatory and safety guidelines has affected the development of NNM products toward timely and effective clinical translation [59,60,85]. For example, polymers have been widely investigated as an effective platform for NNM strategies; however, their safety and efficacy is highly dependent on the polymer molecular weight, polydispersity, molecular structure, and conjugation chemistry [100,101]. Due to the increased number of novel polymeric materials and complex polymeric-based NNM formulations, there is an urgent need for an appropriate regulatory framework to assist in evaluation [101]. As each polymer-based NNM is different, it is important to consider each individually based on doses, administration routes, dosing frequency, and proposed clinical use. This would be the same for most other NNM platforms.

NNMs are currently regulated within the conventional framework governed by the key regulatory authority of each country (e.g. FDA, TGA and EMA). Although NNMs have been on the market for nearly two decades, the first generation of NNM products passed regulatory approval by only having to meet general standards, applicable to medicinal compounds. These regulations are no longer appropriate to confirm the quality, safety, and efficacy of NNMs for clinical use [59,60,85]. Reasons for this are based on the complex structure of NNMs, their unclear interaction with cells and tissues within the human body, increased complexity of clinical use, and the multi-functional nature of some formulations (e.g. integration of therapeutics with imaging diagnostics) [59,60,85]. Regulatory standards and protocols validated specifically for nanoparticles are needed that bridge both medicine and medical devices regulations. This should take into account a NNM's complexity, route of administration, pharmacokinetics, pharmacodynamics and safety profile, as well as provide information on the most appropriate clinical trial design and patient selection [60]. There needs to be a fine balance to ensure the safety and quality of NNMs without over-regulation, which can negatively affect the progress of innovative products to the market, by escalating costs for achieving regulatory approval and/or consuming a significant portion of the life of a patent.

Development of global regulatory standards for NNMs should be established alongside key countries with invested interest. Although major steps have been taken in the last 5 years, a closer collaboration between regulatory agencies, academia, research and industry is needed [72,85,97]. This is of particular importance due to the limited availability of contract manufacturing organizations world-wide that specialize in producing NNM products, in accordance with the requirements for good manufacturing practice (GMP) [72]. It should be noted that this limited number of manufacturing organizations may be further divided based on their infrastructure capabilities of producing specific NNM platforms (e.g. liposomes, polymeric nanoparticles, dendrimers and drug-polymer conjugates). Therefore, NNMs produced in these manufacturing organizations will likely be marketed in multiple countries and thus should be governed under the same regulatory standards [72]. There will need to be complete evaluation and documentation of production processes for NNMs, incorporating appropriate industrial standards for both quality control and prevention of environmental issues [85]. Manufactured NNMs will still need to meet general pharmaceutical standards such as purity, sterility, stability, manufacturing operations, and related industrial control standards [85]. In addition, new analytical tools and standardized methods will need

to be implemented to evaluate key physical characteristics of NNMs that can affect in vivo performance such as particle size and size distribution, surface chemistry, morphology, surface area, surface coating, hydrophilicity, porosity, and surface charge density [59,60,85]. These methods will vary for different nanomaterials and nanostructures. Thus, regulatory authorities should work together to develop the testing methods and appropriate standardized protocols for toxicity studies and regulatory requirements, which will be needed to ensure the efficacy and safety of current and emerging NNMs.

Perspectives on the translational development of nanomedicines

From a therapeutic perspective, increasing drug accumulation at target tissues and minimizing systemic adverse effects are still the biggest design challenges to meet when developing new drug delivery systems. Even though promising NNMs may demonstrate significant efficacy in in vitro or ex vivo studies, it is important to evaluate the platforms in vivo using appropriate animal models of the disease. It is here where many of the current NNM platforms have shown limited specificity, accumulation and/or stability, therefore providing unsatisfactory results to warrant progression in the R&D process [11]. Efficacy in an animal model also does not necessarily equate to efficacy in humans, as drug delivery within the human body is complex and can be highly variable, especially when associated with disease [3]. Therefore, this concept of designing nanomedicines that act like a "magic bullet", which refers to the exclusive delivery of active compounds to specific organs, tissues or cells, is just not realistic when taking into account the pharmacokinetic and pharmacodynamic processes that occur following administration into the body [15]. This term should refer to the development of realistic therapeutic platforms, in which therapeutic effects are maximized, doses are minimized, and complexity in dosage form design is reduced [15].

Complexity in dosage form design is a key factor in the ability for a NNM formulation to be translated to the clinic, irrelevant of its therapeutic efficacy. Simplification in formulation design is required to allow efficient and reproducible large-scale manufacturing [15,16,73]. Any added complexities to the basic NNM platform would need to show significantly improved benefits that is reliable and reproducible in animal models and patients, due to the added costs and complexity in the manufacturing process. For example, further studies are required to examine the benefits of ligand-targeted delivery systems over basic NNM platforms, in particular the reliability and consistency of the expression of the target across disease severity and in different patients [3,3,11]. In addition, when translating findings from animal models to hu-

mans, we need to determine how to modify these formulations so that they are appropriate for human administration [11]. In vivo studies are typically conducted in animal models of experimental diseases, especially in mice and rats, which can place limitations on the size and consistency of the dosage form that can be administered – for example, via oral, topical or intraperitoneal delivery [4,11]. The practicability of designing dosage forms that are both acceptable to humans and efficacious needs to be further explored for clinical studies. Thus, there needs to be a balance between complexity, therapeutic efficacy and clinical translation.

To transition NNMs to the clinic, attention should be given to nanosized carriers that are stable following in vivo administration, easily able to be up-scaled for manufacturing with high control over their physicochemical properties (e.g. size and polydispersity, morphology, drug encapsulation efficiency, and charge), as well as being composed of materials that are biocompatible, biodegradable and non-toxic. As nanoparticles are able to enter cells and interfere with molecular pathways, synthetic polymers and lipids should be carefully evaluated for potential short-term and long-term toxicity for clinical application [101]. For example, recent studies have identified potentially toxic in vitro and in vivo effects with the use of cationic lipids and polymers, including cell shrinking, reduced number of mitoses, vacuolization of the cytoplasm, and detrimental effects on key cellular proteins (e.g. protein kinase C) [102].

Pathway to translation and commercialization

The experimental development of NNMs is progressing at a fast pace, however significant challenges still exist in promoting these platforms into clinically feasible therapies (**Table 3**). The majority of NNMs in the clinic are for the treatment of cancer, predominantly by the parenteral route of administration. They are structurally based on simple nanomedicine platforms, in particular basic nanoparticles, surface charge-modified nanoparticles, and PEGylated nanoparticles [59,72]. Although clinical applications of nanotechnology for non-cancer diseases are increasing based on promising experimental results, there are several barriers that have slowed progress in the preclinical and, especially, clinical stages of development. This includes issues surrounding complexity in manufacturing and characterization, lack of understanding of in vivo pharmacokinetics and pharmacodynamics, acute and chronic toxicity, and cost-effectiveness [1,59,60,72,85]. These challenges are even greater with increasing complexity of the NNM design.

The pace for the clinical translation of NNMs has been relatively slow as the development trajectory is very costly, complex and time-consuming, which

has affected the attitudes of the pharmaceutical industry and capital investors [28-30]. There has to be a clear positive benefit-to-risk ratio that will accompany the clinical implementation of products and procedures based on nanotechnology. In particular, the cost-benefit analysis may be a limitation to the clinical translation of some NNMs when compared to an approved counterpart or existing therapies. This analysis has to be clear before starting the development process. Emerging NNM products, which are more complex in structure and more expensive than conventional therapies, need to provide an overall reduction in health care costs and provide a worthwhile opportunity for the pharmaceutical industry to invest its R&D budgets [72]. This reduction in health care costs is likely to be obtained by increasing therapeutic efficacy, improving quality of life, reducing adverse effects or toxicities in non-target organs, and/or reducing the need for surgical or other high-risk interventions [103]. Nanopharmaceuticals can offer the ability to extend the economic life of proprietary drugs and create additional revenue streams [60]. In addition, market analysis, investment risk, potential profit margins, and value proposition of novel NNMs are important factors for the pharmaceutical industry and investors. Typically, pharmaceutical products that are developed to address larger disease populations with treatment expected in a primary or secondary care setting are preferred by the pharmaceutical industry. From a business perspective, the necessary infrastructure, understanding of NNMs, and skill set required for the commercial development of NNMs are not currently well represented at most pharmaceutical companies. These factors should be taken into account when assessing the overall cost-effectiveness of NNMs in comparison to existing therapies.

Nanomedicines generally face a number of regulatory approval hurdles. The control of materials in the nanosize range often presents greater scientific and technical challenges compared to conventional formulations [1,59,60,72,85]. NNMs encompass a number of different types of nanomaterials and nanostructures, which make it even more challenging to establish appropriate regulatory protocols and tools to ensure standardized GMP manufacturing and characterization, safety and toxicology evaluation, and clinical trial design. These procedures are paramount to confirming therapeutic efficacy and safety prior to marketing approval for use in patients on a larger scale. Effective clinical translation will require an interdisciplinary approach to develop novel protocols, assays and infrastructure for the manufacturing and characterization of NNMs [1,59,60,72,85]. This will need to involve experts from academia and industry with specialty in pharmaceutics, engineering, biology, medicine, and toxicology. Potential approaches to fast-track promising novel NNMs to

clinical trials include the establishment or coordination of laboratories and centers that have expertise in (i) characterizing NNM platforms, (ii) conducting preclinical studies on NNMs for submission to regulatory agencies, (iii) scale up laboratory preparation of nanomaterials according to regulatory and industry standards for early clinical trials, and (iv) designing and conducting clinical trials of NNM platforms [72].

Conclusion

Overall, the use of nanotechnology in medicine has the potential to have a major impact on human health. It has been suggested to facilitate the development of personalized medicine for specific patient sub-groups, in which therapy is tailored by the patient's individual genetic and disease profile [1,104,105]. For example, disease-specific characteristics such as capillary permeability [106], cellular receptor expression and molecular pathway activation could be analyzed and used to design personalized nanomedicines [1,104,105]. The physicochemical properties (e.g. size and structure) of the delivery system can also be modified according to the severity of the disease for optimal therapeutic benefits [11]. This concept would significantly advance the way in which we treat patients. However, for this to occur, there are still a number of issues that need to be addressed as detailed in this review – from our basic understanding of the biology of specific diseases and the biological interaction of NNMs in patients, to commercialization hurdles related to manufacturing, costs, and regulatory standards. Finally, researchers need to consider minimizing the complexity of NNMs and take into account the final dosage form for human use, in order for a formulation to have the potential to be translated into a clinically applicable therapeutic. Reducing complexity to the minimum required for pathophysiological or medical need is paramount in nanoparticle design and synthesis to generate clinically translatable nanosized therapeutics.

Author Contributions

All authors were involved in drafting the manuscript and revising the manuscript critically for important intellectual content.

Acknowledgements

The authors wish to thank The Pharmacy Research Trust of New South Wales, The Rebecca L. Cooper Medical Research Foundation, Gladys M Brawn Fellowship, ausEE Research Foundation, and The University of Newcastle for providing financial support for our research.

References

[1] Teli MK, Mutalik S, Rajanikant GK. Nanotechnology and nanomedicine: going small means aiming big. Curr Pharm Des. 2010;16(16):1882-92.
[2] Allen TM, Cullis PR. Drug delivery systems: entering the mainstream. Science. 2004;303(5665):1818-22.
[3] Hare JI, Lammers T, Ashford MB, Puri S, Storm G, Barry ST. Challenges and strategies in anti-cancer nanomedicine development: An industry perspective. Adv Drug Deliv Rev. 2017;108:25-38.
[4] Sercombe L, Veerati T, Moheimani F, Wu SY, Sood AK, Hua S. Advances and Challenges of Liposome Assisted Drug Delivery. Front Pharmacol. 2015;6:286.
[5] Kim HJ, Kim A, Miyata K, Kataoka K. Recent progress in development of siRNA delivery vehicles for cancer therapy. Adv Drug Deliv Rev. 2016;104:61-77.
[6] Larsson M, Huang WT, Liu DM, Losic D. Local co-administration of gene-silencing RNA and drugs in cancer therapy: State-of-the art and therapeutic potential. Cancer Treat Rev. 2017;55:128-35.
[7] Mishra DK, Balekar N, Mishra PK. Nanoengineered strategies for siRNA delivery: from target assessment to cancer therapeutic efficacy. Drug Deliv Transl Res. 2017;7(2):346-58.
[8] Shajari N, Mansoori B, Davudian S, Mohammadi A, Baradaran B. Overcoming the Challenges of siRNA Delivery: Nanoparticle Strategies. Curr Drug Deliv. 2017;14(1):36-46.
[9] Talekar M, Tran TH, Amiji M. Translational Nano-Medicines: Targeted Therapeutic Delivery for Cancer and Inflammatory Diseases. AAPS J. 2015;17(4):813-27.
[10] Hua S. Targeting sites of inflammation: intercellular adhesion molecule-1 as a target for novel inflammatory therapies. Frontiers in Pharmacology. 2013;4:127.
[11] Hua S, Marks E, Schneider JJ, Keely S. Advances in oral nano-delivery systems for colon targeted drug delivery in inflammatory bowel disease: Selective targeting to diseased versus healthy tissue. Nanomedicine. 2015;11(5):1117-32.
[12] Mastrobattista E, Koning GA, Storm G. Immunoliposomes for the targeted delivery of antitumor drugs. Adv Drug Deliv Rev. 1999;40(1-2):103-27.
[13] Luxenhofer R, Barz M, Schillmeier M. Quo vadis nanomedicine? Nanomedicine (Lond). 2014;9(14):2083-6.
[14] Nehoff H, Parayath NN, Domanovitch L, Taurin S, Greish K. Nanomedicine for drug targeting: strategies beyond the enhanced permeability and retention effect. Int J Nanomedicine. 2014;9:2539-55.
[15] Barz M, Luxenhofer R, Schillmeier M. Quo vadis nanomedicine? Nanomedicine (Lond). 2015;10(20):3089-91.
[16] Lammers T. Smart drug delivery systems: back to the future vs. clinical reality. Int J Pharm. 2013;454(1):527-9.
[17] Rizzo LY, Theek B, Storm G, Kiessling F, Lammers T. Recent progress in nanomedicine: therapeutic, diagnostic and theranostic applications. Curr Opin Biotechnol. 2013;24(6):1159-66.
[18] Milane LS, Amiji M. Nanomedicine for inflammatory diseases. New York: CRC Press; 2017.
[19] Hashizume H, Baluk P, Morikawa S, McLean JW, Thurston G, Roberge S, et al. Openings between defective endothelial cells explain tumor vessel leakiness. Am J Pathol. 2000;156(4):1363-80.
[20] Danhier F. To exploit the tumor microenvironment: Since the EPR effect fails in the clinic, what is the future of nanomedicine? J Control Release. 2016;244(Pt A):108-21.
[21] Maeda H, Nakamura H, Fang J. The EPR effect for macromolecular drug delivery to solid tumors: Improvement of tumor uptake, lowering of systemic toxicity, and distinct tumor imaging in vivo. Adv Drug Deliv Rev. 2013;65(1):71-9.
[22] Hobbs SK, Monsky WL, Yuan F, Roberts WG, Griffith L, Torchilin VP, et al. Regulation of transport pathways in tumor vessels: role of tumor type and microenvironment. Proc Natl Acad Sci U S A. 1998;95(8):4607-12.
[23] Matsumura Y, Maeda H. A new concept for macromolecular therapeutics in cancer chemotherapy: mechanism of tumoritropic accumulation of proteins and the antitumor agent smancs.

Cancer Res. 1986;46(12 Pt 1):6387-92.
[24] van der Meel R, Vehmeijer LJ, Kok RJ, Storm G, van Gaal EV. Ligand-targeted particulate nanomedicines undergoing clinical evaluation: current status. Adv Drug Deliv Rev. 2013;65(10):1284-98.
[25] Nakamura H, Fang J, Maeda H. Development of next-generation macromolecular drugs based on the EPR effect: challenges and pitfalls. Expert Opin Drug Deliv. 2015;12(1):53-64.
[26] Lammers T, Kiessling F, Hennink WE, Storm G. Drug targeting to tumors: principles, pitfalls and (pre-) clinical progress. J Control Release. 2012;161(2):175-87.
[27] Ojha T, Pathak V, Shi Y, Hennink WE, Moonen CTW, Storm G, et al. Pharmacological and physical vessel modulation strategies to improve EPR-mediated drug targeting to tumors. Adv Drug Deliv Rev. 2017;119:44-60.
[28] Theek B, Gremse F, Kunjachan S, Fokong S, Pola R, Pechar M, et al. Characterizing EPR-mediated passive drug targeting using contrast-enhanced functional ultrasound imaging. J Control Release. 2014;182:83-9.
[29] Nichols JW, Bae YH. EPR: Evidence and fallacy. J Control Release. 2014;190:451-64.
[30] Rahman AM, Yusuf SW, Ewer MS. Anthracycline-induced cardiotoxicity and the cardiac-sparing effect of liposomal formulation. Int J Nanomedicine. 2007;2(4):567-83.
[31] Lyass O, Uziely B, Ben-Yosef R, Tzemach D, Heshing NI, Lotem M, et al. Correlation of toxicity with pharmacokinetics of pegylated liposomal doxorubicin (Doxil) in metastatic breast carcinoma. Cancer. 2000;89(5):1037-47.
[32] Willis M, Forssen E. Ligand-targeted liposomes. Adv Drug Deliv Rev. 1998;29(3):249-71.
[33] Coimbra M, Banciu M, Fens MH, de Smet L, Cabaj M, Metselaar JM, et al. Liposomal pravastatin inhibits tumor growth by targeting cancer-related inflammation. J Control Release. 2010;148(3):303-10.
[34] Danhier F, Feron O, Preat V. To exploit the tumor microenvironment: Passive and active tumor targeting of nanocarriers for anti-cancer drug delivery. J Control Release. 2010;148(2):135-46.
[35] Kuijpers SA, Coimbra MJ, Storm G, Schiffelers RM. Liposomes targeting tumour stromal cells. Mol Membr Biol. 2010;27(7):328-40.
[36] Ferrari M. Nanovector therapeutics. Curr Opin Chem Biol. 2005;9(4):343-6.
[37] Puri A, Loomis K, Smith B, Lee JH, Yavlovich A, Heldman E, et al. Lipid-based nanoparticles as pharmaceutical drug carriers: from concepts to clinic. Crit Rev Ther Drug Carrier Syst. 2009;26(6):523-80.
[38] Riehemann K, Schneider SW, Luger TA, Godin B, Ferrari M, Fuchs H. Nanomedicine--challenge and perspectives. Angew Chem Int Ed Engl. 2009;48(5):872-97.
[39] Kirpotin D, Park JW, Hong K, Zalipsky S, Li WL, Carter P, et al. Sterically stabilized anti-HER2 immunoliposomes: design and targeting to human breast cancer cells in vitro. Biochemistry (Mosc). 1997;36(1):66-75.
[40] Kirpotin DB, Drummond DC, Shao Y, Shalaby MR, Hong K, Nielsen UB, et al. Antibody targeting of long-circulating lipidic nanoparticles does not increase tumor localization but does increase internalization in animal models. Cancer Res. 2006;66(13):6732-40.
[41] Park JW, Hong K, Kirpotin DB, Colbern G, Shalaby R, Baselga J, et al. Anti-HER2 immunoliposomes: enhanced efficacy attributable to targeted delivery. Clin Cancer Res. 2002;8(4):1172-81.
[42] Needham D, Anyarambhatla G, Kong G, Dewhirst MW. A new temperature-sensitive liposome for use with mild hyperthermia: characterization and testing in a human tumor xenograft model. Cancer Res. 2000;60(5):1197-201.
[43] Bertrand N, Wu J, Xu X, Kamaly N, Farokhzad OC. Cancer nanotechnology: the impact of passive and active targeting in the era of modern cancer biology. Adv Drug Deliv Rev. 2014;66:2-25.
[44] Jang B, Kwon H, Katila P, Lee SJ, Lee H. Dual delivery of biological therapeutics for multimodal and synergistic cancer therapies. Adv Drug Deliv Rev. 2016;98:113-33.
[45] Min Y, Caster JM, Eblan MJ, Wang AZ. Clinical Translation of Nanomedicine. Chem Rev. 2015;115(19):11147-90.
[46] Oude Blenke E, Mastrobattista E, Schiffelers RM. Strategies for triggered drug release from tumor targeted liposomes. Expert Opin Drug Deliv. 2013;10(10):1399-410.

[47] Sawant RR, Torchilin VP. Challenges in development of targeted liposomal therapeutics. AAPS J. 2012;14(2):303-15.
[48] Shi J, Kantoff PW, Wooster R, Farokhzad OC. Cancer nanomedicine: progress, challenges and opportunities. Nat Rev Cancer. 2017;17(1):20-37.
[49] Torchilin VP. Multifunctional nanocarriers. Adv Drug Deliv Rev. 2006;58(14):1532-55.
[50] Kono K. Thermosensitive polymer-modified liposomes. Adv Drug Deliv Rev. 2001;53(3):307-19.
[51] Wagner V, Dullaart A, Bock AK, Zweck A. The emerging nanomedicine landscape. Nat Biotechnol. 2006;24(10):1211-7.
[52] Caster JM, Patel AN, Zhang T, Wang A. Investigational nanomedicines in 2016: a review of nanotherapeutics currently undergoing clinical trials. Wiley Interdiscip Rev Nanomed Nanobiotechnol. 2017;9(1).
[53] Deamer DW. From "banghasomes" to liposomes: a memoir of Alec Bangham, 1921-2010. FASEB J. 2010;24(5):1308-10.
[54] Sessa G, Weissmann G. Phospholipid spherules (liposomes) as a model for biological membranes. J Lipid Res. 1968;9(3):310-8.
[55] Gregoriadis G, Leathwood PD, Ryman BE. Enzyme entrapment in liposomes. FEBS Lett. 1971;14(2):95-9.
[56] Gregoriadis G, Ryman BE. Liposomes as carriers of enzymes or drugs: a new approach to the treatment of storage diseases. Biochem J. 1971;124(5):58P.
[57] Allen TM, Cullis PR. Liposomal drug delivery systems: from concept to clinical applications. Adv Drug Del Rev. 2013;65(1):36-48.
[58] Kim M, Williams S. Daunorubicin and Cytarabine Liposome in Newly Diagnosed Therapy-Related Acute Myeloid Leukemia (AML) or AML With Myelodysplasia-Related Changes. Ann Pharmacother. 2018:1060028018764923.
[59] Sainz V, Conniot J, Matos AI, Peres C, Zupancic E, Moura L, et al. Regulatory aspects on nanomedicines. Biochem Biophys Res Commun. 2015.
[60] Tinkle S, McNeil SE, Muhlebach S, Bawa R, Borchard G, Barenholz YC, et al. Nanomedicines: addressing the scientific and regulatory gap. Ann N Y Acad Sci. 2014;1313:35-56.
[61] Narang AS, Chang RK, Hussain MA. Pharmaceutical development and regulatory considerations for nanoparticles and nanoparticulate drug delivery systems. J Pharm Sci. 2013;102(11):3867-82.
[62] Zhang L, Gu FX, Chan JM, Wang AZ, Langer RS, Farokhzad OC. Nanoparticles in medicine: therapeutic applications and developments. Clin Pharmacol Ther. 2008;83(5):761-9.
[63] Park K. The drug delivery field at the inflection point: Time to fight its way out of the egg. J Control Release. 2017;267:2-14.
[64] Maeda H. Toward a full understanding of the EPR effect in primary and metastatic tumors as well as issues related to its heterogeneity. Adv Drug Deliv Rev. 2015;91:3-6.
[65] Maiseyeu A, Mihai G, Kampfrath T, Simonetti OP, Sen CK, Roy S, et al. Gadolinium-containing phosphatidylserine liposomes for molecular imaging of atherosclerosis. J Lipid Res. 2009;50(11):2157-63.
[66] Crielaard BJ, Lammers T, Schiffelers RM, Storm G. Drug targeting systems for inflammatory disease: one for all, all for one. J Control Release. 2012;161(2):225-34.
[67] Metselaar JM, Van den Berg WB, Holthuysen AE, Wauben MH, Storm G, Van Lent PL. Liposomal targeting of glucocorticoids to synovial lining cells strongly increases therapeutic benefit in collagen type II arthritis. Ann Rheum Dis. 2004;63(348-53).
[68] Metselaar JM, Wauben MH, Wagenaar-Hilbers JP, Boerman OC, Storm G. Complete remission of experimental arthritis by joint targeting of glucocorticoids with long-circulating liposomes. Arthritis Rheum. 2003;48(7):2059-66.
[69] Hua S, Cabot PJ. Targeted Nanoparticles that Mimic Immune Cells in Pain Control Inducing Analgesic and Anti-inflammatory Actions: A Potential Novel Treatment of Acute and Chronic Pain Condition. Pain Physician. 2013;16(3):E199-216.
[70] Kraft JC, Freeling JP, Wang Z, Ho RJ. Emerging research and clinical development trends of liposome and lipid nanoparticle drug delivery systems. J Pharm Sci. 2014;103(1):29-52.

[71] Hua S, Wu SY. The use of lipid-based nanocarriers for targeted pain therapies. Frontiers in Pharmacology. 2013;4:143.
[72] Hafner A, Lovric J, Lakos GP, Pepic I. Nanotherapeutics in the EU: an overview on current state and future directions. Int J Nanomedicine. 2014;9:1005-23.
[73] Grainger DW. Connecting drug delivery reality to smart materials design. Int J Pharm. 2013;454(1):521-4.
[74] Jaafar-Maalej C, Elaissari A, Fessi H. Lipid-based carriers: manufacturing and applications for pulmonary route. Expert Opin Drug Deliv. 2012;9(9):1111-27.
[75] Svenson S. Clinical translation of nanomedicines. Curr Opin Solid State Mater Sci. 2012;16(6):287-94.
[76] Nystrom AM, Fadeel B. Safety assessment of nanomaterials: implications for nanomedicine. J Control Release. 2012;161(2):403-8.
[77] Accomasso L, Cristallini C, Giachino C. Risk Assessment and Risk Minimization in Nanomedicine: A Need for Predictive, Alternative, and 3Rs Strategies. Frontiers in Pharmacology. 2018;9:228.
[78] Storm G, Oussoren C, Peeters P, Barenholz C. Tolerability of liposomes in vivo. In: Gregoriadis G, editor. Liposome Technology. 3. Florida: CRC Press; 1993. p. 345-83.
[79] Jackman JA, Meszaros T, Fulop T, Urbanics R, Szebeni J, Cho NJ. Comparison of complement activation-related pseudoallergy in miniature and domestic pigs: foundation of a validatable immune toxicity model. Nanomedicine. 2016;12(4):933-43.
[80] Szebeni J, Storm G. Complement activation as a bioequivalence issue relevant to the development of generic liposomes and other nanoparticulate drugs. Biochem Biophys Res Commun. 2015;468(3):490-7.
[81] Szebeni J. Complement activation-related pseudoallergy: a new class of drug-induced acute immune toxicity. Toxicology. 2005;216(2-3):106-21.
[82] Moghimi SM, Hunter AC. Capture of stealth nanoparticles by the body's defences. Crit Rev Ther Drug Carrier Syst. 2001;18(6):527-50.
[83] Szebeni J, Moghimi SM. Liposome triggering of innate immune responses: a perspective on benefits and adverse reactions. J Liposome Res. 2009;19(2):85-90.
[84] Dobrovolskaia MA, McNeil SE. Understanding the correlation between in vitro and in vivo immunotoxicity tests for nanomedicines. J Control Release. 2013;172(2):456-66.
[85] Gaspar R. Regulatory issues surrounding nanomedicines: setting the scene for the next generation of nanopharmaceuticals. Nanomedicine (Lond). 2007;2(2):143-7.
[86] Dusinska M, Boland S, Saunders M, Juillerat-Jeanneret L, Tran L, Pojana G, et al. Towards an alternative testing strategy for nanomaterials used in nanomedicine: lessons from NanoTEST. Nanotoxicology. 2015;9 Suppl 1:118-32.
[87] Nel A, Xia T, Meng H, Wang X, Lin S, Ji Z, et al. Nanomaterial toxicity testing in the 21st century: use of a predictive toxicological approach and high-throughput screening. Acc Chem Res. 2013;46(3):607-21.
[88] Oomen AG, Bos PM, Fernandes TF, Hund-Rinke K, Boraschi D, Byrne HJ, et al. Concern-driven integrated approaches to nanomaterial testing and assessment--report of the NanoSafety Cluster Working Group 10. Nanotoxicology. 2014;8(3):334-48.
[89] Kunjachan S, Ehling J, Storm G, Kiessling F, Lammers T. Noninvasive Imaging of Nanomedicines and Nanotheranostics: Principles, Progress, and Prospects. Chem Rev. 2015;115(19):10907-37.
[90] Szebeni J, Barenholz Y. Adverse immune effects of liposomes: complement activation, immunogenicity and immune suppression. In: Publishing PS, editor. Harnessing biomaterials for nanomedicine: preparation, toxicity and applications. Singapore: Pan Stanford Publishing 2009. p. 1-19.
[91] Senior JH. Fate and behavior of liposomes in vivo: a review of controlling factors. Crit Rev Ther Drug Carrier Syst. 1987;3(2):123-93.
[92] Poste G, Papahadjopoulos D, Vail WJ. Lipid vesicles as carriers for introducing biologically active materials into cells. Methods Cell Biol. 1976;14:33-71.
[93] Satalkar P, Elger BS, Shaw DM. Defining Nano, Nanotechnology and Nanomedicine: Why Should It Matter? Science and engineering ethics. 2015.

[94] Paradise J, Wolf SM, Kuzma J, Kuzhabekova A, Tisdale AW, Kokkoli E, et al. Developing U.S. oversight strategies for nanobiotechnology: learning from past oversight experiences. J Law Med Ethics. 2009;37(4):688-705.
[95] Bawa R. Patents and nanomedicine. Nanomedicine (Lond). 2007;2(3):351-74.
[96] Bawa R, Melethil S, Simmons WJ, Harris D. Nanopharmaceuticals - patenting issues and FDA regulatory challenges. American Bar Association SciTech Lawyer. 2008;5:10-5.
[97] Murday JS, Siegel RW, Stein J, Wright JF. Translational nanomedicine: status assessment and opportunities. Nanomedicine. 2009;5(3):251-73.
[98] Bawa R. Will the nanomedicine "patent land grab" thwart commercialization? Nanomedicine. 2005;1(4):346-50.
[99] Bawa R, Bawa SR, Maebius SB, Flynn T, Wei C. Protecting new ideas and inventions in nanomedicine with patents. Nanomedicine. 2005;1(2):150-8.
[100] Diab R, Jaafar-Maalej C, Fessi H, Maincent P. Engineered nanoparticulate drug delivery systems: the next frontier for oral administration? AAPS J. 2012;14(4):688-702.
[101] Gaspar R, Duncan R. Polymeric carriers: preclinical safety and the regulatory implications for design and development of polymer therapeutics. Adv Drug Deliv Rev. 2009;61(13):1220-31.
[102] Lv H, Zhang S, Wang B, Cui S, Yan J. Toxicity of cationic lipids and cationic polymers in gene delivery. J Control Release. 2006;114(1):100-9.
[103] Gandjour A, Chernyak N. A new prize system for drug innovation. Health Policy. 2011;102(2-3):170-7.
[104] Laroui H, Rakhya P, Xiao B, Viennois E, Merlin D. Nanotechnology in diagnostics and therapeutics for gastrointestinal disorders. Dig Liver Dis. 2013;45(12):995-1002.
[105] Mura S, Couvreur P. Nanotheranostics for personalized medicine. Adv Drug Deliv Rev. 2012;64(13):1394-416.
[106] Calcagno C, Lobatto ME, Dyvorne H, Robson PM, Millon A, Senders ML, et al. Three-dimensional dynamic contrast-enhanced MRI for the accurate, extensive quantification of microvascular permeability in atherosclerotic plaques. NMR Biomed. 2015;28(10):1304-14.

Part II | Introduction to cytotoxic lectins

Chapter 3 -Quantitative analysis of receptor-mediated uptake and pro-apoptotic activity of mistletoe lectin-1 by high content imaging

Nataliia Beztsinna, Maria B.C. de Matos, Johanna Walther, Christopher Heyder, Ellen Hildebrandt, Gero Leneweit, Enrico Mastrobattista, Robbert Jan Kok

Scientific Reports (2018)

DOI:10.1038/s41598-018-20915-y

Abstract

Ribosome inactivating proteins (RIPs) are highly potent cytotoxins that have potential as anticancer therapeutics. Mistletoe lectin 1 (ML1) is a heterodimeric cytotoxic protein isolated from European Mistletoe and belongs to RIP class II. The aim of this project was to systematically study ML1 cell binding, endocytosis pathway(s), subcellular processing and apoptosis activation. For this purpose, state of the art cell imaging equipment and automated image analysis algorithms were used. ML1 displayed very fast binding to sugar residues on the membrane and energy-dependent uptake in CT26 cells. The co-staining with specific antibodies and uptake blocking experiments revealed involvement of both clathrin-dependent and -independent pathways in ML1 endocytosis. Co-localization studies demonstrated the toxin transport from early endocytic vesicles to Golgi network; a retrograde road to the endoplasmic reticulum. The pro-apoptotic and antiproliferative activity of ML1 were shown in time lapse movies and subsequently quantified. ML1 cytotoxicity was less affected in multidrug resistant tumor cell line 4T1 in contrast to commonly used chemotherapeutic drug (ML1 resistance index 6.9 vs 13.4 for doxorubicin; IC_{50}: ML1 1.4 ng/ml vs doxorubicin 24000 ng/ml). This opens new opportunities for the use of ML1 as an alternative treatment in multidrug resistant cancers.

Introduction

Ribosome inactivating proteins (RIPs) are highly potent cytotoxins that interfere in protein biosynthesis. RIPs have been found and isolated from various natural resources such as plants, bacteria, fungi and algae. Plant derived RIPs play an important role as defense against herbivores [1,2]. From clinical point-of-view, RIPs are considered as anticancer therapeutics[3,4]. The large RIP family comprises all enzymes EC 3.2.2.22 that catalytically inactivate eukaryotic protein synthesis by hydrolyzation of the N-glycosidic bond between adenine-4324 and the nucleotide in the 28S rRNA of the 60S subunit of ribosomes. The rRNA is fragmented and it ultimately results in protein synthesis inhibition[1,2,5–10] and caspase-mediated apoptosis and necrosis[8]. Toxic RIPs act at very low doses (less than equimolar ratio to the substrate) since the inactivation of ribosome protein production is irreversible[1,2,5–10].

RIPs can be generally classified in three groups. The class of monomeric ~30 kDa RIP-I contains an enzymatic chain only. The class of heterodimeric ~60 kDa RIP-II cytotoxins has the enzymatic chain linked to a lectin chain, often referred as B-chain. The B-chain has high affinity for sugar moieties on the cells surface which promotes protein binding and mediates the protein uptake[1,2,5–9,11]. Due to the absence of a lectin chain, RIP-I do not internalize as efficiently as RIP-II and some of them are considered relatively safe.9 Specific cell binding ligands could be conjugated to RIP-I to increase the therapeutic value. In addition to these two classes, RIP type III cytotoxins consist of a toxic unit linked to a peptide with unknown function[10].

Ricin and Abrin are among the best well studied plant derived RIP-II cytotoxins. Mistletoe lectin 1 (ML1) is also categorized as RIP-II and it is one of the main active components of Viscum album extracts. Although Viscum album extracts are used as an adjuvant in alternative medicine practices[12,13], there is a lack of scientific understanding of how ML1 as a major extract component contributes to the perceived gain in quality of life, and thus the human-beneficial potentialities might be underestimated or misunderstood.

Scientific reports on ML1 are mostly referring to Korean ML or recombinant variations of ML1. Reports on European ML1 are however scarce. Although European ML1 shares 84% homology with Korean ML[14–19], it cannot be assumed they have the same subcellular modes of action and pathways; the same is true for recombinant variations of mistletoe lectin or plant extracts containing ML1[20–23].

ML extracts as well as isolated and recombinant versions of the protein have

shown potent cytotoxic activity against tumor cells in vitro[21,24–27] as well as has contributed to prolonged cancer-free survival in some clinical studies[12,28–30]. Interestingly, ML1 was pointed out as a suitable candidate for treatment of breast cancer in clinical and preclinical trials but despite the promising initial results, no follow up research was done[31,32]. Other studies have suggested that ML1, especially the B-chain, has an immunomodulatory activity[21,33,34]. However, this information is sometimes contradictory and/or lacking proper controls. The mechanisms of ML1 uptake and subsequent cell processing are often equated in the literature to other similar toxins such as ricin or Shiga toxin[35–38]; but direct data on the cellular fate of ML1 is limited and most of the studies were performed on paraformaldehyde prefixed cells[36,37,39].

Our aim was to take the first steps towards a better understanding of the uptake mechanism and cytotoxicity of European ML1. We investigated in detail ML1 binding, uptake pathways and endosomal escape mechanisms in correlation with its cytotoxic activity in living cells. For this purpose, state-of-the-art high content imaging was used in combination with advanced image analysis algorithms. The present study sheds light on the ML1 mechanism of action that can be helpful for cancer treatment, but also provides advanced methodological tools for the investigation of the interaction of proteins, macromolecules or nanoparticles with cells in real time with high speed and accuracy.

Results and Discussion

ML1 isolation and labeling.

Mistletoe lectin 1 (ML1) is composed of a cytotoxic A chain and a galactose binding B chain (**Figure 1 A**). It shares 52% sequence homology with ricin, one of the most common RIP-II[40]. ML1 was extracted and isolated from plant material as described previously[41]. characterized with FPLC and PAGE (**Supplementary information, Figure S1**) and subsequently labeled with Alexa Fluor 647 NHS (AF647) via covalent conjugation. ML1 – AF647 conjugates (further abbreviated as ML1, **Figure 1 B**) were purified and analyzed by size exclusion chromatography (**Figure 1 C**). The fluorophore to protein molar ratios after conjugation were around 1:1. The activity of fluorophore conjugated ML1 was compared to the native protein and no significant differences were found (**Supplementary information, Figure S2**). To exclude non-specific uptake of labeled proteins, AF647 was conjugated to bovine serum albumin (BSA) as a negative control. As expected, there was no uptake of this conjugate in CT26 cells after 1h incubation (data not shown).

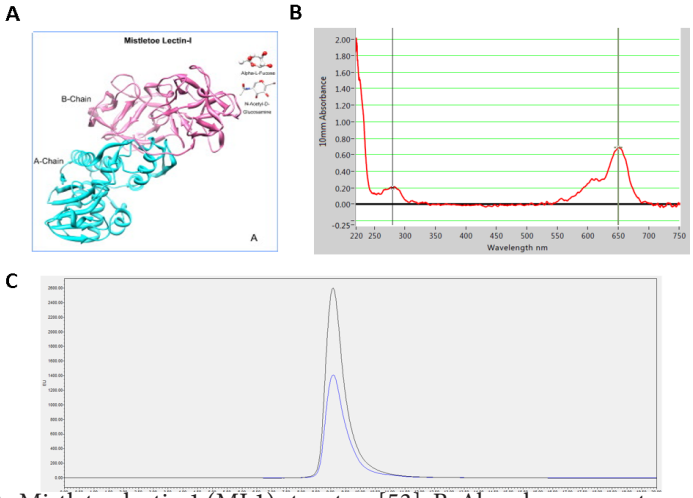

Figure 1. A. Mistletoe lectin 1 (ML1) structure[53]; B. Absorbance spectrum of AF647 labeled ML 1; C. GPC chromatogram of AF647 labeled ML1 (absorbance at 280 nm –blue, at 650 nm – black).

ML1 uptake in CT26 cells

The uptake of ML1 conjugates was examined in living murine colon carcinoma cells (CT26) by fluorescence confocal microscopy using the Yokogawa Cell Voyager CV7000s (**Figure 2**). Their murine origin makes CT26 tumor cells especially suitable for use in cancer models in immunocompetent mice, which are more representative of clinical cancer than xenograft models in nude athymic mice. The CV7000s imaging platform consists of an automated confocal laser-scanning microscope placed in the environmental chamber therefore allowing the acquisition of live cell images in real time. The high speed of auto-focusing and image acquisition allowed capturing the earliest steps of ML1 binding. As seen on the **Figure 2**, the protein immediately binds to cells outlining their membrane on the microscopy image. The same binding pattern is observed when cells are incubated with ML1 at 4 °C and fixed (**Supplementary Information, Figure S3**). As early as 15 minutes after addition of the protein to cells, ML1 appears in cytoplasmic vesicular structures and their number and fluorescence intensity increases over time. Moreover, at later time points these vesicles seem to get closer to the perinuclear region.

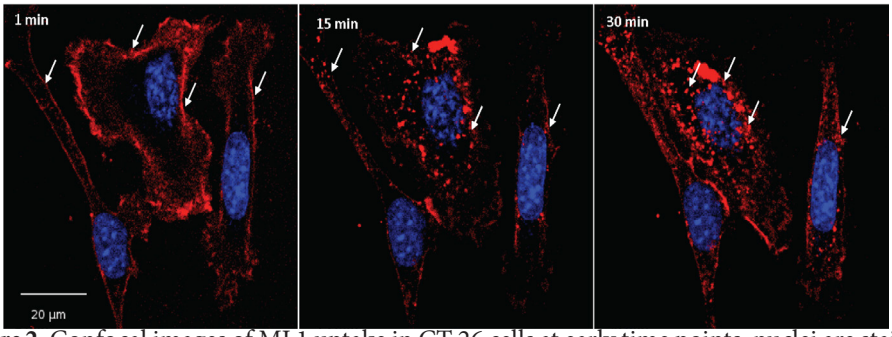

Figure 2. Confocal images of ML1 uptake in CT 26 cells at early time points; nuclei are stained in blue, ML1 – red; arrows indicate changes in the uptake patterns from membrane binding to vesicles that move closer to the nuclei in time; size bar 20 µm.

Comparison of ML1 uptake with other toxins

The binding and uptake of ML1 in CT26 cells was simultaneously compared to Oregon Green labeled Wheat Germ Agglutinin (WGA) and Alexa Fluor 488 labeled Cholera Toxin subunit B conjugate (CTsB). All three proteins displayed very similar uptake pattern with membrane binding in first minutes followed by location in vesicles in the cytoplasm (**Figure 3 A, B**).

The co-localization of ML1 and either of the toxins in intracellular vesicles was quantified with the help of Columbus Suit software calculating Pearson correlation coefficient (P coloc). P coloc is a well-established measure of correlation and ranges from +1 (perfect correlation) to -1 (perfect negative correlation) with values close to 0 meaning an absence of correlation. For the two fluorophores P coloc measures the correlation between their intensities in a given picture and is meant to reflect on a molecular interaction between molecules or with subdomains of a cellular compartment[42]. Columbus co-localization algorithm P coloc calculation provided correlation plots in a faster and more automated manner than classical image analysis tools such as Image J Software (Coloc 2 tool). Both software tools were applied on the same dataset (ML1 and CTsB after 1h of co-incubation) and yielded almost identical P coloc values 0.44±0.13 and 0.45±0.15 for Image J and Columbus, respectively.

Co-localization analysis in time showed similar degree of association between ML1 and WGA or ML1 and CTsB (**Figure 3C, 3D**). **Figure 3D** shows an example of P coloc distribution analysis in one of the images of ML1 and CTsB after 1h of co-incubation. The Pearson's correlation coefficient varied from 0.2-0.3 at the first minutes of experiment (membrane binding step) to 0.4-0.6 after 15-60 minutes of continuous incubation with both protein pairs. Although theoretical P coloc maximum is 1, the correlation of 0.5 and higher is con-

sidered high enough to show the co-localization in biological systems[43,44]. The observed P coloc values indicate high degree of similarity between ML1, WGA and CTsB in terms of cellular uptake, although their targeted receptors on the cell surface are different[45]. CTsB is frequently used in the literature as a marker of lipid-raft associated caveolin-mediated uptake while it was also shown to enter cells through clathrin-dependent pathway and clathrin- and caveolin- independent pathways[46,47].

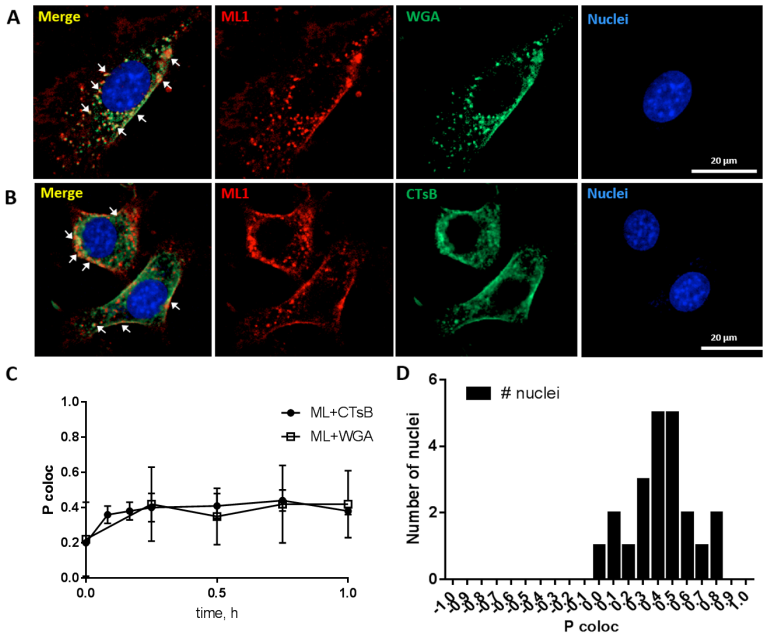

Figure 3. Confocal images of ML1 (in red) co-localization with: A. WGA (in green); B. CTsB (in green). C. Pearson correlation coefficient calculated with Columbus Suit software (P coloc) of ML1 co-localization with WGA or CTsB at various time points. D. Frequency distribution of P coloc between ML1 and CTsB after 1h incubation; CT 26 cells, nuclei are stained in blue; size bar 20µm.

Inhibition of ML1 uptake

Various uptake inhibitors were applied to elucidate the key mechanisms involved in ML1 uptake by the cells. The results are based on microscopic observations and subsequent quantitative image analysis (**Supplementary figures S4 and S5**). Incubation of the cells with ML1 at 4 ^{0}C resulted in binding to the outer membrane surface without any observable intracellular signal (**Supplementary information, Figure S2**). This result suggests that ML1 uptake is energy-dependent. The molecular target for ML1 on the cell surface is a specific polysaccharide ligand containing a terminal sialic acid residue and D-ga-

lactose. Non-surprisingly, the pre-incubation of cells with excessive amounts of galactose (10-100 mM) inhibited both uptake and membrane binding of ML1. It was previously reported that high amounts of galactose in the cell medium could protect cells from ML1 associated toxicity[48]. Inhibitors of clathrin-dependent uptake, chlorpromazine and high concentration of sucrose, noticeably decreased ML1 uptake and binding but did not inhibit it completely suggesting the involvement of clathrin-independent mechanism in ML1 uptake. Finally, methyl-β-cyclodextrin, a cholesterol-depleting agent that abolishes caveolae mediated endocytosis[49], did not show any influence on ML1 membrane binding and uptake.

ML1 co-localization with subcellular compartments

The dynamic accumulation of ML1 in various subcellular compartments was studied by coincubation with various markers that are compatible with microscopy of living cells (summarized table of all used cell markers is presented in **Supplementary Information, Table S1**). CT26 cells were first pre-incubated with endosomal, lysosomal and Golgi vesicular markers in separate experimental setups (pHrodo™ Green Dextran was used for endosomes, LysoTracker® Green for lysosomes and BODIPY® TR C5-ceramide complexed to BSA for Golgi). Then the cells were incubated with 10 μg/mL of ML1 and imaged. **Figure 4** shows gradual increase in time in the overlapping between the green signal from endosomes (pHrodo™) and red signal from ML1. Co-localization analysis at short (up to 3h, and long (up to 28h) kinetics revealed time-dependent increase in correlation of intracellular ML1 signal with endosomal labelling (**Figure 4**).

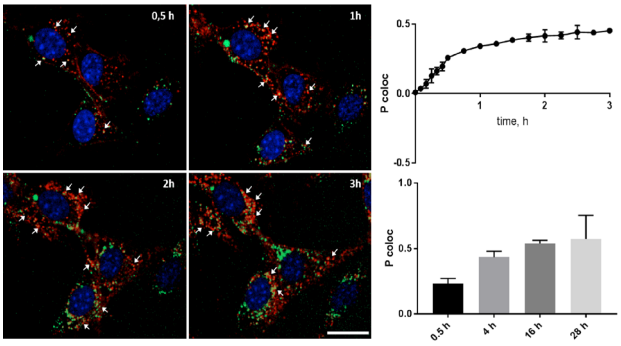

Figure 4. Confocal images of ML1 (in red) co-localization with endosomal marker (pHrodo™ Green Dextran, in green) at different time points (left) and Pearson correlation coefficient dynamics of co-localization ML1 with endosomes at early (up, right) and late time points (lower, right). CT 26 cells, nuclei are stained in blue; arrows indicate co-localization regions; size bar – 20 μm.

Co-localization analysis of ML1 with lysosomal marker (LysoTracker® Green) revealed little to no correlation (P coloc around 0, **Figure 5**). In contrast, Golgi apparatus labeling with BODIPY® TR C5-ceramide complexed with BSA showed substantially higher co-localization with intracellular ML1 already at 30 min incubation (P coloc 0.38 for Golgi versus 0.03 for lysosomes). This indicates that ML1 does not go through the endolysosomal pathway leading to protein degradation, but instead follows a retrograde pathway from endosomes to Golgi and endoplasmic reticulum as previously shown for ricin, Shiga toxin and Cholera toxin[50].

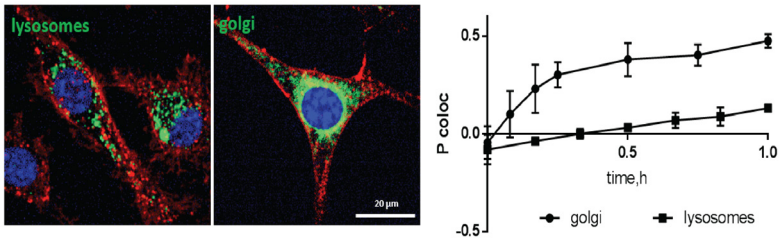

Figure 5. Confocal images of ML1 (in red) co-localization with lysosomal or Golgi markers (in green) after 1h incubation and Pearson correlation coefficient dynamics of co-localization ML1 with lysosomes and Golgi. CT 26 cells, nuclei are stained in blue; arrows indicate co-localization regions; size bar – 20 µm.

To confirm live imaging data, ML1 uptake was analyzed with a set of endolysosomal pathway specific antibodies (**Figure 6, Supplementary information, Figure S6**). CT26 cells were incubated with ML1 for 2h, fixed and then stained with anti EE1 and anti Rab5 for early endosomes, anti Rab7 for late endosomes, anti Rab11 for lysosomes, anti-clathrin and anti-caveolin. Subsequent co-localization and statistical analysis revealed the ML1 association with both clathrin and caveolin staining with slight preference towards the former. This is in accordance with the uptake inhibition experiments and the co-localization data described above, indicating a progressively decreasing amount of ML1 associated with later stages of endolysosomal pathway (Rab5, Rab7 and Rab11) and thus confirming its redirection towards Golgi and retrograde transport to the ER. The exact "endosomal escape" mechanism remains unclear for plant derived toxins in general and for ML1. Ricin toxin, shares a lot of similarities with ML1, induces membrane destabilization and structural changes at low pH (fusion and lysis), which allows it to escape endocytic vesicles and undergo retrograde transport to the ER with subsequent translocation to the cytoplasm[51,52].

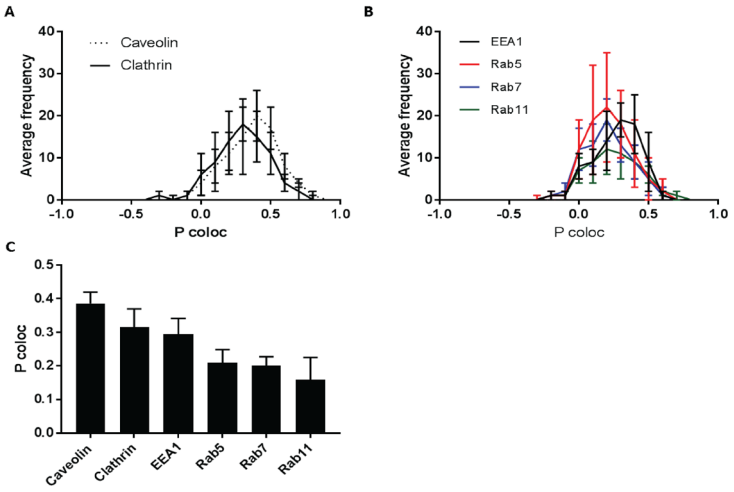

Figure 6. Co-localization analysis of ML1 and endosomal pathway specific antibodies: A. Pearson's coefficient frequency distribution of ML1 co-localization with caveolin or clathrin specific antibodies; B. Pearson's coefficient frequency distribution of ML1 co-localization with early, late endosome or lysosome specific antibodies; C. Median Pearson's coefficient of ML1 and endosomal pathway specific antibodies co-localization. CT26 cells were incubated with 10 μg/mL of ML1 for 2h, then fixed, permeabilized and stained with specific antibodies.

ML1 cytotoxicity

Pro-apoptotic and anti-proliferative activity of ML1 were demonstrated in viability and caspase activation assays in live-cell imaging (**Figures 7 and 8**). ML1 demonstrated a dose-dependent induction of apoptosis in CT26 cells through caspase activation mechanism. The latter was determined by CellEvent™ green pan caspase activation marker. It consists of nucleic acid binding dye coupled to a fluorescence quenching peptide. In healthy cells CellEvent™ can be freely taken up but is not fluorescent. But if caspases 3/7 or 8 are present in the cell, quenching peptide is cleaved, the dye binds to DNA in the nuclei and displays bright green fluorescence. In this way, early apoptosis could be detected and quantified by image analysis tools. Moreover, the assay itself is not toxic to the cells and could be monitored continuously over time with live imaging (**Figure 7, Supplementary information, movies 1 and 2**).

Even though the ML1 uptake and translocation towards retrograde Golgi transport were very fast (minutes to hours), the caspase mediated apoptosis activation was detectable much later, after at least one day (**Figure 7, Supplementary movies 1 and 2**). The total cell number was visibly lower in ML1 treated cells indicating not only pro-apoptotic but also anti-proliferative activity of ML1 (**Figure 7, A**). In the literature ML1 was shown to activate apoptosis

though various pathways such as TNF-α induction, external caspase 8 activation as well as Bax and Bad proteins translocation to the mitochondria53.

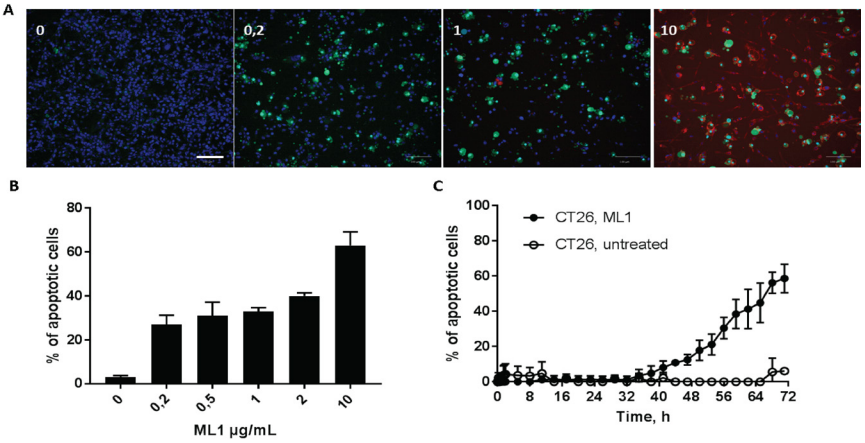

Figure 7. A. Confocal images of apoptosis in CT 26 cells after 71 h incubation with ML1 at different concentrations; nuclei are stained in blue, apoptotic cells in green (CellEvent® live staining), ML1 in red; size bar 100 µm. B. CT 26 cell viability after 71 h incubation with different concentrations of ML1; C. Percentage of apoptotic cells at different time points during incubation with 10 µg/mL of ML1.

The anti-proliferative activity of ML1 was investigated in additional cell lines (**Figure 8A**). Interestingly, the IC_{50} of studied murine cancerous cell lines was 3.5 to 100-fold lower compared to murine inflammatory cell line RAW264.7. These differences could be potentially attributed to variations in cell glycosylation patterns, which results in lower or higher sensitivity to ML1[26]. The altered glycosylation pattern was also shown to influence multidrug resistant tumor cell's sensitivity to ML1[26]. Experiments performed using a chemoresistant variant of the murine triple negative (TNBC) breast cancer cell line 4T1 are represented on **Fig 8A, B**. When compared to the reported values of doxorubicin[43], a standard chemotherapeutic for treatment of breast cancer patients, ML1 was 2x less affected by antineoplastic resistance (ML1 resistance index 6.9 vs 13.4 for doxorubicin). Furthermore, ML1 is almost 4 orders of magnitude more cytotoxic than doxorubicin in the chemo-sensitive cell line (IC_{50}: ML1 1.4 ng/ml in **Figure 8 A**, as compared to doxorubicin 24000 ng/ml reported by Chen et al[43]). Real-time apoptosis imaging revealed a very similar pattern to the one observed for CT26 cells (**Figure 8C**). The slightly higher spontaneous apoptosis rate in non-treated chemoresistant 4T1 cells may be due to increased expression levels of caspases or nonspecific proteases that will generate false positive signals in the CellEvent™ assay (**Supplementary**

information, movies 3 and 4). Nevertheless, the subtraction of spontaneous caspase activation in non-treated 4T1 Res cells from ML1 incubated still gives the net increase in apoptosis rate of around 60%, which is comparable to 53% for CT26 cells reported **Figure 7C**. Even though the IC_{50} of sensitive and drug resistant cells was different, the ML1 uptake profile and its co-localization with cell organelles were very similar for both cell lines (**Supplementary information, Figure S7**).

A

Cell line	CT26	RAW 264.7	4T1	4T1-Res
IC50 (ML1 ng/mL)	36.6	128.7	1.3	9.4

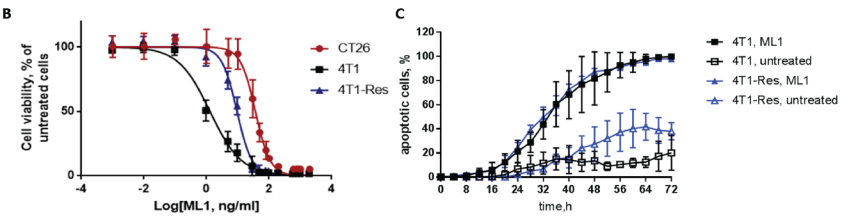

Figure 8. A. Comparative cytotoxicity of ML1 in different cell lines. B. IC_{50} curves for CT26, 4T1 parental and 4T1 Dox Resistant cell lines; C. Percentage of apoptotic cells at different time points during incubation of 4T1 parental and 4T1 Dox Resistant with 200 μg/mL of ML1. Non-treated cells were used as negative control.

Conclusions

The present study clearly demonstrated crucial steps for the uptake of isolated ML1: i. glycan binding on the cell surface; ii. clathrin-dependent and -independent endocytosis; iii. redirection of the protein from endocytic vesicles to Golgi network and presumably its subsequent retrograde transport to the ER. These steps are crucial for the protein to reach its molecular target in the cytosol and ensure anti-proliferative and pro-apoptotic activity. In this context, ML1 is a potential cytotoxin which can be applied for eradication of multidrug resistant tumor cells which respond poorly to anticancer drugs that are transported via ABC transporters (including P-glycoprotein [P-gp] and multi-drug resistance proteins). While those mechanisms alter the performance of conventional chemotherapeutic drugs (taxanes, platinum drugs etc.), ML1 might overcome the resistance due to a specific uptake pathway, subcellular processing and sorting.

Materials and Methods

Materials

All cell labeling reagents and fluorescent dyes were purchased from Thermo Fisher Scientific, Naarden, The Netherlands unless stated otherwise. Cell medium and supplements were from GibcoBRL, Thermo Fisher Scientific, Naarden, The Netherlands.

Methods

1. Purification and characterization of Mistletoe lectin I.

For ML1 isolation, mistletoe plant material was harvested in June from ash tree (Fraxinus excelsior L.) and extraction was performed by affinity chromatography as described previously41, using the affinity of ML1 for D-galactose. After purification, ML-1 was characterized by FPLC using a Mono S cation exchange column (Pharmacia/GE Healthcare, Uppsala, Sweden) and a 0.6M NaCl salt gradient in 0.015M citrate buffer (pH 4.0) at a detection wavelength of 280 nm (**Supplementary information, Figure S1 A**). Further characterization was performed by non-denaturing and denaturing SDS-PAGE to confirm the size of native ML-1, and presence of the A and B chains (12% PAA, 1h at 160V, LMW SDS Marker; GE Healthcare, Munich, Germany). For non-denaturing SDS-PAGE, ML was pretreated with saturated iodoacetamide solution (1:2) for 30 min at RT to prevent autolytic cleavage of the single disulfide bond which covalently links A and B chains. Gels were stained using Coomassie blue (**Supplementary information, Figure S1 B**). ML-1 was quantified at 280 nm using an extinction coefficient of 1.41 and by ELISA using monoclonal (5F5) and POD-labelled polyclonal (5H8) anti-ML A chain antibodies (Sifin Diagnostics GmbH, Berlin, Germany).

1.1 ML1 fluorescent tagging

ML1 conjugation to Alexa Fluor 647 (AF647) succinimidyl ester was performed in accordance to manufacturer protocol. In brief, the protein was dissolved in PBS buffer at 5.6 mg/mL and then diluted with 0.02 M bicarbonate buffer (2000+250µL) to ensure basic pH. The 2250µL of diluted protein were added to aliquoted dye (100 µg) diluted in 20 µL of anhydrous DMSO. The mixture (protein to dye molar ratio – 1:5) was stirred at room temperature for 1h. The protein-dye conjugate was purified with a PD10 size exclusion column and then analyzed with GPC (Bio Sep 3000 column, 20 min, PBS 1mL/min). The labeled protein stock solution was filtered through 0.45 µm syringe filter and protein concentration was quantified by absorbance at 280 nm with NanoDrop® spectrophotometer (Isogen Life Sciences B.V., Utrecht, The Netherlands).

2. Cell culture

The murine colon carcinoma cells (CT26 WT) were obtained from American Type Culture Collection (ATCC) and cultured in RPMI-1640 medium (Sigma Aldrich) supplemented with 10% FBS (Sigma Aldrich). The murine breast cancer cells (4T1) – mother and doxorubicin resistant cell lines were kindly provided by Prof. Twan Lammers from Uniklinik RWTH Aachen, Germany and cultured in RPMI-1640 medium (Sigma Aldrich) supplemented with 10% FBS (Sigma Aldrich). The murine macrophages (RAW 264.7) were also obtained from ATCC and cultured in DMEM (Sigma Aldrich) supplemented with 10% FBS (Sigma Aldrich). All cells were maintained at 37°C in a 5% CO2 and humidified atmosphere.

2.1 Organelle labeling

All subcellular structures labeling was performed according to the manufacturer instructions. For the nuclei staining, the cells were incubated with 10 nM Hoechst 33342 in PBS for 10 min at 37°C. Lysosomes were stained with 75 nM LysoTracker Green solution in PBS for 30 min at 37°C. Endosomes were labeled with pHrodo Green Dextran conjugate diluted in complete growth medium to a final concentration of 0.05 mg/mL for 20 min at 37°C. For Golgi staining cells were first incubated on ice with cold solution of BODIPY® TR C5 -ceramide complexed to BSA at final concentration of 5 μM, then washed with cold PBS and incubated with fresh medium for further 30 min at 37°C. Summarized table of all used cell markers is presented in **Supplementary Information, Table S1**.

2.2 ML1 uptake

Cells were seeded into 96-well μClear® black plates (Greiner, 10000 cells/ well) and incubated overnight. Then, medium was replaced with fresh complete medium and appropriate amount ML1-AF647 conjugate (ML1, from 0.0002 to 20 μg/mL) was added. For live imaging experiments the cells were placed in the microscope and imaged immediately with CV7000s and then as often and as long as it was required for a particular experiment. For endpoint imaging, the cells were incubated with ML1 for desired time, then washed with PBS and fixed with 10 % formaldehyde solution (30 min at room temperature). The uptake at low temperatures was performed with pre-cooled cells (15 min at 4^0 C), cold medium and PBS. The cells were incubated with cold solution of ML1 (10 μg/mL) for 1 hour, then washed and fixed with 10 % formaldehyde solution as described above.

2.3 WGA and cholera toxin subunit b uptake

Cells were seeded into 96-well μClear® black plates (Greiner, 10000 cells/ well) and incubated overnight. The medium was replaced with fresh complete me-

dium and Wheat Germ Agglutinin Oregon green or Cholera toxin subunit b. Alexa Fluor 488 conjugates were added to the cells to a final concentration of 5 and 10 μg/mL, respectively. In co-localization experiments 10 μg/mL of ML1-AF647 conjugates were added to the cells as well. The cells were imaged immediately with CV7000s.

2.4 Inhibition of ML1 endocytosis

For the uptake inhibition experiments cells were seeded into 96-well μClear® black plates (Greiner, 10000 cells/ well) and incubated overnight. Next day the medium was replaced with fresh full growth medium containing appropriate concentration of the inhibitor and cells were pre-incubated for 15-30 min (galactose 10-100 mM, sucrose 0,4 M, chlorpromazine 12.5-100 μM, methyl-β-cyclodextrin 10-250 mM). Then 10 μg/mL of ML1-AF647 conjugates were added to the cells and after 1 h incubation cells were imaged with CV7000s and ML1 uptake was quantified. Non-treated cells were used as positive uptake control. For the low temperature experiments, cells were first washed with ice-cold medium, pre-incubated 15 min at 4^0 C and then incubated with 10 μg/mL of ML1-AF647 conjugates at 4^0 C for 1 h. After incubation, cells were washed twice with ice-cold PBS and fixed with 4 % PFA solution (10 min at room temperature). After fixation, cells were washed twice with PBS and imaged with CV7000s. The same procedure was performed for the control plate that was incubated at 37^0 C. To facilitate subsequent image analysis, prior imaging cell nuclei were labeled with Hoechst 33342 as described above.

2.5 Endosomal pathways labeling with antibodies

Endosomal Marker Antibody Sampler Kit #12666 was purchased from Cell Signaling Technology Europe, B.V. (Leiden, The Netherlands) and used according to manufacturer instructions. Briefly, cells were seeded into 96-well μClear® black plates (Greiner, 10000 cells/ well) and incubated overnight. Then the medium was refreshed with full complete growth medium and 10 μg/mL of ML1-AF647 conjugates were added to the cells. After 2 h incubation cells were washed twice with PBS and fixed with 4 % PFA solution (10 min at room temperature). Cell nuclei were labeled with Hoechst 33342 as described above. Then cells were pre-incubated with blocking buffer (5 % FBS, 0,3 % Triton in PBS) for 1 h. Antibodies were diluted in antibody dilution buffer (1 % BSA, 0,3 % Triton in PBS) as following: anti-caveolin 1:400, anti-clathrin 1:50, anti-EEA1 1:100, anti-Rab5 1:200, anti-Rab7 1:100 and anti-Rab11 1:100. Cells were incubated with diluted antibodies overnight at 4^0 C, then washed 3 times with PBS and incubated with secondary antibody (Anti-Goat conjugated to Alexa Fluor 488, dilution 1:100) for 2 h at room temperature. Finally, cells were washed twice with PBS and imaged with CV7000s.

2.4 Cytotoxicity assays

Cells were seeded in 96 well plates (CT26 and 4T1 10000 cells/well; RAW264.7 5000 cells/well) and left to adhere for 24 h. Various concentrations of ML1 (2 µg/ml – 0.001 ng/ml) were incubated with cells for 48 h, after which cell survival was determined by MTS conversion (CellTiter 96® AQueous One Solution Cell Proliferation Assay) at 490 nm in a well plate reader. IC_{50} (the concentration of drug causing 50% reduction of the survival of the control) was calculated from the survival growth curves by fitting using GraphPad Prism software.

2.5 Apoptosis induction detection

To investigate the caspase-mediated pro-apoptotic activity of ML1 commercially available CellEvent™ caspase-3/7 Green Detection Reagent was used. Cells were seeded into 96-well µClear® black plates (Greiner, 10000 cells/well) and incubated overnight. First, cell nuclei were labeled with Hoechst 33342 as described above. 30 min before the experiment, cell medium was refreshed with full complete growth medium containing 10 µM of CellEvent™ Caspase-3/7 Green Detection Reagent. Then various concentrations of ML1-AF647 conjugates (200-0.0002 µg/mL) were added. The cells were imaged immediately with CV7000s with images taken every 4 h for up to 72h in total.

3. Image analysis

Customized image analysis protocols were developed with Columbus Software (U.S. National Institutes of Health, Bethesda, Maryland, USA).

Acknowledgements

This work was supported by the People Program (Marie Curie Actions) of the European Union's Seventh Framework Program FP7/2007–2013/ under REA grant agreement n° 324275 (project acronym: decent AID).

Contributions

N.B., E.M. G.L. and R.J.K designed the study. C.H. isolated the mistletoe lectin. M.B.C.dM. performed mistletoe lectin labeling and viability experiments. N.B. performed live-cell confocal imaging experiments, fixed cell experiments, antibody staining and optimized image analysis protocols. J.W. contributed to image analysis. E.H. contributed to viability studies. N.B. and M.B.C.dM wrote the manuscript. All authors discussed the results and commented on the manuscript.

References

[1] Pizzo, E. & Di Maro, A. A new age for biomedical applications of Ribosome Inactivating Proteins (RIPs): from bioconjugate to nanoconstructs. J. Biomed. Sci. 23, 54 (2016).
[2] Stirpe, F. Ribosome-inactivating proteins: From toxins to useful proteins. Toxicon 67, 12–16 (2013).
[3] de Virgilio, M., Lombardi, A., Caliandro, R. & Fabbrini, M. S. Ribosome-inactivating proteins: from plant defense to tumor attack. Toxins 2, 2699–2737 (2010).
[4] Zeng, M. et al. Anti-tumor activities and apoptotic mechanism of ribosome-inactivating proteins. Chin. J. Cancer 34, 325–334 (2015).
[5] Bolognesi, A., Bortolotti, M., Maiello, S., Battelli, M. G. & Polito, L. Ribosome-Inactivating Proteins from Plants: A Historical Overview. Mol. Basel Switz. 21, (2016).
[6] Das, M. K., Sharma, R. S. & Mishra, V. Induction of apoptosis by ribosome inactivating proteins: Importance of N-glycosidase activity. Appl. Biochem. Biotechnol. 166, 1552–1561 (2012).
[7] Barbieri, L. et al. Enzymatic activity of toxic and non-toxic type 2 ribosome-inactivating proteins. FEBS Lett. 563, 219–222 (2004).
[8] Narayanan, S., Surendranath, K., Bora, N., Surolia, A. & Karande, A. A. Ribosome inactivating proteins and apoptosis. FEBS Lett. 579, 1324–1331 (2005).
[9] Walsh, M. J., Dodd, J. E. & Hautbergue, G. M. Ribosome-inactivating proteins: potent poisons and molecular tools. Virulence 4, 774–84 (2013).
[10] Puri, M., Kaur, I., Perugini, M. a. & Gupta, R. C. Ribosome-inactivating proteins: Current status and biomedical applications. Drug Discov. Today 17, 774–783 (2012).
[11] Cummings, R. D. & Etzler, M. E. Chapter 28 R-type Lectins. 1–15 (2014).
[12] Marvibaigi, M., Supriyanto, E., Amini, N., Abdul Majid, F. A. & Jaganathan, S. K. Preclinical and clinical effects of mistletoe against breast cancer. BioMed Res. Int. 2014, 785479 (2014).
[13] Kienle, G. S. & Kiene, H. Complementary cancer therapy: a systematic review of prospective clinical trials on anthroposophic mistletoe extracts. Eur. J. Med. Res. 12, 103–119 (2007).
[14] Maletzki, C., Linnebacher, M., Savai, R. & Hobohm, U. Mistletoe lectin has a shiga toxin-like structure and should be combined with other Toll-like receptor ligands in cancer therapy. Cancer Immunol. Immunother. 62, 1283–1292 (2013).
[15] Park, H. J. et al. TLR4-mediated activation of mouse macrophages by Korean mistletoe lectin-C (KML-C). Biochem. Biophys. Res. Commun. 396, 721–725 (2010).
[16] Kim, J. J. et al. Enhanced dendritic cell maturation by the B-chain of Korean mistletoe lectin (KML-B), a novel TLR4 agonist. Int. Immunopharmacol. 21, 309–319 (2014).
[17] Lee, J. Y. et al. In vitro immunoregulatory effects of Korean mistletoe lectin on functional activation of monocytic and macrophage-like cells. Biol. Pharm. Bull. 30, 2043–2051 (2007).
[18] Khil, L. Y. et al. Mechanisms involved in Korean mistletoe lectin-induced apoptosis of cancer cells. World J. Gastroenterol. 13, 2811–2818 (2007).
[19] Lee, C. H., Kim, J. K., Kim, H. Y., Park, S. M. & Lee, S. M. Immunomodulating effects of Korean mistletoe lectin in vitro and in vivo. Int. Immunopharmacol. 9, 1555–1561 (2009).
[20] Pevzner, I. B. et al. Differences in amino acid sequences of mistletoe lectin I and III B-subunits determining carbohydrate binding specificity. Biochim. Biophys. Acta - Gen. Subj. 1675, 155–164 (2004).
[21] Elsässer-Beile, U., Voss, M., Schühle, R. & Wetterauer, U. Biological effects of natural and recombinant mistletoe lectin and an aqueous mistletoe extract on human monocytes and lymphocytes in vitro. J. Clin. Lab. Anal. 14, 255–259 (2000).
[22] Boneberg, E. M. & Hartung, T. Mistletoe lectin-1 increases tumor necrosis factor-alpha release in lipopolysaccharide-stimulated whole blood via inhibition of interleukin-10 production. J. Pharmacol. Exp. Ther. 298, 996–1000 (2001).
[23] Lee, A. L. Z. et al. Efficient intracellular delivery of functional proteins using cationic polymer core/shell nanoparticles. Biomaterials 29, 1224–1232 (2008).
[24] Yau, T., Dan, X., Ng, C. C. W. & Ng, T. B. Lectins with Potential for Anti-Cancer Therapy. Mol-

ecules 20, 3791–3810 (2015).
[25] Hong, C. E., Park, A. K. & Lyu, S. Y. Synergistic anticancer effects of lectin and doxorubicin in breast cancer cells. Mol. Cell. Biochem. 394, 225–235 (2014).
[26] Valentiner, U., Pfüller, U., Baum, C. & Schumacher, U. The cytotoxic effect of mistletoe lectins I, II and III on sensitive and multidrug resistant human colon cancer cell lines in vitro. Toxicology 171, 187–199 (2002).
[27] Hildebrandt, E. et al. Liposomal formulations of mistletoe produced by centrifugal technologies and cell proliferation analysis of both mistletoe extracts and isolated mistletoe lectin I = Liposomale Formulierung von Mistelextrakten durch Zentrifugationsverfahren und Analyse der Zellproliferation von Gesamtextrakten und isoliertem Mistellektin I. Mistel Tumortherapie 4 AktuellerStand Forsch. Klin. Anwend. Hrsg R Scheer (2016).
[28] Lenartz, D., Dott, U., Menzel, J., Schierholz, J. M. & Beuth, J. Survival of glioma patients after complementary treatment with galactoside-specific lectin from mistletoe. Anticancer Res. 20, 2073—2076 (2000).
[29] Mabed, M., El-Helw, L. & Shamaa, S. Phase II study of viscum fraxini-2 in patients with advanced hepatocellular carcinoma. Br. J. Cancer 90, 65–69 (2004).
[30] Tröger, W. et al. Viscum album [L.] extract therapy in patients with locally advanced or metastatic pancreatic cancer: a randomised clinical trial on overall survival. Eur. J. Cancer Oxf. Engl. 1990 49, 3788–3797 (2013).
[31] Timoshenko, a. V., Lan, Y., Gabius, H. J. & Lala, P. K. Immunotherapy of C3H/HeJ mammary adenocarcinoma with interleukin-2, mistletoe lectin or their combination: Effects on tumour growth, capillary leakage and nitric oxide (NO) production. Eur. J. Cancer 37, 1910–1920 (2001).
[32] Timoshenko, a. V., Gorudko, I. V., André, S. & Gabius, H. J. Cell-type dependence of stability modulation of lectin-initiated contacts by impairment of multivalent carbohydrate binding and intracellular signaling. Biosci. Rep. 20, 199–209 (2000).
[33] Hajto, T., Hostanska, K., Frei, K., Rordorf, C. & Gabius, H. J. Increased secretion of tumor necrosis factors alpha, interleukin 1, and interleukin 6 by human mononuclear cells exposed to beta-galactoside-specific lectin from clinically applied mistletoe extract. Cancer Res. 50, 3322–3326 (1990).
[34] Thies, A., Nugel, D., Pfüller, U., Moll, I. & Schumacher, U. Influence of mistletoe lectins and cytokines induced by them on cell proliferation of human melanoma cells in vitro. Toxicology 207, 105–116 (2005).
[35] Sandvig, K. & van Deurs, B. Endocytosis and intracellular sorting of ricin and Shiga toxin. FEBS Lett. 346, 99–102 (1994).
[36] Moisenovich, M., Agapov, I., Marx, U., Bereiter-Hahn, J. & Tonevitsky, A. Intracellular transport of plant toxins ricin and viscumin from different plasma membrane sites. Arzneimittelforschung. 53, 470–475 (2003).
[37] Spooner, R. A. & Lord, J. M. Ricin Trafficking in Cells. Toxins 7, 49–65 (2015).
[38] Mulsow, K. et al. Impact of Mistletoe Triterpene Acids on the Uptake of Mistletoe Lectin by Cultured Tumor Cells. PLOS ONE 11, e0153825 (2016).
[39] Pohl, P. et al. Membrane fusion mediated by ricin and viscumin. Biochim. Biophys. Acta 1371, 11–16 (1998).
[40] Sweeney, E. C. et al. Mistletoe lectin I forms a double trefoil structure. FEBS Lett. 431, 367–370 (1998).
[41] Eifler, R., Pfuller, K., Gockeritz, W. & Pfuller, U. Improved procedures for isolation of mistletoe lectins and treir subunits: lectin pattern of th Eropean Mistletoe. Lectins Biol. Biochem. Clin. Biochem. 9, (1993).
[42] Adler, J. & Parmryd, I. Quantifying colocalization by correlation: the Pearson correlation coefficient is superior to the Mander's overlap coefficient. Cytom. Part J. Int. Soc. Anal. Cytol. 77, 733–742 (2010).
[43] Chen, Y. et al. Overcoming multidrug resistance using folate receptor-targeted and pH-responsive polymeric nanogels containing covalently entrapped doxorubicin. Nanoscale 9, 10404–10419 (2017).
[44] Zinchuk, V. & Grossenbacher-Zinchuk, O. Recent advances in quantitative colocalization analysis: Focus on neuroscience. Prog. Histochem. Cytochem. 44, 125–172 (2009).
[45] S. Coulibaly, F. & C. Youan, B.-B. Current status of lectin-based cancer diagnosis and therapy.

AIMS Mol. Sci. 4, 1–27 (2017).
[46] Chinnapen, D. J.-F., Chinnapen, H., Saslowsky, D. & Lencer, W. I. Rafting with cholera toxin: endocytosis and tra/cking from plasma membrane to ER. FEMS Microbiol. Lett. 266, 129–137 (2007).
[47] Mayor, S. & Pagano, R. E. Pathways of clathrin-independent endocytosis. Nat. Rev. Mol. Cell Biol. 8, 603–612 (2007).
[48] Frantz, M., Jung, M. L., Ribereau-Gayon, G. & Anton, R. Modulation of mistletoe (Viscum album L.) lectins cytotoxicity by carbohydrates and serum glycoproteins. Arzneimittelforschung. 50, 471–478 (2000).
[49] Vercauteren, D. et al. The Use of Inhibitors to Study Endocytic Pathways of Gene Carriers: Optimization and Pitfalls. Mol. Ther. 18, 561–569 (2010).
[50] Sandvig, K. & Van Deurs, B. Transport of protein toxins into cells: Pathways used by ricin, cholera toxin and Shiga toxin. FEBS Lett. 529, 49–53 (2002).
[51] Day, P. J., Pinheiro, T. J. T., Roberts, L. M. & Lord, J. M. Binding of Ricin A-Chain to Negatively Charged Phospholipid Vesicles Leads to Protein Structural Changes and Destabilizes the Lipid Bilayer. Biochemistry (Mosc.) 41, 2836–2843 (2002).
[52] Sun, J. et al. Membrane destabilization by ricin. Eur. Biophys. J. 33, 572–579
[53] Fu, L.-L. et al. Plant lectins: Targeting programmed cell death pathways as antitumor agents. Int. J. Biochem. Cell Biol. 43, 1442–1449 (2011).

Supplementary information

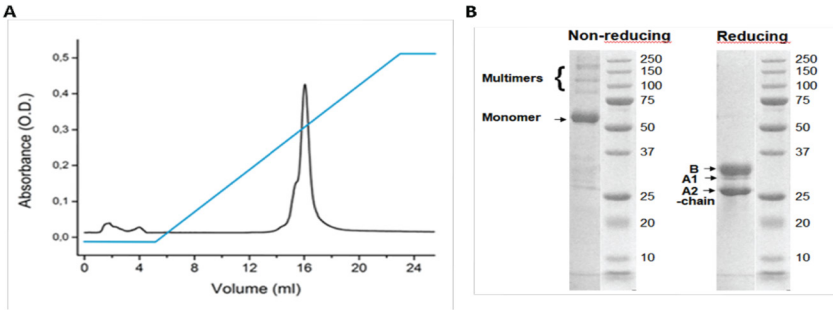

Figure S1 A. FPLC elution profile for ML1 (0.6M NaCl gradient). The main peak represents purified ML1 cytotoxin, with a small left shoulder comprising the variant (A1) of the apoptotic A chain typical for winter mistletoe harvest. B. SDS-PAGE analysis of ML1 under non-reducing and reducing conditions. Monomer ML-1 and multimers of ML-1 are observed under non-reducing conditions. Disruption of disulfide bonds under reducing SDS-PAGE conditions separates the covalently linked A and B chain of ML-1 into 26 kDa and 30 kDa fragments, respectively. A third band was detected at 29 kDa, which is a variant (A1) of the A chain found in winter harvests of the mistletoe plant.

Figure S2. Comparative cytotoxicity of native and Alexa Fluor 647 labeled ML1. Respective IC50 values are 36,6 and 33,2 ng/mL.

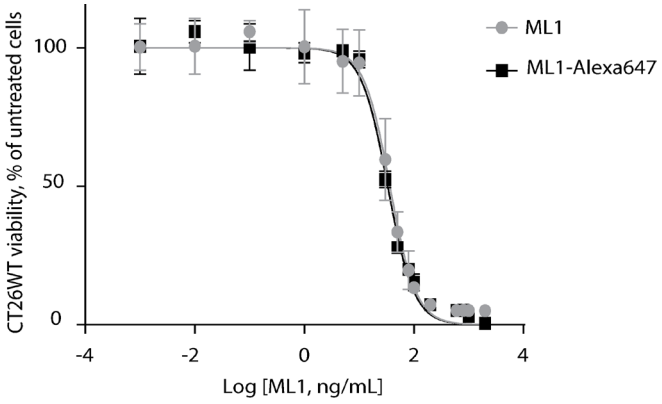

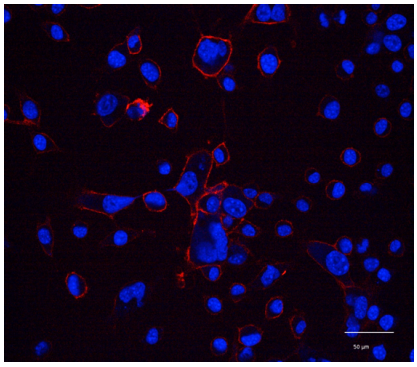

Figure S3. Confocal image of CT26 cells incubated with ML1 at 4^0C for 1h (10 μg/mL). Nuclei are stained in blue; size bar – 50 μm.

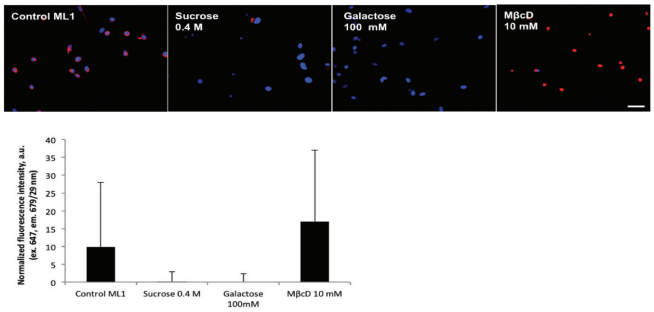

Figure S4. Confocal images of CT26 cells pre-incubated with uptake inhibitors and then incubated with ML1 for 2h (10 μg/mL) (up); Average ML1 fluorescence (n=4) in the cells quantified with Columbus suite software and normalized by subtraction of baseline cell fluorescence; nuclei are stained in blue, ML1 – red; size bar 50 μm.

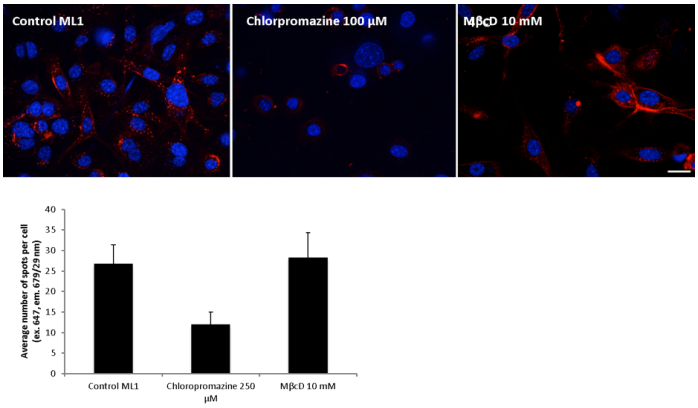

Figure S5. Confocal images of CT26 cells pre-incubated with uptake inhibitors and then incubated with ML1 for 1h (10 µg/mL) (up); Average number of spots per cell (n=3) quantified with Columbus suite software; nuclei are stained in blue, ML1 – red; size bar 20 µm.

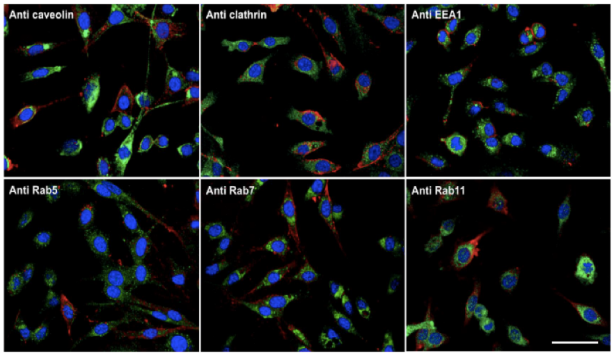

Figure S6. Confocal images of ML1 uptake (10 µg/mL, 2h) and co-staining with endo-lysosomal pathway specific antibodies; nuclei are stained in blue, ML1 – red, secondary antibody (Anti-Goat conjugated to Alexa Fluor 488) - green; size bar 50 µm.

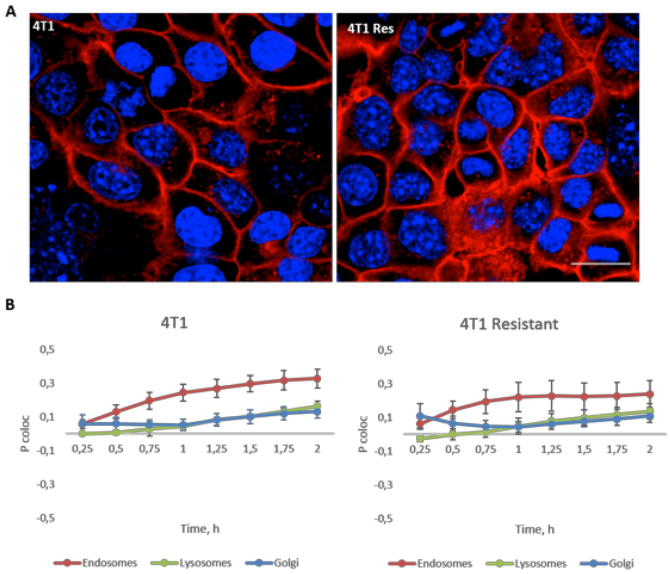

Figure S7. A. Confocal images of ML1 uptake in 4T1 control and doxorubicin resistant cells at 30 min incubation with 10 μg/mL ML1; nuclei are stained in blue, ML1 – red; size bar 20 μm.; B. Pearson correlation coefficient dynamics of co-localization ML1 with endosomes, lysosomes and Golgi in 4T1 mother and resistant cells.

Supplementary movies (available online):
1 and 2: Time-lapse movies of ML1 induced apoptosis in CT26 cells (1) or untreated CT26 cells in the same experiment (2); nuclei are stained in blue, apoptotic cells in green (CellEvent® live staining), ML1 in red, magnification 60x. The first 8 frames of each movie are taken every 15 min for 2h and the rest 24 frames every 3 hours up to 72h.
3 and 4: Time-lapse movies of ML1 induced apoptosis in 4T1 Res cells (3) or untreated 4T1 Res cells in the same experiment (2); nuclei are stained in blue, apoptotic cells in green (CellEvent® live staining), ML1 in red, magnification 40x. In total 18 frames are taken with imaging every 4 hours up to 72h.

Table S1. Summary of fluorescent labels used for various experiments with living or fixed cells.

Target	**Live-cell experiments***	**Fixed cells experiments**
Nuclei	Hoechst 33342	Hoechst 33342
Lysosomes	LysoTracker Green	Anti-Rab11†
Golgi	BODIPY TR C5 -ceramide complexed to BSA	-
Endosomes early	pHrodo Green Dextran conjugate	Anti-EEA1, Anti-Rab5
Endosomes late	-	Anti-Rab7
Cell membrane/		
protein transport	Wheat Germ Agglutinin Oregon Green conjugate	-
Caveolin-mediated uptake	Cholera toxin subunit b Alexa Fluor 488 conjugate	Anti-caveolin
Clathrin-mediated uptake	-	Anti-clathrin
Apoptotic cells	CellEvent caspase-3/7 Green Detection Reagent	CellEvent caspase-3/7 Green Detection Reagent

* All live cell labeling reagents and fluorescent dyes were purchased from Thermo Fisher Scientific, Naarden, The Netherlands.
† Endosomal Marker Antibody Sampler Kit #12666 was purchased from Cell Signaling Technology Europe, B.V., Leiden, The Netherlands.

Part III | Efficient macromolecule delivery by triggered release

Chapter 4 -Thermosensitive liposomes for triggered release of cytotoxic proteins

Maria B. C. de Matos, Nataliia Beztsinna, Christoph Heyder, Marcel Fens, Enrico Mastrobattista, Raymond Schiffelers, Gero Leneweit, Robbert Jan Kok

European Journal of Pharmaceutics and Biopharmaceutics (2018)

DOI: 10.1016/j.ejpb.2018.09.010

Abstract

Lysolipid-containing thermosensitive liposomes (LTSL) are clinically-relevant drug nanocarriers which have been used to deliver small molecule cytostatics to tumors in combination with local hyperthermia (42 °C) to trigger local drug release. The objective of this study was to investigate the feasibility of LTSL for encapsulation and triggered release of macromolecular drugs such as plant-derived cytotoxins. As therapeutic protein, we used Mistletoe lectin-1 (ML1) - a ribosome-inactivating protein with potent cytotoxic activity in tumor cells.
Model macromolecules (dextrans, albumin) and ML1 were encapsulated in small unilamellar LTSL with varying lipid compositions by the thin film hydration method and extrusion. LTSLs showed molecular weight dependent heat-triggered release of the loaded cargo. The most promising composition, ML1 formulated in LTSL composed of 86:10:4 %mol DPPC:MSPC:DSPE-PEG2000, was further studied for bioactivity against murine CT26 colon carcinoma cells. Confocal live-cell imaging showed uptake of released ML1 after mild hyperthermia at 42 °C, subsequently leading to potent cytotoxicity by LTSL-ML1. Our study shows that LTSL in combination with localized hyperthermia hold promise as local tumor delivery strategy for macromolecular cytotoxins.

Keywords: Lysolipid-containing thermosensitive liposomes; hyperthermia; triggered drug release; macromolecule encapsulation and release; live-cell imaging

1. Introduction

Over the past decades, nanomedicines have gained attention as targeted formulations for cancer therapy. Due to the leakiness of tumor blood vessels and impaired lymphatic system, long-circulating nanoparticles such as PEGylated liposomes extravasate and accumulate in tumors, a phenomenon described as the enhanced permeability and retention (EPR) effect [1]. A more recent development in the nanomedicine field are nanocarrier systems that can be triggered with an external stimulus like heat, light or ultrasound [2–7]. Triggerable nanocarrier systems are especially interesting for cancer therapy, as they allow local controlled drug release thus limiting the toxicity of the payload to normal tissues and intensifying the peak concentrations of the active compounds within the tumor [2,8–14]. Lysolipid containing thermosensitive liposomes (LTSL), like the ThermoDox® formulation, are a well-studied example. They have shown superior activity in progression-free survival as well as in overall survival in clinical trials [14].

When thermosensitive liposomes are exposed to heating, the lipid bilayer undergoes a melting phase transition from a gel to a liquid-crystalline phase, allowing a rapid increase in bilayer permeability and thus rapid release of small solutes. The exact temperature and broadness of the phase transition depend on the lipid composition and can be adjusted to clinically relevant mild-hyperthermia temperatures (39-43 °C) [2,12,15]. The increased bilayer permeability in ThermoDox®, compared with traditional thermosensitive liposomes, relies on the inclusion of the lysolipid 1-stearoyl-2-hydroxy-sn-glycero-3-phosphatidylcholine (MSPC or Lyso-PC) in a 1,2-dipalmitoyl-sn-glycero-3-phosphocholine (DPPC) and N-(carbonyl-methoxypolyethyleneglycol2000)-1,2-distearoyl-sn-glycero-3-phosphoethanolamine (mPEG2000-DSPE) (10:86:4 molar ratio, respectively).

Up to now, thermosensitive liposomes have been mainly used for the encapsulation and triggered release of small molecule drugs like doxorubicin, cisplatin, taxol, melphalan, methotrexate, plumbagin, dacarbazine, mitomycin C, TNF-α and paclitaxel [7,8,10,15–21]. Encapsulation of macromolecular drugs in LTSL may seem counterintuitive, as they may not be released from this type of nanocarriers upon changes in bilayer fluidity. Still, a few examples of LTSL loaded with macromolecules exist. They report successful, though incomplete, release under mild hyperthermia [22,23]. We now report on LTSL-encapsulation of mistletoe lectin I (ML1), a potent cytotoxin that is one of the main active components of Viscum album extracts used as an adjuvant in complementary medicine practices [24,25]. Combining LTSL/intratumoral

triggered release with the potent cytotoxins can be promising for cancer treatment.

Mistletoe lectin-I belongs to the class of plant derived ribosome inactivating proteins (of class II, RIP-II) which interfere in protein biosynthesis via their rRNA N-glycosidase activity. The cytotoxic activity has been ascribed to the A-chain, which is linked to the B-chain that binds to cell-surface expressed receptors on target cells and hence mediates internalization of the RIP-II protein [26–30]. ML1 displays very fast binding to sugar residues on the cell membrane and its endocytosis involves both clathrin-dependent and -independent pathways [31]. ML1 is then transported from early endocytic vesicles to Golgi network and in a retrograde way to the endoplasmic reticulum, where it inactivates the ribosomes, leading to the disruption of protein biosynthesis, and eventually cell death [26–30]. RIP-II glycoproteins and plant extracts containing these cytotoxins have also been associated with activation of the immune system, which serves as alternative mechanism of anticancer activity. [29,30]

Intratumoral delivery and on-site release via thermosensitive liposomes seems an attractive strategy to improve the therapeutic window of ML1 and similar cytotoxins. We therefore explored the encapsulation and hyperthermia triggered release of model macromolecules and ML1. Our final obtained formulation showed good storage stability and stability at conditions reflecting the circulation of liposomes in the blood stream, while triggered release was induced by mild hyperthermia of 42 °C. Functional bioactivity of ML1 released from hyperthermia-triggered LTSL was studied by live-cell confocal fluorescence imaging and cell viability assays, demonstrating uptake of released ML1 by tumor cells and subsequent cytotoxic activity.

2. Materials and methods

2.1. Chemicals

The phospholipids 1,2-dipalmitoyl-sn-glycero-3-phosphocholine (DPPC), and 1,2- distearoyl-sn-glycero-3-phosphoethanolamine-N-PEG2000 (DSPE-PEG2000) were purchased from Lipoid (Ludwigshafen, Germany). 1-stearoyl-2-hydroxy-sn-glycero-3-phosphocholine (MSPC) were purchased from Avanti Polar Lipid Inc (Alabaster, USA). FITC labelled BSA and Dextran 4000 Da were obtained from Sigma Aldrich (Zwijndrecht, Netherlands), while FITC labelled Dextran 10000 Da was purchased from Nanocs (New York, USA). Isolated Mistletoe Lectin-1 and control standard for ELISA (4.5 µg/ml) were isolated according to the protocols provided by Eifler et al. [32]. Anti-ML-A-5F5, and Anti-ML-A-5H8-POD monoclonal antibodies with specificity to ML1 A-chain were both obtained from SIFIN (Berlin, Germany). CellTiter

96® AQueous One Solution Cell Proliferation Assay (MTS) was provided by Promega (Leiden, The Nederlands). The lipophilic fluorescent dye 3,3'-dioctadecyloxacarbocyanine perchlorate ('DiO'; DiO-C18(3)) and Alexa Fluor® 647 succinimidyl ester (Alexa 647 NHS) were purchased from Invitrogen (Landsmeer, The Netherlands). Chemicals used in cell culture (RPMI, FBS, tripsin, PBS) were purchased from Sigma-Aldrich (Zwijndrecht, Netherlands). The murine colon carcinoma cell line CT26 was obtained from American Type Culture Collection (ATCC, Wesel, Germany).

2.2. Mistletoe lectin-1 isolation and characterization

For ML1 isolation, mistletoe plant material was harvested in June from ash tree (Fraxinus excelsior L.) and extraction was performed at ABNOBA GmbH by affinity chromatography as described previously [32], using the affinity of ML1 for D-galactose. After purification, ML1 was characterized by FPLC using a Mono S cation exchange column (Pharmacia/GE Healthcare, Uppsala, Sweden) and a0.6 M NaCl salt gradient in 0.015 M citrate buffer (pH 4.0) at a detection wavelength of 280 nm. For chromatograms, see [31].

2.2.1. SDS-PAGE

The identification of molecular weight of native ML1 was performed by non-reducing SDS-PAGE (50 min at 165 V). ML1 was pretreated with saturated iodoacetamide solution (1:2) for 30 min at room temperature to prevent autolytic cleavage of the disulfide bond which covalently links A and B chains. NuPAGE Bis-Tris Gels (12% polyacrylamide, Novex, Life Technologies) were stained using Coomassie blue.

2.2.2. Quantification by NanoDrop and ELISA

ML-1 was quantified by UV/Vis using NanoDrop ND-1000 (Thermo Fisher Scientific) at 280 nm using an extinction coefficient of 104850 $M^{-1}cm^{-1}$. ML1 was also experimentally quantified by sandwich ELISA. Briefly, the wells of a 96 well plate were coated with primary antibodies (9 µg/mL, bicarbonate buffer, Anti-ML-A-5F5, 100 µL per well) by incubating at room temperature for 30 min. Following three washes with PBS–Tween (each 100 µL), the plate was incubated for 30 min with ML1 samples and standards (each 100 µL/well). The plate was again washed with PBS-Tween buffer (3 × 100 µL/well). Then wells were coated with the secondary peroxidase antibodies Anti-ML-A-5H8 (10 µg/mL, 100 µL/well) and incubated at room temperature for 30 min. After PBS-Tween buffer wash, the plate was incubated with 100 µL/well of TBM substrate. Finally, the reaction was stopped by addition of 100 µL/well

1 M sulfuric acid. The yellow colored reaction product was detected at 450 nm with the spectrometric plate reader.

2.2.3. Labeling with AlexaFluor 647

ML1 conjugation to Alexa Fluor 647 (AF647) succinimidyl ester was performed in accordance to manufacturer's protocol. In brief, 250 µL of 0.02 M bicarbonate buffer pH 8.3 was added to 2 mL of ML1 5.6 mg/mL (12 mg, 0.2 µmol). The diluted protein was reacted with AF647 dye (5:1 dye:protein mol/mol; 100 µg/in 20 µl DMSO)20 5:1 dye: ML1 ratio) The mixture was stirred at room temperature for 1h and purified by size exclusion chromatography (PD10 disposable columns, GE Healthcare Life Sciences). Purified AF647-ML1 was characterized by analytical size-exclusion chromatography on a Bio Sep 3000 column, 20 min, PBS 1mL/min). The labeled ML1 was kept protected from the light at 4 °C until further use.

2.3. Preparation of LTSL

Liposomes with different lipid compositions (lipid molar ratio of DPPC/MSPC/DSPE-PEG2000 for LTSL5: 91/5/4; for LTSL10: 86/10/4; for LTSL15: 81/15/4) were prepared by the lipid film and extrusion. Typically, 250 µmol of lipids (and DiO at 0.5% mol of total lipid, for lipid bilayer labeling) were dissolved in 1:1 chloroform/methanol; and the organic solvents were evaporated for 20 min in the rotavapor (thin-film) at 60 °C. The films were kept for 1 hour in nitrogen stream and later hydrated at 50 °C with HBS (10 mM HEPES buffer with 0.9% w/v NaCl), with or without macromolecules dissolved. Lipid film formation and reconstitution, typically in 5 mL of buffer, resulted in a final lipid concentration of 50 mM. Extrusion was done 15 times over 400 and 100 nm pore-size polycarbonate filters at 50 °C. The lipid concentration of LTSL encapsulating ML1 was 50 mM, but the batch size was smaller (1 mL, 50 µmoL total lipid). When applicable, liposomes were separated from non-encapsulated cargo by ultracentrifugation (Beckmann ultracentrifuge, 3x, 55000 rpm 60 min 4 °C), and stored at 4 °C.

2.4. Characterization of LTSL

2.4.1. Size, polydispersity index, zeta potential

The hydrodynamic diameter and polydispersity index of all liposomes were measured by dynamic light scattering using a Malvern ALV/CGS-3 multiangle goniometer with He–Ne laser source (λ = 632.8 nm, 22 mW output power) under an angle of 90° (ALV, Langen, Germany). The zeta-potential of the liposomes was measured using laser Doppler electrophoresis on a Zetasizer

Nano-Z (Malvern Instruments) with samples dispersed in 10 mM HEPES buffer pH 7.4 (with no additional salts added).

2.4.2. Encapsulation efficiency

An aliquot of 50 µL of liposome suspension was diluted in 450 µL of HBS, to which TritonX-100 0.1% v/v was added to destroy the liposomes. The amount of encapsulated compound was determined by fluorometry (in the case of model compounds) or by ELISA (in the case of ML1, see above) and calculated as follows:

$$EE\% = \frac{total\ amount\ of\ payload\ in\ liposomes}{initial\ amount\ of\ payload} \times 100 \quad (1)$$

2.4.3. Storage stability

Storage stability of LTSL at 4 °C was extrapolated from size/PDI variations (using the same methods as presented above) and drug retention capacity over a period of 3 weeks. At each time point, an aliquot of liposomes suspension was separated from the free drug by means of ultrafiltration (Vivaspin 500 MWCO 300 000 Da). The flow-through was analyzed by fluorometry (in the case of model compounds) or by ELISA (in the case of ML1; see below) and calculated as:

$$Drug\ retention\ [\%] = \frac{payload_t}{payload_i} \times 100 \quad (2)$$

where $payload_t$ is mass of compound found outside (in the flow-through) the LTSL at a certain time point, $payload_i$ is the mass found inside the liposomes in the beginning of the experiment.

2.4.4. Differential Scanning Calorimetry

DSC was carried out to a have a better insight about the thermal properties of the LTSLs, for further studies of thermal-induced release, live-imaging with mild hyperthermia in cells. DSC measurements (DSC Discovery, TA Instruments, New Castle, USA) were carried out in duplicate, starting by equilibrating the samples and reference at 25 °C for 5 min and then ramping from 25 °C to 55°C, at 1 °C/min.

2.5. Release experiments

2.5.1. Temperature-dependent release

LTSL suspensions were incubated in preconditioned HBS (22, 37, 40 and 42°C) under stirring (300 rpm) in a thermomixer. After incubation at the designated temperature for 15 min, the samples were immediately transferred to

an ice bath to avoid further leakage. LTSL samples kept at 4 °C were considered as a blank and LTSL samples destroyed with TritonX-100 were considered as the 100 % release. Separation of released cargo from LTSL was done by ultrafiltration with Vivaspin columns and the flow-through was analyzed by fluorometry (model compounds) or ELISA (ML1) as described above.

2.5.2 Time-dependent release

Time-dependent release profiles of LTSLs were performed at 37°C and 42°C. LTSL suspensions were diluted in pre-heated HBS during fixed intervals (5, 10, 15, 30 min) under stirring (300 rpm) in a thermomixer. LTSL samples kept at 4 °C were considered as a blank and LTSL samples destroyed with TritonX-100 were considered as the 100 % release. Separation of released cargo from LTSL by Vivaspin ultrafiltration and analysis of labeled macromolecules (fluorometry) or ML1 (ELISA) was done as described above.
In all release experiments, the percent release of the compounds was quantified by using the equation:

$$Release\ \% = \frac{payload_t - payload_0}{payload_{triton} - payload_0} \times 100 \qquad (3)$$

where $payload_t$ is mass determined of compound at a certain time point or fixed temperature, $payload_0$ is the mass found outside the liposomes in the beginning of the experiment (typically zero) and $payload_{triton}$ is total mass found after liposomes were treated with Triton X-100.

2.6. Bioactivity of LTSL-ML1 under normothermia and mild hyperthermia conditions

Bioactivity of ML1 was studied using CT26 colon carcinoma cells, which are sensitive to ML1 at low nM ranges [31]. CT26 cells were culture in RPMI supplemented with 10 % FBS, at 37°C in a 5% CO_2 and humidified atmosphere. Two different heat treatment schedules were used to explore bioactivity of ML1. While the first approach demonstrates the functional activity of ML1 loaded in LTSL, the second approach simulated the hyperthermia treatment of tumor nodules in which ML1 is released from liposomes after intratumoral accumulation by EPR.
For all the experiments and for both experimental setups (see experimental details below), CT26 colon carcinoma cells were first seeded in 96-well plates (10000 cells/well) 24 h prior to the experiment. For live cell confocal imaging microscopy experiments, DiO' labeled liposomes loaded with AF647-labeled ML1 were used and nuclei of CT26 cells were prestained with Hoechst 33342.

Non-labeled ML1 and liposomes were used for cell-viability experiments and nuclei were not prestained with Hoechst 33342.

2.6.1. Heat-treatment schedules and ML1 bioactivity for setup 1

LTSL10-DiO' loaded with AF-647-labeled ML1 and control formulations as specified in the result section were diluted in OptiMEM (final concentrations 10 µg/mL AF647-ML-1 and 8 mM total lipid) and incubated for 1 h at 42°C (hyperthermia triggered media) or for 1 h at 37°C (normothermic media) in a pre-thermostated Eppendorf thermoshaker. The incubated media were then transferred without any separation/purification step onto CT26 cells kept at 37°C and previously stained with Hoechst 33342. Live cell images were taken for 4 h in a fluorescent confocal Yokogawa Cell Voyager CV7000s microscope (Tokyo, Japan).

To determine cytotoxic activity, ML1 formulated in LTSL10 or ML1 loaded in control PEG liposomes were diluted in OptiMEM to final concentration ranges of 0.3-10 µg/mL ML-1 (5-167 nM); corresponding to 0.2-8 mM total lipid. Spiked media were incubated for 1 h at 42 °C (hyperthermia triggered media) or for 1 h at 37 °C (normothermic control media) in a pre-thermostated Eppendorf thermoshaker. The preconditioned media were then transferred without any separation/purification step onto CT26 cells that were subsequently cultured at 37 °C under standard culture conditions (see above) for 4h. After the 4 h contact period, the drug containing media were refreshed with drug-free culture medium and cells were cultured for an additional 44h at 37 °C in the incubator. ML1 bioactivity was assessed by its effect on cell survival as assessed by MTS conversion (CellTiter 96® AQueous One Solution Cell Proliferation Assay) at 490 nm in a well plate reader. IC_{50} values of each treatment were calculated by non-linear curve fitting using GraphPad Prism software. OptiMEM spiked with ML1, empty LTSL10, and conventional liposomes (NTL, non-thermosensitive liposomes) loaded with ML1 were submitted to the same protocol and used as controls.

2.6.2. Heat-treatment schedules and ML1 bioactivity for setup 2

The second heat treatment schedule involved mild hyperthermia of CT26 cells in the presence of ML1-loaded LTSL treatment (42°C for 1h; versus normothermic conditions of 37°C for 1h), which was either effectuated directly in the microscope plate chamber (live cell imaging) or by incubating cells in a water bath (cell viability experiments). For live cell imaging, the CV7000s microscope plate chamber was heated to the desired temperature (37 °C or 42 °C). OptiMEM was spiked with AF647-labeled ML1 formulated in DiO'-

labeled LTSL (final concentration final concentrations 10 μg/mL AF647-ML-1 and 6 mM total lipid), after which media were pipetted onto the cells and well plates were transferred into the microscope plate chamber. Cellular uptake of ML1 was imaged by live-cell confocal microscopy for 1h at the stated temperatures. Confocal images were analyzed with Columbus® image analysis software (PerkinElmer) using automated segmentation protocols for nuclei and cytoplasm detection and build-in functionalities for average fluorescence intensity determination.
In a parallel experiment, OptiMEM was spiked with various concentrations of non-labeled ML1 formulated in LTSL10 (final concentration of ML1: 0.22-10 μg/mL or 4-167 nM; corresponding total lipid concentration range 0.2-6 mM). Drug-spiked media were transferred onto CT26 cells after which the well plates were tightly sealed with parafilm and subsequently incubated for 1h at 42 °C or for 1 h at 37 °C in a water bath, previously heated to the desired temperatures. Next, after refreshing the media with drug-free culture medium, CT26 cells were cultured for an additional 47 h at 37 °C in the incubator. Cell number was determined by MTS conversion as described above.

2.7. Statistical analysis

Data are presented as average with standard deviation. Statistical differences between groups were computed using GraphPad Prism7 with 95% confidence one-way ANOVA and using Tukeys multicomparison test.

3. Results and discussion

Characterization of Mistletoe Lectin-1

ML1 was isolated from freshly harvested mistletoe plant material as described in the materials and methods section and was characterized by SDS-PAGE, ELISA and bioactivity (MTS) as presented in **Supplementary Figure 1**. As expected from its structure (UniProtKB-P81446, EC 3.2.2.22; MW 62628 Da), ML1 migrated in SDS-PAGE around 60 kDa; no bands were observed at higher molecular weights indicating that there were no multimers in the isolated product. In addition, no bands were observed in the 20-30 kDa range, meaning that the ML1 was intact and had not dissociated into the two (A and B) chains. The concentration of the ML1 stock solution was quantified by two different methods, UV-absorbance at 280 nm and an anti-ML1 sandwich ELISA, which both yielded similar values (5.6 and 4.6 mg/mL for UV absorbance and ELISA respectively). For the remaining experiments, we used the ELISA method in view of its higher sensitivity.

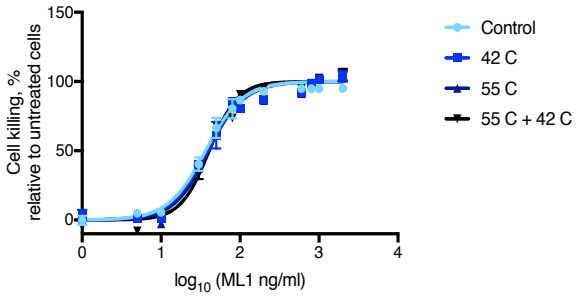

	Control	42°C	55°C	55°C+42°C
IC_{50}, ng/mL	36.55	38.86	39.73	40.69

Figure 1 - Bioactivity of ML1 exposed to different heat conditions versus CT26 colon carcinoma cells after 48h incubation: light blue line control (untreated) ML1; royal blue 42°C line represents the effect of mild hyperthermia; dark blue 55 °C line represents the effect of extrusion temperature and shear forces; black 55°C+42°C line represents the combination effect of extrusion and mild hyerthermia.

The bioactivity of ML1 after different heat treatments, was tested against CT26 cells after an incubation period of 48 h, using MTS cell viability assay; the untreated ML1 control IC_{50} (36.6 ± 0.01 ng/mL) was in agreement with previous reports [31]. The effect of extrusion and mild-hyperthermia were determined by exposing ML1 to: 55°C and 100 nm extrusion membrane, 42°C in the Eppendorf shaker, and to their combination (55°C+42°C). The effect of heat slightly increased the IC_{50}, however the values were still in the same order of magnitude and therefore, not considered to be significant.
Collectively, the characterization data confirmed the identity and bioactivity of the isolated ML1 in line with previously reported studies [31].

Characterization of LTSL: size, polydispersity index, encapsulation efficiency, thermal properties and shelf-life

Table 1 shows characterization data of LTSL with different lipid compositions that had been loaded by the film hydration method with fluorescein-labeled macromolecules ranging in MW from 4kD-67 kDa, with diverse structures (dextrans, albumin and ML1). The size (111 – 146 nm) and polydispersity (0.04 – 0.15) of LTSL were similar between loaded and non-loaded formulations, irrespectively of the loaded macromolecule (**Table 1**). Similar encapsulation efficiencies were found for all samples (6-10%), i.e. no specific trend was observed towards the lipid composition and/or the loaded molecule.

Table 1 – Initial physicochemical features of all the LTSL formulations prepared with varying mixtures of DPPC/MSPC/DSPE-PEG2000. LTSL5: 91/5/4 %mol; LTSL10: 86/10/4 %mol; LTSL15: 81/15/4 %mol. Average ± standard deviation of 2 independent samples; n.a. = non-applicable.

Formulation		Size, nm	PDI	Zeta potential, mV	EE%
Control	LTSL5	132 ± 0	0.08 ± 0.00	-13.6 ± 0.8	n.a.
	LTSL10	136 ± 2	0.04 ± 0.01	-8.5 ± 0.3	n.a.
	LTSL15	146 ± 3	0.05 ± 0.05	-12. 0 ± 0.4	n.a.
4 kDa dextran	LTSL5	115 ± 0	0.07 ± 0.03	-8.7 ± 0.1	8.6 ± 0.1
	LTSL10	134 ± 4	0.03 ± 0.00	-2.3 ± 0.4	7.9 ± 0.3
	LTSL15	120 ± 1	0.15 ± 0.02	-8.1 ± 1.1	9.3 ± 0.6
10 kDa dextran	LTSL5	111 ± 0	0.05 ± 0.04	-8.5 ± 0.3	7.8 ± 0.6
	LTSL10	141 ± 9	0.10 ± 0.09	-12.8 ± 0.1	10.1 ± 0.1
	LTSL15	119 ± 1	0.15 ± 0.04	-8.5 ± 0.3	6.2 ± 0.1
60 kDa ML1	LTSL5	137 ± 3	0.10 ± 0.01	-11.3 ± 0.1	6.1 ± 0.5
	LTSL10	133 ± 7	0.06 ± 0.01	-12.9 ± 0.2	8.8 ± 1.3
	LTSL15	193 ± 2	0.16 ± 0.06	-10.7 ± 0.6	4.3 ± 2.1
67 kDa BSA	LTSL5	131 ± 4	0.06 ± 0.01	-11.2 ± 1.7	7.8 ± 0.6
	LTSL10	133 ± 7	0.06 ± 0.01	-5.6 ± 4.5	6.8 ± 1.3
	LTSL15	133 ± 8	0.09 ± 0.04	11.2 ± 3.7	6.7 ± 0.4

Ultracentrifugation was used to purify the LTSL and their stability was analyzed after each step in terms of size, phosphate recovery and quantification of ML1 present inside the aqueous core (**Supplementary Figure SI-2**). Not only the initial (untreated) formulations kept the same size throughout the process, but also the cargo quantification indicates that the ultracentrifugation is not inducing any significant premature release.

The capability of LTSL to release their loaded cargo upon mild hyperthermia is attributed to phase transitions of the bilayer during the melting of DPPC around 40-42°C. All three formulations with different percentages of MSPC showed similar transition temperature (T_m) of the bilayer (ca. 41 °C; T_{onset} 40 °C), although a broader melting track was observed for LTSL with 15% MSPC (**Supplementary Figure SI-3**). Incorporation of different mol% of MSPC did not alter the Tm, which remained constant around 41 °C as previously shown [33]. A small side peak was visible in the thermogram for LTSL containing 15 % mol MSPC, which is indicative of mismatched phase mixtures caused by two different populations in the composition, as previously reported [33,34].

The transition temperature was not affected by the presence of encapsulated macromolecules (**Table 2**). Minor differences were observed in the transition enthalpy (ca. 0.15 J/g) between dextran loaded and BSA loaded LTSL, and our hypothesis is that protein hydrophobic domains of BSA may interact with the lipid bilayer, energetically favoring the solid to liquid transition by acting like a membrane defect. Melting enthalpy and T_m were comparable for LTSL10 incubated in buffer or media containing 10% serum.

Table 2 – Thermal properties of all the LTSL formulations prepared, determined by DSC: LTSL5 DPPC/MSPC/DSPE-PEG2000 91/5/4 %mol; LTSL10: DPPC/MSPC/DSPE-PEG2000 86/10/4 %mol; LTSL15: DPPC/MSPC/DSPE-PEG2000 81/15/4 %mol. Where indicated, formulations were analyzed in the presence of 10% serum. The samples indicated with asterisk presented two peaks in the thermograms and the calculated values refer to the peak integration of both peaks.

		Differential scanning calorimetry		
Formulation		Onset T, °C	Melting T, °C	Enthalpy, J/g
Control	LTSL5	39.9	40.9	0.955
	LTSL10	40.2	41.5	0.838
	LTSL10 + serum	40.1	41.5	0.935
	LTSL15*	40.5	41.4	0.989
4kDa dextran	LTSL5	40.0	41.2	1.202
	LTSL10	40.9	41.2	1.087
	LTSL15*	40.1	41.5	1.137
10kDa dextran	LTSL5	39.9	41.1	1.197
	LTSL10	40.4	41.3	1.073
	LTSL15*	40.1	41.4	1.183
ML1	LTSL5	40.6	40.9	0.957
	LTSL10	40.4	41.4	0.839
	LTSL10 + serum	40.4	41.5	0.838
	LTSL15	40.4	41.0	0.930
BSA	LTSL5	40.6	41.2	1.048
	LTSL10	40.6	41.3	0.837
	LTSL10 + serum	40.7	41.6	0.839
	LTSL15	40.2	41.4	1.018

All three LTSL compositions were stable with respect to particle size and PDI when stored at 4 °C up to 3 weeks (**Figure 2A-B**). Leakage of encapsulated cargo during storage was most pronounced for the formulations with 5% or 15% MSPC and correlated inversely to the molecular weight (size) of the en-

capsulated compound, i.e. LTSL loaded with larger macromolecules retained higher percentages of the loaded cargo by the end of the study. It is worth noticing that BSA- and ML1-loaded LTSLs showed comparable profiles and leaked amounts. LTSL10 exhibited a superior ML1 retention over the assessed period with approximately 95% ML1 retention after 1 week and 70% after 3 weeks (**Figure 2F**). Our storage stability data indicated that the physic-chemical instability of LTSL is related to the lysolipid content, with 10% MSPC affording the best stability. This lipid composition is similar to Thermodox® LTSL formulation.

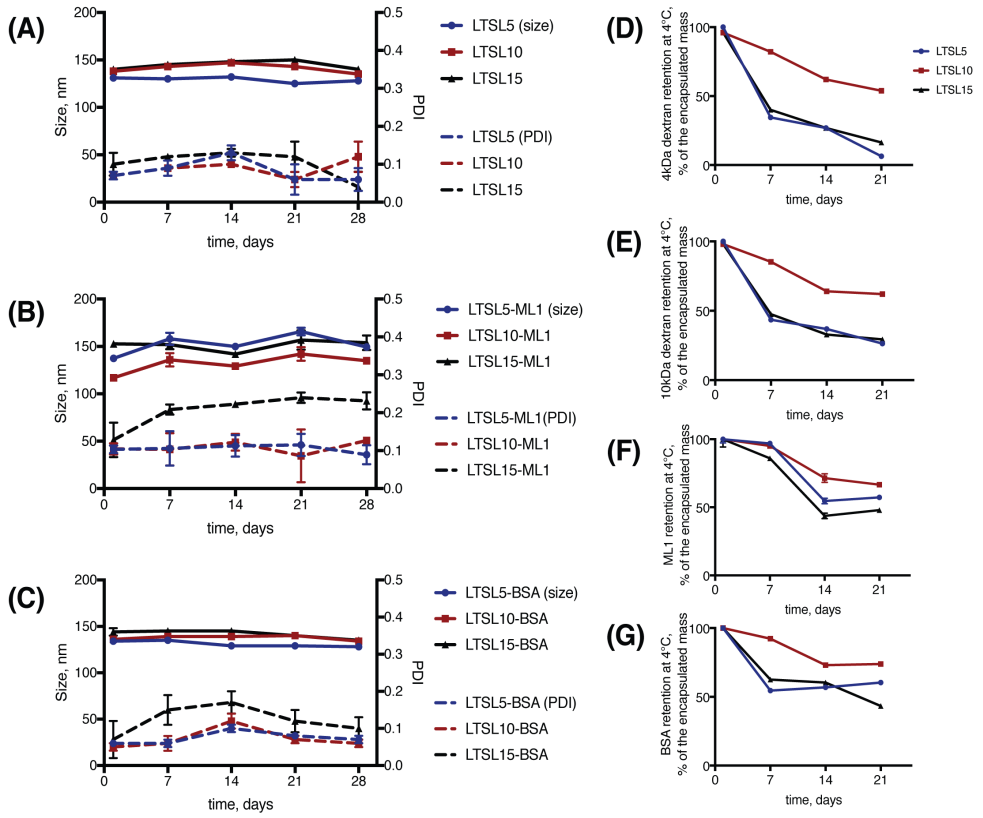

Figure 2 - Storage stability of LTSL at 4°C in HBS buffer. Left-hand panels show nanoparticles characteristics determined by DLS (continuous lines: size; broken lines: polydispersity); right-hand panels concern retention of loaded cargo in LTSL during storage. A) control (buffer loaded) LTSL. B) ML1-loaded LTSL. C) BSA-loaded LTSL. D) 4 kDa dextran–loaded LTSL. E) 10 kDa dextran-loaded LTSL. F) ML1-loaded LTSL G) BSA-loaded LTSL. In all graphs, the colors of the lines correspond to the same lipid composition: blue line LTSL5 containing 5%mol MSPC; Red line LTSL10 containing 10 %mol MSPC; Black line LTSL15 containing 15 %mol MSPC. Error bars represent average ± standard deviation of 2 independent samples.

Temperature- and time-dependent release kinetics of model macromolecules

To test hyperthermia-triggered release of macromolecular drugs from LTSL, we assessed temperature and time-dependent release of small and medium-sized dextrans, ML1 and albumin, thus covering a wide-range of macromolecular model compounds. **Figure 3** shows the temperature dependent release of model compounds of the tested liposome formulations after a 15-min heating period. LTSL10 showed the preferred release profile for all model compounds. Minor leakage of loaded cargo at 37 °C was observed in all cases. Increasing the temperature to mild hyperthermia, i.e. 42 °C, resulted in up to 46% release of the smallest macromolecular cargo (4 kDa dextran), while approximately 15% of the loaded content was released for the largest model compounds BSA and ML1. LTSL5 and LTSL15 showed a poorer release of all the molecules as compared to LTSL10, indicating that 10% mol MSPC is the optimal MSPC concentration. **Figure 4** shows the time-dependent release at 37 °C and 42 °C of all the macromolecules from LTSL10. For all the molecular weight compounds, the release profiles of the LTSL10 exposed to 37°C revealed minor leakages for during the 30-min period, in contrast with the LTSL10 incubated at 42 °C for the same period of time.

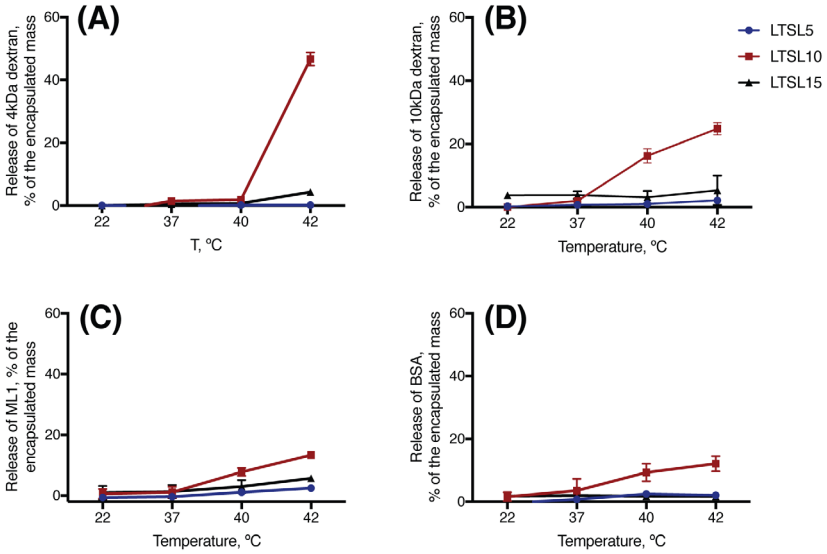

Figure 3 - Hyperthermia triggered release of loaded cargo from LTSL after 15 min incubation at the indicated temperature. A) LTSL loaded with 4 kDa dextran. B) LTSL loaded with 10 kDa dextran. C) LTSL loaded with ML1 (60 kDa). D) LTSL loaded with BSA (67 kDa). DPPC/MSPC/DSPE-PEG2000 molar ratios: LTSL5 91/5/4 mol% (blue line); LTSL10: 86/10/4 mol% (red line); LTSL15: 81/15/4 mol% (black line).

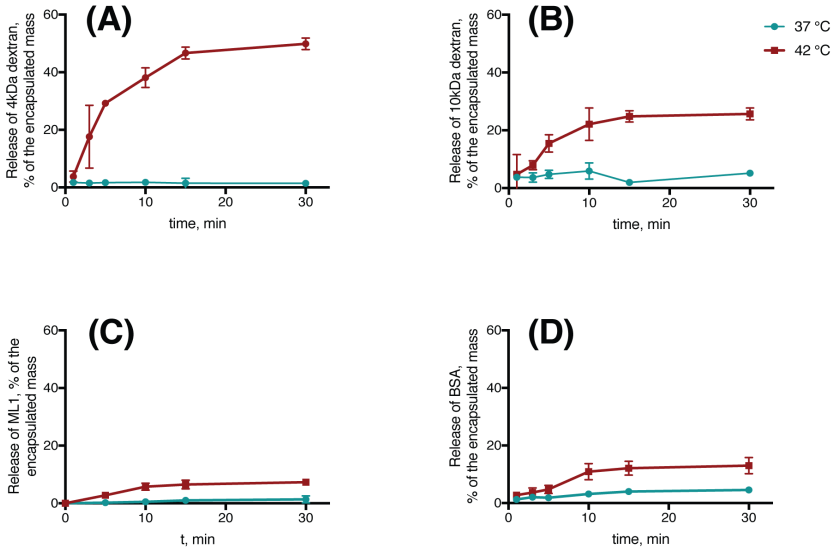

Figure 4 - Time-dependent release of loaded cargo from LTSL10 exposed to 37°C (blue lines) or 42°C (red lines) for 15 min. A) LTSL10 loaded with 4 kDa dextran. B) LTSL10 loaded with 10 kDa dextran. C) LTSL10 loaded with ML1 (60 kDa). D) LTSL10 loaded with BSA (67 kDa).

Zhang et al (2011) investigated the heat triggered release of BSA from temperature sensitive liposomes and they demonstrated that approximately 60 % of the entrapped BSA can be released within 5 min at 42 ºC. The same authors also recovered found that a rather high percentage of the protein is in the bilayer, i.e. aberrantly inserted in the lipid membrane, which could influence the results of release by over quantification [35]. In a recent report [23], the authors also found a size- and time- dependent mechanism for release of macromolecules, including 4 kDa Dextran and FITC-albumin. All these results are in line with the profiles obtained in the present paper: the smaller the entrapped molecule, the more is released from LTSL which suggests that size-restricted membrane passage or diffusion through pores in the bilayer plays a role.

Although the true mechanism behind thermosensitivity in liposomes is still up for debate, it is expected that the transfer (diffusivity) of molecules through the bilayer (from the inner aqueous solution of the liposomes, to the outside) is slower and energetically more unfavorable than permeation of a very small extremely hydrophilic molecule such as water. This process depends on the partition coefficient (for amphiphilic molecules) and on the size, structure and nature of the solute [36,37]. When defects or pores are created in the liposomes by lysolipids, the overall diffusion energy will be lowered, but still

the packing defects may be too small to allow free pore diffusion of macromolecules of all size ranges [37].
Overall, our results indicate that, although incomplete, the release obtained from LTSL for macromolecules is most efficient when 10% mol of Lyso-PC is incorporated in the bilayer. We therefore continued the remainder of our studies with this formulation.

Effect of serum on the release of Mistletoe Lectin-1
It has been reported that the proteins in the release medium alter the release properties of LTSL formulations in the in vitro and in vivo setups. To investigate this, release studies with ML1 loaded LTSL10 were performed in normothermia and hyperthermia conditions in RPMI culture medium without serum or RPMI culture medium supplemented with 10% serum; the quantification of ML1 release was made by ELISA (**Figure 5**). Our results suggest that there is a minor leakage (below 5%) at physiological temperature in the presence of serum. The release at hyperthermia conditions (42 °C) was not influenced by the presence of serum and it is comparable with the results obtained with HBS buffer (see **Figure 4C**).

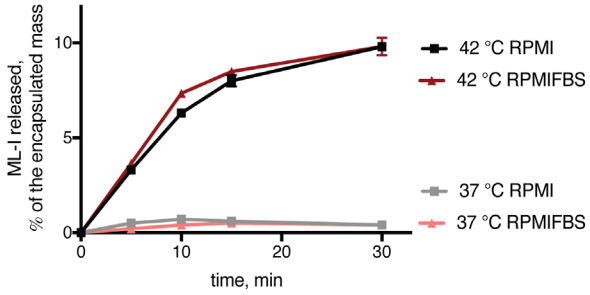

Figure 5 - Effect of serum in hyperthermia triggered release of ML1 from LTSL10. Black line: LTSL diluted in RPMI (no serum) at 42 ºC; dark red line: LTSL diluted in RPMI with 10% serum at 42 ºC. Grey line: LTSL diluted in RPMI (no serum) at 37 ºC; light red line: LTSL diluted in RPMI with 10% serum at 37 ºC.

Release, uptake and cytotoxicity in tumor cells
Several treatment and hyperthermia protocols have been proposed to maximize the thermal sensitization of cancer cells and intratumoral drug accumulation, either aiming at intravascular release within the tumor blood vessels (thus avoiding EPR and requiring uptake of released drug from the circulation) or intratumoral drug release (i.e. after a lag time allowing accumulation of LTSL within the tumor by EPR). Other heating protocols use a two-step method aiming for more uniform drug distribution throughout the tumor

by maximizing tumor perfusion and vascular leakiness in the first step and maximizing drug release in the second step [10,38,39]. The optimal timing between LTSL administration and local hyperthermia may depend not only on the tumor physiology, but also on the lipid composition and on the biopharmaceutical properties of the loaded drug, i.e. its capability to enter and stay within the tumor microenvironment. Intravascular release of doxorubicin from LTSL (that is, LTSL administration directly followed by hyperthermia for 30-60 min) proved approximately two-fold more efficacious than intratumoral release (based on EPR accumulation of LTSL, followed by hyperthermia), which was attributed to deeper and more extensive tumor penetration of free doxorubicin as compared to tumor distribution of liposomes [21,40]. Such differences between free doxorubicin and the applied liposomes may largely relate to the efficient uptake of the drug itself and may not be applicable to macromolecules like ML1.

To investigate the overall bioactivity of the formulated ML1 we studied two phenomena related to the two different functional chains of the protein. First, we studied the in vitro uptake in cancer cells by live cell imaging over a time period of 4h, and we studied ML1 induced cytotoxicity which is only occurring 2 days later (as described before) [31]. ML1 is composed of a cytotoxic A-chain linked to the lectin B-chain responsible for cellular binding and for mediating the protein uptake [41]; thus cytotoxic activity is ensured if the structure of both chains of the protein is conserved. Obviously, uptake and killing of cancer cells should only occur upon hyperthermia treatment of LTSL. In a different setup, we studied the uptake and cytotoxic efficacy when cells were heated together with the LTSL, to observe any bystander effect of the heating procedure.

Figure 6 shows the microscopy pictures of the uptake study. After hyperthermia treatment (42 °C) ML1 released from LTSL was internalized by CT26, resulting in a punctuated red pattern in the cells cytoplasm and leading to potent cytotoxic efficacy after 48 h (IC_{50}= 2.25 µg/mL). As expected, incubating the LTSL10 at 37 °C resulted in a minor release of ML1, and its internalization was less pronounced than at 42 °C. Heating resulted in an 8-fold reduction in IC50 (**Supplementary Figure SI-4**), which is comparable to the differences in ML1 release between normothermia or hyperthermia conditions (~10-fold increase in release, see **Figure 5**).
ML1 formulated in conventional PEG-liposomes was not released and hence showed no uptake (**Figure 6**) nor cytotoxicity (**Figure 7**). As expected, buffer

loaded LTSL and NTL did not induce cytotoxicity. These results indicate that the lipid formulation used are non-toxic, even at high concentrations. Only LTSL and their combination with hyperthermia results in potent cytotoxic activity of ML1, which thus supports the planned approach of applying localized hyperthermia to the tumor area after administration of ML1-loaded LTSL.

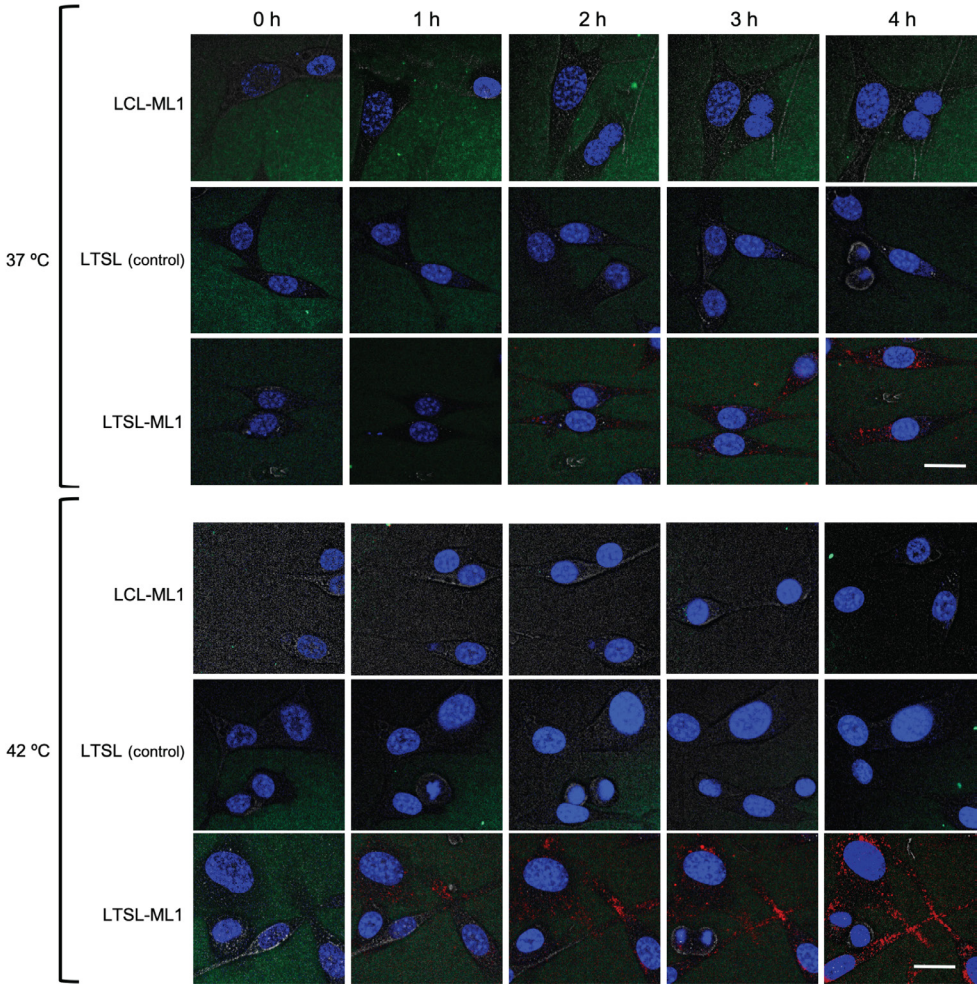

Figure 6 - Uptake of ML1 released from LTSL (setup 1). LTSL were diluted in cell culture media and exposed to mild hyperthermia for 1h. The resulting media were transferred without further processing onto CT26 and cells were evaluated for 4 h uptake of ML1 by live cell imaging. For the uptake studies, liposomes were labeled with DiO' (green) while ML1 was labeled with AF647 (red). Nuclei of CT26 were stained with Hoechst 33342 (blue) prior to addition of the preconditioned culture media. Scale bar applies for all live cell images, 20 μm.

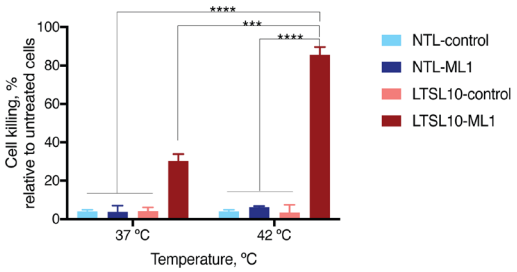

Figure 7 - Bioactivity of ML1 released from LTSL (setup 1). Several concentrations of ML1-loaded LTSL (formulated ML1 10 - 0.3 µg/mL) were diluted in cell culture media and exposed to mild hyperthermia for 1h. The resulting media were transferred without further processing onto CT26 After the 4-h uptake period, the cell culture medium was refreshed and cells were cultured for additional 44 h for cytotoxicity (MTS) measurement. Toxicity values represent 48 h cell killing effect of the formulations containing 10 mg/ml of formulated ML1.

In the second setup, LTSL and cells were heated at 42 °C collectively. As can be observed, the uptake (during an incubation period of 1 h, **Figure 8 A** and **B**) and cytotoxicity (after 48 h, **Figure 9A**) were strongly enhanced by hyperthermia at 42 °C for 1 h. In the absence of ML1 or liposomes, the control cells exposed at 37 °C or at 42 °C for 1h (**Figure 9B**) showed little differences in terms of cell viability. Thus, these results demonstrate that that the release of the encapsulated toxin can exert potent cytotoxic effects in tumor cells. We therefore conclude that ML1 keeps its bioactivity, which was shown by its cell-binding and uptake, and by tumor cells killing.

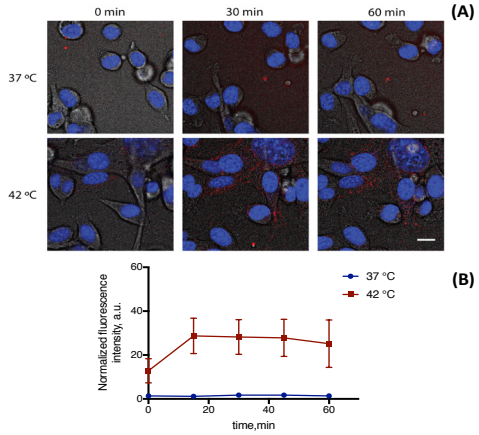

Figure 8 – Release and uptake of ML1 released from LTSL (setup 2). LTSL and CT26 cells were collectively exposed to mild hyperthermia for 1h and the release and uptake events were evaluated by live cell imaging. (A) For the microscopy studies, ML1 was labeled with AF647 (red). Nuclei of CT26 were stained with Hoechst 33342 (blue) prior to experiment. Scale bar applies for all live cell images, 20 µm. (B) semi-quantitative analysis of the ML1AF647 cell uptake microscopy studies. Blue line: 37 °C; red line 42 °C.

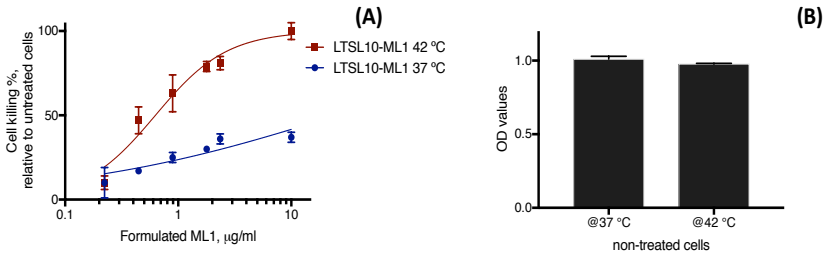

Figure 9 – (A) Bioactivity of ML1 released from LTSL (setup 2). CT26 cells and ML1-loaded LTSL were collectively exposed to mild hyperthermia or normothermic conditions for 1 h; the cell culture medium was refreshed and cells were cultured for additional 47 h for cytotoxicity (MTS) measurement. ML1-loaded LTSL exposed to 42 °C had an IC_{50} of 0.6 mg/ml, while the same formulation exposed to 37 °C had an extrapolated IC_{50} of 25 mg/ml. (B) Effect of heat treatment on CT26 cells, without ML1 or liposomes. Cells were exposed to mild hyperthermia (42 °C) or normothermic (37 °C) conditions for 1 h, and kept for additional 47 h at 37 °C, for MTS measurement. The OD values are presented in this figure. The OD values of the ML1 or liposome treated samples in (A) were normalized by the correspondent negative control OD value in (B).

Conclusions

We have demonstrated the potential of thermosensitive liposomes as nanocarriers for high-molecular weight cytotoxins like ML1. The most suitable liposomal formulation, containing 10 mol% MSPC, complied with all requirements i.e. a homogeneous size, temperature range for hyperthermia and in vitro release tests. Our experiments with CT26 cells confirmed that ML1-LTSL potently inhibited tumor cell viability upon hyperthermia treatment, either after a preheating treatment or when cells were coincubated with ML1-LTSL. These promising results warrant further investigation of the developed thermosensitive formulation of ribosome-inactivating cytotoxins.

Acknowledgments

This work was supported by the People Programme (Marie Curie Actions) of the European Union's Seventh Framework Programme FP7/2007–2013/ under REA grant agreement n° 324275. The authors acknowledge Phospholipid Research Center (Heidelberg) for funding and Lipoid GmbH for the generous supplying of lipids.

References

[1] Y. Matsumura, H. Maeda, Cancer Res. 1986, 46, 6387.
[2] E. Oude Blenke, E. Mastrobattista, R. M. Schiffelers, Expert Opin. Drug Deliv. 2013, 10, 1399.
[3] A. Wicki, D. Witzigmann, V. Balasubramanian, J. Huwyler, J. Control. Release 2015, 200, 138.
[4] M. Karimi, A. Ghasemi, P. Sahandi Zangabad, R. Rahighi, S. M. Moosavi Basri, H. Mirshekari, M. Amiri, Z. Shafaei Pishabad, A. Aslani, M. Bozorgomid, D. Ghosh, A. Beyzavi, A. Vaseghi, A. R. Aref, L. Haghani, S. Bahrami, M. R. Hamblin, Smart Micro/Nanoparticles in Stimulus-Responsive Drug/Gene Delivery Systems, Royal Society Of Chemistry, 2016.
[5] C. Alvarez-Lorenzo, A. Concheiro, Chem. Commun. (Camb). 2014, 50, 7743.
[6] S. Mura, J. Nicolas, P. Couvreur, Nat. Mater. 2013, 12, 991.
[7] Z. Al-Ahmady, K. Kostarelos, Chem. Rev. 2016, 116, 3883.
[8] L. Li, T. L. M. ten Hagen, D. Schipper, T. M. Wijnberg, G. C. van Rhoon, A. M. M. Eggermont, L. H. Lindner, G. A. Koning, J. Control. Release 2010, 143, 274.
[9] S. M. Park, M. S. Kim, S. J. Park, E. S. Park, K. S. Choi, Y. S. Kim, H. R. Kim, J. Control. Release 2013, 170, 373.
[10] L. Li, T. L. M. Ten Hagen, M. Bolkestein, A. Gasselhuber, J. Yatvin, G. C. Van Rhoon, A. M. M. Eggermont, D. Haemmerich, G. A. Koning, J. Control. Release 2013, 167, 130.
[11] B. M. Dicheva, G. A. Koning, Expert Opin. Drug Deliv. 2014, 11, 83.
[12] T. Ta, T. M. Porter, J. Control. Release 2013, 169, 112.
[13] D. Chen, W. Liu, Y. Shen, H. Mu, Y. Zhang, R. Liang, A. Wang, K. Sun, F. Fu, Int. J. Nanomedicine 2011, 6, 2053.
[14] Y. Dou, K. Hynynen, C. Allen, J. Control. Release 2017, 249, 63.
[15] W. J. M. Lokerse, E. C. M. Kneepkens, T. L. M. ten Hagen, A. M. M. Eggermont, H. Grüll, G. A. Koning, Biomaterials 2016, 82, 138.
[16] B. M. Dicheva, T. L. M. Ten Hagen, D. Schipper, A. L. B. Seynhaeve, G. C. Van Rhoon, A. M. M. Eggermont, G. A. Koning, J. Control. Release 2014, 195, 37.
[17] B. M. Dicheva, T. L. M. Ten Hagen, L. Li, D. Schipper, A. L. B. Seynhaeve, G. C. Van Rhoon, A. M. M. Eggermont, L. H. Lindner, G. A. Koning, Nano Lett. 2013, 13, 2324.
[18] L. Li, T. L. M. Ten Hagen, M. Hossann, R. Süss, G. C. Van Rhoon, A. M. M. Eggermont, D. Haemmerich, G. a. Koning, J. Control. Release 2013, 168, 142.
[19] G. A. Koning, A. M. M. Eggermont, L. H. Lindner, T. L. M. ten Hagen, Pharm. Res. 2010, 27, 1750.
[20] D. K. Chang, C. Y. Chiu, S. Y. Kuo, W. C. Lin, A. Lo, Y. P. Wang, P. C. Li, H. C. Wu, J. Biol. Chem. 2009, 284, 12905.
[21] C. D. Landon, J.-Y. Park, D. Needham, M. W. Dewhirst, Open Nanomed. J. 2011, 3, 38.
[22] V. Saxena, C. Gacchina Johnson, A. H. Negussie, K. V. Sharma, M. R. Dreher, B. J. Wood, Int. J. Hyperth. 2015, 31, 67.
[23] X. Huang, M. Li, R. Bruni, P. Messa, F. Cellesi, Int. J. Pharm. 2017, 524, 279.
[24] M. Marvibaigi, E. Supriyanto, N. Amini, F. A. Abdul Majid, S. K. Jaganathan, Biomed Res. Int. 2014, 2014, 785479.
[25] M. Horneber, G. Bueschel, R. Huber, K. Linde, M. Rostock, M. Horneber, G. Bueschel, R. Huber, K. Linde, M. Rostock, Cochrane Libr. 2010, 4.
[26] M. Puri, I. Kaur, M. a. Perugini, R. C. Gupta, Drug Discov. Today 2012, 17, 774.
[27] F. Stirpe, Toxicon 2013, 67, 12.
[28] G. Ribéreau-Gayon, S. Dumont, C. Muller, M. L. Jung, P. Poindron, R. Anton, Cancer Lett. 1996, 109, 33.
[29] A. Thies, D. Nugel, U. Pfüller, I. Moll, U. Schumacher, Toxicology 2005, 207, 105.
[30] A. Thies, P. Dautel, A. Meyer, U. Pfüller, U. Schumacher, Br. J. Cancer 2008, 98, 106.
[31] N. Beztsinna, M. B. C. de Matos, J. Walther, C. Heyder, E. Hildebrandt, G. Leneweit, E. Mastrobattista, R. J. Kok, Sci. Rep. 2018, 8, 2768.
[32] R. Eifler, K. Pfuller, W. Gockeritz, U. Pfuller, in Lectins 9 Biol. Biochem. Clin. Biochem. (Eds: J. Basu, M. Kundu, P. Chakrabari, T. Bog-Hansen), Wiley Eastern Limited, New Delhi, 1993, pp. 1–5.

[33] J. K. Mills, D. Needham, Biochim. Biophys. Acta - Biomembr. 2005, 1716, 77.
[34] D. Needham, M. W. Dewhirst, Adv. Drug Deliv. Rev. 2001, 53, 285.
[35] X. Zhang, P. F. Luckham, A. D. Hughes, S. Thom, X. Y. Xu, Int. J. Pharm. 2011, 421, 291.
[36] M. Hossann, T. Wang, M. Wiggenhorn, R. Schmidt, A. Zengerle, G. Winter, H. Eibl, M. Peller, M. Reiser, R. D. Issels, L. H. Lindner, J. Control. Release 2010, 147, 436.
[37] T.-X. Xiang, B. D. Anderson, Adv. Drug Deliv. Rev. 2006, 58, 1357.
[38] A. M. Ponce, B. L. Viglianti, D. Yu, P. S. Yarmolenko, C. R. Michelich, J. Woo, M. B. Bally, M. W. Dewhirst, JNCI J. Natl. Cancer Inst. 2007, 99, 53.
[39] L. Li, T. L. M. Ten Hagen, A. Haeri, T. Soullié, C. Scholten, A. L. B. Seynhaeve, A. M. M. Eggermont, G. A. Koning, J. Control. Release 2014, 174, 202.
[40] A. A. Manzoor, L. H. Lindner, C. D. Landon, J. Park, A. J. Simnick, M. R. Dreher, S. Das, G. Hanna, W. Park, A. Chilkoti, G. A. Koning, T. L. M. Hagen, D. Needham, M. W. Dewhirst, 2012, 72, 5566.
[41] E. Pizzo, A. Di Maro, J. Biomed. Sci. 2016, 23, 54.

Supplementary information

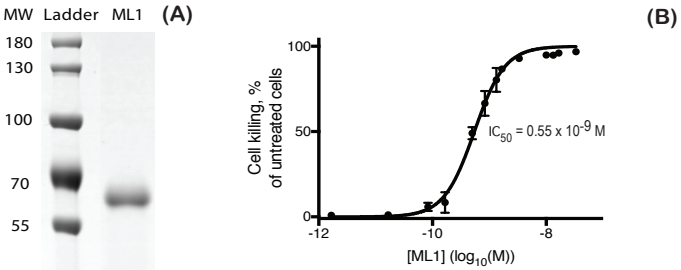

	ML1 concentration after dialysis, mg/mL
UV absorbance λ=280 nm	5.6 (93 μM)
ELISA	4.6 (77 μM)

Supplementary Figure SI-1 – Characterization of isolated ML1. A) Non-reducing SDS PAGE analysis. B) Bioactivity of ML1 versus CT26 colon carcinoma cells after 48h incubation.

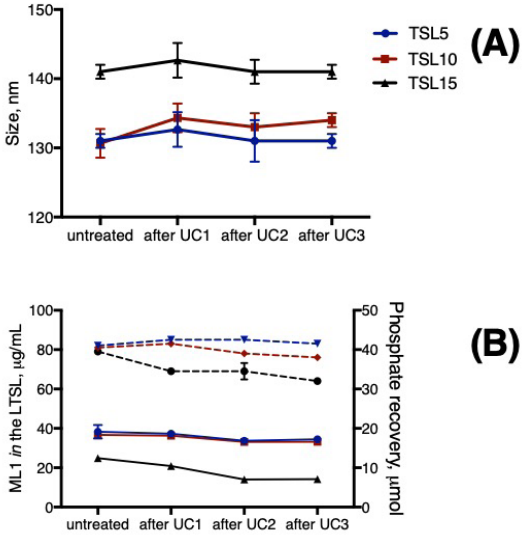

Supplementary Figure SI-2 – Validation of the ultracentrifugation method for the LTSL purification. LTSL were separated from non-encapsulated cargo by 3 cycles of ultracentrifugation; at the end of each step, an aliquot of the liposomal suspension was analyzed in terms of size (A) and encapsulation efficiency determined by ELISA (continuous lines in B) and phosphate recovery (dashed lines in B) and compared with the non-purified sample. In both graphs, the colors of the lines correspond to the same lipid composition: blue line LTSL5 containing 5%mol MSPC; Red line LTSL10 containing 10 %mol MSPC; Black line LTSL15containing 15 %mol MSPC. Error bars represent average ± standard deviation of 2 independent samples.

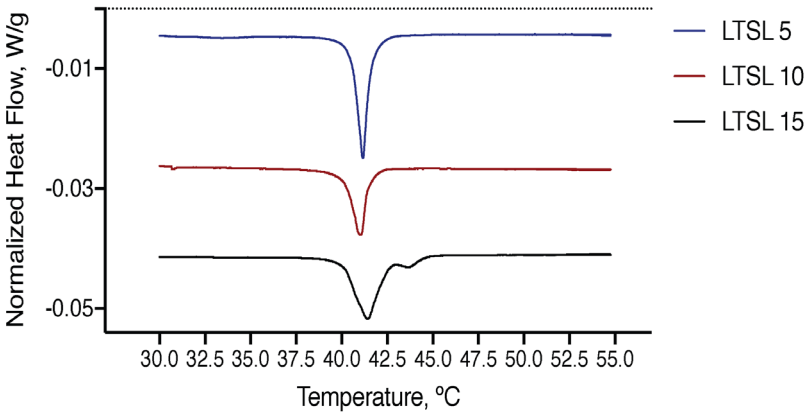

Supplementary Figure SI-3 - Phase transition of LTSL as determined by DSC analysis. Top line (blue) LTSL5: DPPC/MSPC/DSPE-PEG2000 91/5/4 %mol; middle line (red) LTSL10: DPPC/MSPC/DSPE-PEG2000 86/10/4 %mol; bottom line (black) LTSL15: DPPC/MSPC/DSPE-PEG2000 81/15/4 %mol.

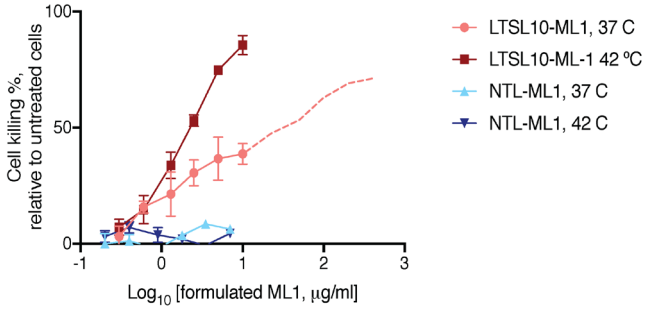

Supplementary Figure SI-4 – Bioactivity of ML1 released from LTSL (setup 1). Several concentrations of ML1-loaded LTSL (formulated ML1 10 - 0.3 µg/mL) were diluted in cell culture media and exposed to mild hyperthermia for 1h. The resulting media were transferred without further processing onto CT26 After the 4-h uptake period, the cell culture medium was refreshed and cells were cultured for additional 44 h for cytotoxicity (MTS) measurement. The LTSL10 formulation exposed to 42 °C (red line) had an IC_{50} of 2 µg/ml. The same formulation exposed to 37 °C (peach-color line) had an extrapolated (dashed line) IC_{50} value of 17 µg/ml.

Chapter 4b
Additional study

Cationic thermosensitive liposomes for encapsulation and triggered release of macromolecules

Summary

In this chapter, we investigated cationic thermosensitive liposomes (CTSL) as potential carrier for cytotoxic macromolecules. We studied the encapsulation and release of the model macromolecule bovine serum albumin (BSA) in liposomal formulations composed of 1,2-dipalmitoyl-sn-glycero-3-phosphocholine (DPPC), 1,2- distearoyl-sn-glycero-3-phosphoethanolamine-N-PEG_{2000} (DSPE-PEG_{2000}), 1-stearoyl-2-hydroxy-sn-glycero-3-phosphocholine (MSPC) and the cationic lipid dimethyldioctadecylammonium bromide (DDAB). We demonstrated that the encapsulation and release of BSA is increased to almost double when compared with non-cationic formulations. In conclusion, the CTSL here described are strong candidates for encapsulations and heat-triggered release of macromolecular compounds.

Introduction

The aim of this chapter was to provide additional experimental insights on thermosensitive drug release systems that are suitable for encapsulation of mistletoe lectin 1 (ML1). Further improvements on the formulation of Chapter 4a have been made by incorporation of cationic lipids in the lysolipid containing formulation. Cationic lipids may promote interactions with target cells by electrostatic interactions. In case of ML1, cationic lipids may also improve encapsulation as ML1 has a negative charge at physiological pH.
Cationic thermosensitive liposomes (CTSL) have been studied for tumor delivery of small molecules like doxorubicin (Dox) in the Gerben Koning lab [1–8]. In their research they have used 1,2- dipalmitoyl-3-trimethylammonium-propane (DPTAP chloride salt) as cationic lipid in combination with DPPC, DSPC and DSPE-PEG_{2000}. They showed that the Dox-CTSL had superior uptake and toxicity in different tumor cell lines and endothelial cells compared to conventional TSL. In the in vivo experiments, the intravital microscopy revealed that Dox-CTSL delivered 3-fold higher Dox quantity to tumors than TSL upon heat treatment [9].
Thus, we investigated the potential of CTSL as carrier for macromolecules. We studied the encapsulation and release of un-labelled bovine serum albumin (BSA) in formulations composed of DPPC, DSPE-PEG_{2000}, MSPC and DDAB. Formulation, encapsulation and release studies were done according to methods similar to **Chapter 4a**.

Materials and methods

Chemicals

The phospholipids 1,2-dipalmitoyl-sn-glycero-3-phosphocholine (DPPC), and 1,2- distearoyl-sn-glycero-3-phosphoethanolamine-N-PEG2000 (DSPE-PEG_{2000}) were purchased from Lipoid (Ludwigshafen, Germany). DDAB (dimethyldioctadecylammonium bromide) and 1-stearoyl-2-hydroxy-sn-glycero-3-phosphocholine (MSPC) were purchased from Avanti Polar Lipid Inc (Alabaster, USA). BSA was obtained from Sigma Aldrich (Zwijndrecht, Netherlands). Isolated Mistletoe Lectin-1 and control standard for ELISA (4.5 µg/ml) were isolated according to the protocols provided by Eifler et al [10]. MicroBCA kit was purchased from ThermoFisher and used to measure BSA concentration according to the manufacturer's instructions.

Isoelectric point of ML1

The isoelectric point of ML1 was determined by changes in zeta potential according to the buffer's pH. At the isoelectric point of the protein, its net charge or zeta potential is zero. The protein solutions were titrated from pH value 7.6 to 2.6 using Citric Acid – Na_2HPO_4 buffer solutions as electrolytes. Before titration, freshly prepared protein solutions were filtered through 0.45 µm filters. All measurements were made using protein solutions with a concentration of 1 mg/mL. Each media was measured using laser Doppler electrophoresis on a Zetasizer Nano-Z (Malvern Instruments) [11].

Liposomes preparation

Liposomes with different lipid compositions (**Table 1**) were prepared by the lipid film and extrusion method. Typically, 150 µmol of lipids were dissolved in 4 mL of a 1:1 chloroform/methanol solvent mixture. The organic solvents were evaporated for 20 min in the rotavapor (thin-film) at 60 °C. The films were kept for 1 hour in nitrogen stream and later hydrated with 3 mL with HBS (10 mM HEPES buffer with 0.9% w/v NaCl) at 50 °C, with or without BSA (2mg/mL). After reconstitution, a total lipid (TL) concentration of 50 mM was obtained. Samples were hand-extruded 15 times over 400 and 100 nm pore-size polycarbonate filters at 50 °C. When applicable, liposomes were separated from non-encapsulated cargo by ultracentrifugation (Beckmann ultracentrifuge, 3x, 55000 rpm 60 min 4 °C), and stored at 4 °C.

Table 1 – Lipid composition of cationic thermosensitive liposomes.

Formulation	DDAB, mol%	MSPC, mol%	DSPE-PEG$_{2000}$, mol%	DPPC, mol%
C10TSL10	10	10	5	75
C5TSL10	5	10		80
C10TSL5	10	5		80
C5TSL5	5	5		85
LTSL10	0	10		85
LTSL5	0	5		90

Size, PDI and Zeta-potential

The hydrodynamic diameter and polydispersity index of all liposomes were measured by dynamic light scattering using a Malvern ALV/CGS-3 multiangle goniometer with He–Ne laser source (λ = 632.8 nm, 22 mW output power) under an angle of 90° (ALV, Langen, Germany). The zeta-potential of the liposomes was measured using laser Doppler electrophoresis (Zetasizer Nano-Z) with samples dispersed in 10 mM HEPES buffer pH 7.4 (with no additional salts added).

Phosphate content determination

The total phosphate content of the liposome formulations was determined according to the method of Rouser et al [12] with sodium biphosphate as a standard after destruction of the phospholipids with perchloric acid and heating at 180 °C. The blue colored reaction product was detected at 797 nm with the spectrometric plate reader.

Encapsulation efficiency

An aliquot of 50 µL of liposomes suspension was diluted in 450 µL of HBS, to which TritonX-100 0.1% v/v was added to destroy the liposomal bilayer and expose the encapsulated BSA. Separation of released BSA from lipids was done by Vivaspin ultrafiltration (300 kDA MWCO) and analysis of the flow-throw was done by MicroBCA. Loading contents (LC%) and encapsulation efficiencies (EE%) were calculated as follows:

$$LC\% = \frac{nmol\ BSA}{nmol\ total\ lipid} \times 100 \quad (1)$$

$$EE\% = \frac{BSA_{in}}{BSA_{start}} \times 100 \quad (2)$$

where, BSA_{in} is payload of BSA determined experimentally after formulation and purification, and BSA_{start} is the starting amount of payload.

Differential Scanning Calorimetry

DSC was carried out to a have a better insight about the thermal properties of the CTSLs, for further studies of thermal-induced release. DSC measurements (DSC Discovery, TA Instruments, New Castle, USA) were carried out in duplicate, starting by equilibrating the samples and reference at 25 °C for 5 min and then ramping from 25 °C to 55 °C, at 1 °C/min.

Time-dependent release

Time-dependent release profiles of CTSLs were performed at 37 °C and 42°C. CTSL suspensions were diluted in pre-heated HBS during fixed intervals (5, 10, 15, 30 min) under stirring (300 rpm) in a thermomixer. CTSL samples kept at 4 °C were considered as a blank and LTSL samples destroyed with TritonX-100 were considered as the 100 % release. Separation of released BSA from CTSL was done by Vivaspin ultrafiltration (300 kDA MWCO) and analysis of the flow-throw was done by MicroBCA. In all release experiments, the release percentage of BSA was quantified by using the equation:

$$Release\% = \frac{amount\ released}{total\ release\ by\ TritonX100} \quad (3)$$

where *amount released* is the amount of BSA at a certain time point, and *total release by TritonX100* is the total mass found after liposomes were treated with Triton X-100. Non-loaded formulations were used as reference for any possible cross-reactivity between lipids/triton and the kit reagents.

Results and discussion

Isoelectric point of ML1

The isoelectric point of ML1 was determined by laser Doppler electrophoresis, a technique that is commonly used for determination of the zetapotential of nanoparticles. The zetasizer equipment can also be used for microelectrophoresis of proteins. As such, it allows for determination of the mobility of proteins in buffers with different pH values, and thus allows calculation of pI values at which net-neutral charge is obtained. Our experiments revealed that ML1 has an isoelectric point of 5.5, comparable to the pI of BSA (5.4 [13]). Both proteins hence will be negatively charged at pH 7.4 which is the pH of the encapsulation buffer. The encapsulation of BSA and ML1 thus can benefit from the cationic components in the lipid bilayer.

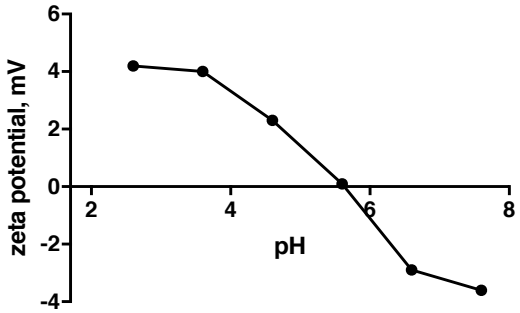

Figure 1 – The isoelectric point of ML1 (5.5) was determined by zeta potential, using citric Acid – Na_2HPO_4 buffer solutions as electrolytes (pH 2.6 to 7.6).

Development of cationic thermosensitive liposomes

Several compositions with different mol% lysolipid MSPC, cationic lipid DDAB and neutral lipid DPPC were prepared by film-hydration technique and extrusion over 100 nm pore size membranes. Similar to the LTSLs in **chapter 4**, the mol% of the PEGylated lipid PEG-$DSPE_{2000}$ was fixed at a concentration of 5 mol% in all formulations.

All liposomes had sizes below 150 nm and polydispersity indexes below 0.2 (**Table 2**). The changes of net surface charge were also monitored and are in line with the composition: positive charges were found when DDAB was introduced, and neutral charges were observed when no DDAB was added. Control formulations (not containing BSA) had similar zetapotential as cationic formulations without BSA, suggesting that only residual BSA is attached to the outer side of the liposomes.

Moreover, we obtained a positive correlation between the net charges of liposomes (zeta potential) and the amount of entrapped BSA.Incorporation of cationic lipid in the bilayer improved the encapsulation of BSA from 0.015% LC to 0.082% LC, i.e. more than five-fold at the same loading conditions. The same trend was observed for the encapsulation efficiency of BSA that was improved from 13% when no DDAB was included, up to 71%. Thus, we confirm that the presence of positive charge of the DDAB lipid is beneficial for the entrapment of this protein.

Table 2 – Features of the prepared cationic thermosensitive liposomes containing BSA as model macromolecule (ns=2).

Formulation	Size, nm	PDI	Zeta-pot., mV	EE,%	LC,%
C10TSL10	134 ± 1	0.07 ± 0.01	12 ± 1	71 ± 6	0.082
C5TSL10	105 ± 0	0.14 ± 0.09	-1 ± 0	46 ± 1	0.053
C10TSL5	141 ±1	0.12 ± 0.00	11 ± 1	45 ± 1	0.041
C5TSL5	142 ± 2	0.24 ± 0.00	-8 ± 1	28 ± 1	0.032
LTSL10	136 ± 2	0.09 ± 0.08	-14 ± 0	19 ± 2	0.027
LTSL5	153 ± 3	0.16 ± 0.03	-11 ± 1	13 ± 3	0.015

The same formulations where analyzed in the presence of serum and the overall increase in size/PDI suggests particles aggregation for the cationic formulations (**Table 3**). Formulations that did not contain any cationic component (LTSL10 and LTSL5, similar to the ones presented in **Chapter 4**) conserved their properties due to the effective polyethylene glycol shell. Thus, although the incorporation of cationic DDAB was successful in raising encapsulation of negatively charged BSA, the aggregation of cationic LTSL can be a serious problem. Cationic particles that aggregate in presence of serum can result in aggregates and thrombi that cause severe in vivo toxicity [12–14]. More research in this type of formulations is needed, for instance by independently controlling the lipid composition of the inner and outer lipid leaflets. Such formulations offer the potential of improving the encapsulation of negatively charged compounds by producing a positively charged inner leaflet, while keeping the outer leaflet with neutral charge and with PEGylated shielding.

Table 3 – Features of the prepared cationic thermosensitive liposomes containing BSA as model macromolecule in the presence of serum (ns=2).

Formulation	Size, nm	PDI
C10TSL10	162 ± 2	0.37 ± 0.03
C5TSL10	139 ± 2	0.34 ± 0.02
C10TSL5	212 ± 3	0.37 ± 0.01
C5TSL5	244 ± 14	0.47 ± 0.00
LTSL10	155 ± 4	0.27 ± 0.02
LTSL5	129 ± 4	0.16 ± 0.00

Thermal analysis (**Table 4**) indicates that the introduction of 5 mol% cationic lipid combined with 5 mol% lysolipid did not interfere with the transition temperature (T_m). In the presence of serum, the transition peaks shape shifts from sharp to broad with minimum changes in the enthalpy (ΔH). Ultimately, this could result in a wider temperature release-sensitivity range; since the onset temperature (T_{Onset}) remained constant (between 40 and 41 °C) one is assured that the temperature at which the thermosensitivity starts is confined to a physiologically and clinically feasible range.

Table 4 – Thermal properties of the prepared cationic thermosensitive liposomes in the absence and in the presence of serum (ns=2).

Media	Formulation	T_{Onset}, ºC	T_m, ºC	ΔH, J/g
HBS	**C10TSL10**	40.2 ± 0.0	42.1 ± 0.1	0.28 ± 0.01
	C5TSL10	40.1 ± 0.0	41.5 ± 0.0	0.67 ± 0.00
	C10TSL5	40.2 ± 0.0	42.2 ± 0.0	0.35 ± 0.01
	C5TSL5	40.9 ± 0.0	41.4 ± 0.0	1.39 ± 0.01
	LTSL10	40.7 ± 0.1	41.2 ± 0.2	1.01 ± 0.01
	LTSL5	40.3 ± 0.0	41.1 ± 0.0	0.98 ± 0.00
HBS+10% serum	**C10TSL10**	40.3 ± 0.2	42.2 ± 0.1	0.75 ± 0.01
	C5TSL10	40.2 ± 0.0	41.5 ± 0.0	0.55 ± 0.00
	C10TSL5	40.3 ± 0.0	42.5 ± 0.0	0.74 ± 0.01
	C5TSL5	40.9 ± 0.0	41.4 ± 0.0	1.08 ± 0.00
	LTSL10	40.7 ± 0.0	41.4 ± 0.0	0.73 ± 0.00
	LTSL5	40.5 ± 0.0	41.2 ± 0.0	0.78 ± 0.00

Temperature triggered release experiments

For all formulations, insignificant BSA release was observed at 37 °C (**Figure 3**, left), which is expected at temperatures below T_{onset} and T_m. On the other hand, raising the temperature to 42 °C (i.e. above T_m) resulted in extensive release of the loaded cargo. Moreover, up to 4-fold higher release was observed as compared to conventional LTSL10/5, as shown in **Figure 3** (right panel). This observation may be counterintuitive as the presence of a cationic lipid both helps in improving encapsulation and in the increased release of BSA. However, during the gel-to-liquid phase transition, there is an increased membrane fluidity and permeability, facilitating lysolipids' rearrangement within the bilayer or complete dissociation from it [17]. This results in the formation of pores and membrane defects through which the loaded drug is released. With increasing temperature and in the presence of BSA, micellization of DDAB

is energetically favored [18]. As DDAB is part of the bilayer and is promoting BSA entrapment, our underlying hypothesis is that the increased bilayer permeability can promote DDAB mobility/dissociation from the bilayer and therefore BSA release. Our hypothesis does not explain the decreased release with higher amounts of DDAB (e.g. C10TSL10 vs C5TSL10). This observation needs additional research on the incorporation of cationic lipids inclusion in thermosensitive liposomes, the molecular interactions and bilayer dissociative processes.

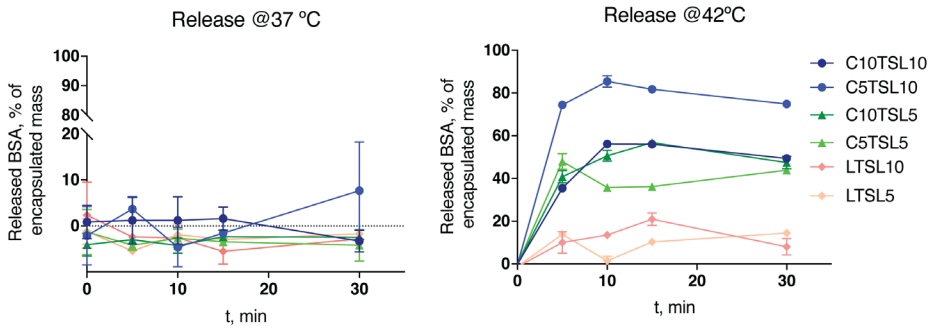

Figure 3 – Heat-triggered release profiles of BSA from cationic thermosensitive formulations. In both graphs, the dark blue line refers to C10TSL10, light blue line to C5TSL10, dark green to C10TSL5, light green to C5TSL5, dark pink to LTSL10 and light pink to LTSL5.

Conclusion

With this additional chapter, we demonstrated the potential of cationic thermosensitive liposomes as nanocarriers for negatively charged protein payloads. The most suitable liposomal formulation, containing 10 mol% MSPC and 5% DDAB, complied with requirements for EPR based nanocarriers. Although much more research is needed to fully characterize these liposomes, these preliminary results collectively underline the potential of using cationic thermosensitive liposomes for the encapsulation and release of macromolecular drugs.

Acknowledgments

Dr. Barbara S. Miranda-Swartjes is kindly acknowledged for fruitful scientific discussions.

References

[1] L. Li, T. L. M. M. Ten Hagen, M. Hossann, R. Süss, G. C. van Rhoon, A. M. M. M. Eggermont, D. Haemmerich, G. A. Koning, J. Control. Release 2013, 168, 142.
[2] W. J. M. Lokerse, M. Bolkestein, S. U. Dalm, A. M. M. Eggermont, M. de Jong, H. Grüll, G. A. Koning, J. Control. Release 2017, 258, 34.
[3] B. M. Dicheva, G. A. Koning, Expert Opin. Drug Deliv. 2014, 11, 83.
[4] B. M. Dicheva, T. L. M. Ten Hagen, L. Li, D. Schipper, A. L. B. Seynhaeve, G. C. Van Rhoon, A. M. M. Eggermont, L. H. Lindner, G. A. Koning, Nano Lett. 2013, 13, 2324.
[5] L. Li, T. L. M. ten Hagen, D. Schipper, T. M. Wijnberg, G. C. van Rhoon, A. M. M. Eggermont, L. H. Lindner, G. A. Koning, J. Control. Release 2010, 143, 274.
[6] W. J. M. Lokerse, E. C. M. Kneepkens, T. L. M. ten Hagen, A. M. M. Eggermont, H. Grüll, G. A. Koning, Biomaterials 2016, 82, 138.
[7] L. Li, T. L. M. Ten Hagen, A. Haeri, T. Soullié, C. Scholten, A. L. B. Seynhaeve, A. M. M. Eggermont, G. A. Koning, J. Control. Release 2014, 174, 202.
[8] B. M. Dicheva, A. L. B. Seynhaeve, T. Soulie, A. M. M. Eggermont, T. L. M. ten Hagen, G. A. Koning, Pharm. Res. 2016, 33, 627.
[9] B. M. Dicheva, T. L. M. Ten Hagen, D. Schipper, A. L. B. Seynhaeve, G. C. Van Rhoon, A. M. M. Eggermont, G. A. Koning, J. Control. Release 2014, 195, 37.
[10] R. Eifler, K. Pfuller, W. Gockeritz, U. Pfuller, Lectins Biol. Biochem. Clin. Biochem. 1993, 9.
[11] S. SALGIN, U. Salgin, S. Bahadır, Int. J. Electrochem. Sci. 2013, 7, 12404.
[12] G. Rouser, S. Fleischer, A. Yamamoto, Lipids 1970, 5, 494.
[13] Q. Shi, Y. Zhou, Y. Sun, Biotechnol. Prog. 2008, 21, 516.
[14] J. Guo, L. Bourre, D. M. Soden, G. C. O. Sullivan, C. O. Driscoll, Biotechnol. Adv. 2011, 29, 402.
[15] M. Kapoor, D. J. Burgess, S. D. Patil, Int. J. Pharm. 2012, 427, 35.
[16] R. M. Schiffelers, G. Storm, Int. J. Pharm. 2008, 364, 258.
[17] D. Needham, M. W. Dewhirst, Adv. Drug Deliv. Rev. 2001, 53, 285.
[18] S. K. Mehta, Bhawna, K. K. Bhasin, A. Kumar, J. Colloid Interface Sci. 2008, 323, 426.

Chapter 5 -Encapsulation and ultrasound-triggered release of mistletoe lectin-1 from liposomes

Maria B. C. de Matos, Roel Deckers, Raymond Schiffelers, Robbert Jan Kok

In Preparation

Abstract

Mistletoe lectin-1 (ML1) is a nature-derived macromolecular cytotoxin that potently induces apoptosis in tumor cells. Non-specific cytotoxicity to normal cells is one of the major risks that prevents its clinical application. We therefore investigated the encapsulation of ML1 in ultrasound-sensitive liposomes (USL) and studied its release by high-intensity focused ultrasound (HIFU). External ultrasound pulses can be focused to a restricted region of interest and can be applied for triggered intratumoral release of drugs from nanomedicines.

USL were prepared by entrapment of perfluorocarbon (PFC) nanodroplets in liposomes. When triggered with HIFU, PFC can undergo phase transition from liquid to gas thus rupturing the lipid capsules. Non-ultrasound-sensitive liposomes (NUSL) were prepared with different DPPC/Cholesterol/DSPE-PEG_{2000} lipid molar ratios (60/20/20 for USL20; 60/30/10 for USL10; 65/30/5 for USL5). The model protein Horseradishperoxidase (HRP) or ML1 were encapsulated in NUSL at 20-40% encapsulation efficiency (EE%). NUSL were subsequently merged with PFC nanoemulsions (composed of perfluoropentane and 0.4 mol% DPPC) by sonication and extrusion to yield USL which were purified over sucrose density gradients. The final EE% of USL was ~4% for both HRP and ML1. USL10 and USL5 showed adequate storage stability, while USL20 lost 50% of the encapsulated cargo when stored at 4°C. Optimized HIFU settings (25 MPa for 1 min exposure) resulted in 80% triggered release of HRP or ML1 for USL10, while 2MPa HIFU for 1 min still effectuated 50% release.

ML1 loaded USL10 were studied for bioactivity against murine CT26 colon carcinoma cells. Confocal live-cell imaging studies with fluorescently labeled ML1-USL10 demonstrated that HIFU treated liposomes released ML1 which was subsequently internalized by target cells. Intact ML1-loaded liposomes (NUSL or USL) were not internalized and prevented uptake of ML1, which shows that nanoencapsulation prevented against the cytotoxic activity. The cytotoxic potential of ML1 was almost fully restored when ML1-USL10 were triggered by HIFU (IC_{50} HIFU triggered ML1-USL10 400 ng/ml; free ML1 281 ng/ml). Our study shows that USL in combination with HIFU hold promise as trigger-sensitive nanomedicines for local delivery of macromolecular cytotoxins.

Keywords: ultrasound-sensitive liposomes; HIFU; triggered drug release; macromolecule encapsulation and release; live-cell imaging.

1. Introduction

Nature-derived cytostatic drug products have long been the source for cancer treatment, with thousands of natural entities identified to possess significant anticancer properties. Semi-synthetic doxorubicin, one of the most studied compounds, found its origins in microorganisms. Taxol (or paclitaxel) and camptothecin are plant derived alkaloids and have been very successful as anti-tumor molecules against refractory ovarian, breast and colon cancer[1–3]. While these anticancer small molecules have shown their potential, nature's medicine toolbox also contains macromolecules that display even higher more targeted cytotoxicity; such macromolecular cytotoxins have great potential for cancer treatment.

Cytotoxins like diphtheria toxin (MW 70 kDa), shiga toxin (MW 40 kDa), ricin (MW 65 kDa) and mistletoe lectin-1 (ML1; MW 60 kDa) are good examples of cytotoxic macromolecules. They come from different natural sources but present a common bifunctional A–B structure and belong to the same class of ribosome inactivating proteins (type 2, RIP-II). Although these proteins vary in the specific mode of action, their cytotoxic effects follows three common steps: 1) B-chain mediated internalization by target cells, 2) translocation of the A-chain into the cytosol and 3) once in the cytosol, irreversible inhibition of the host cells protein synthesis machinery by the toxic polypeptide[4]. With respect to ML1, this cytotoxin is the major active component of mistletoe extracts which are being used in adjuvant cancer treatment[5–8]. Mistletoe extracts are administered subcutaneously as a (neo) adjuvant to radiotherapy and surgery. Intravenous administration of crude mistletoe extracts or purified ML1 is not feasible: the undirected cytotoxicity of ML1 will result in strong adverse effects, which for now prevents its clinical development as tumor directed cytotoxin. Thus, ML1 can greatly benefit from delivery by nanocarriers that direct its anti-cancer activity to tumors, while sparing other tissues.

Nanomedicine-based targeting approaches can increase the therapeutic index of drugs in several aspects, either by increasing localized efficacy or by reducing toxicity to normal tissues; the encapsulated drug compounds can also be protected from degradation or elimination. A good example of nanomedicines are liposomes, which have been used for encapsulation of both hydrophilic and hydrophobic drugs by well-established techniques such as lipid-film hydration or remote loading [9]. The main drawback of these long circulating "stealth" formulations, like Doxil®, is the inadequate release of the drug within the tumor microenvironment: although there is high tumor accumulation of encapsulated drug, levels of free drug are only moderate which

limits the therapeutic efficacy. Thus, novel nanocarrier formulations focus on triggered release rather than spontaneous release of the loaded drug. If adequate release can be achieved intratumorally, the therapeutic availability can be restored once the nanomedicine has reached its intended target tissue [10]. Triggerable nanocarriers make use of endogenous or exogenous stimuli to release their cargo. Endogenous stimuli-responsive nanocarriers exploit factors associated with the tumor microenvironment, for instance low pH, redox gradients or the presence of certain enzymes. Exogenous-responsive nanocarriers respond to external stimuli to trigger drug release, such as temperature, light or ultrasound [11–13]. In addition to small molecules delivery, recent reports have shown temperature-triggered drug delivery systems of macromolecules, including ML1 as shown by our group [14–17]. Such lower-temperature-sensitive liposomes, however, showed only incomplete release of the macromolecular cargo. The aim of the present study is to develop a nanocarrier system that releases macromolecular payloads more efficiently.

We therefore combined liposomes with perfluorocarbon (PFC) nanoemulsions thus creating ultrasound-sensitive liposomes (USL). Upon ultrasound-mediated activation the liposome-encapsulated PFC nanodroplet will vaporize and expand to produce a gas bubble, which will disrupt the liposomal bilayer and trigger drug release [18,19,28–34,20–27]. PFCs microemulsions and PFC microbubbles have found clinical application as oxygen carriers in artificial blood and as contrast agents in medical sonography. Several PFCs such as dodecafluoropentane and perfluorohexane meet the requirements for medical applications [35,36]. First, the protocol for creating USL was optimized using the Horseradish peroxidase (HRP) as model payload. Next, USL formulations of ML1 were prepared and evaluated for their encapsulation efficiency and release by high-intensity focused ultrasound (HIFU). Last, we investigated whether ML1 released from ML1-USL is functionally active, by demonstrating its uptake in cancer cells and cytotoxic activity after HIFU triggered release.

2. Materials and methods

2.1. Chemicals

The phospholipids 1,2-dipalmitoyl-sn-glycero-3-phosphocholine (DPPC), and 1,2- distearoyl-sn-glycero-3-phosphoethanolamine-N-PEG_{2000} (DSPE-PEG_{2000}) were purchased from Lipoid (Ludwigshafen, Germany). Cholesterol, 3,3',5,5'-Tetramethylbenzinide (1-Step™ Ultra TMB-ELISA Substrate Solution) and horseradish peroxidase (HRP) were purchased from Sigma-Aldrich. Perfluoropentane, tech. 90%, was purchased from Alpha Aesar (Germany). ML1 reference standard for ELISA (4.5 µg/ml) was provided by ABNOBA GmbH (Germany). Anti-ML1 monoclonal antibodies with specificity to ML1 A-chain anti-ML-A-5F5, and Anti-ML-A-5H8-horse-radish peroxidase (POD) were obtained from SIFIN (Berlin, Germany). CellTiter 96® AQueous One Solution Cell Proliferation Assay (MTS) was provided by Promega. The lipophilic fluorescent dyes 3,3'-dioctadecyloxacarbocyanine perchlorate (DiOC18(3); DIO') and Alexa Fluor® 647 were purchased from Invitrogen.

2.2. Methods

2.2.1. Mistletoe lectin-1 isolation and characterization

ML1 was isolated from mistletoe plant material as described before [17,37]. In brief, ML1 was isolated by affinity chromatography from mistletoe plant material that was harvested in June from ash tree (Fraxinus excelsior L.). After purification, ML1 was characterized by FPLC using a Mono S cation exchange column (Pharmacia/GE Healthcare, Uppsala, Sweden) and a 0.6 M NaCl salt gradient in 0.015 M citrate buffer (pH 4.0) at a detection wavelength of 280 nm. ML1 concentrations were quantified by UV/Vis at 280 nm (NanoDrop ND-1000, Thermo Fisher Scientific) using an extinction coefficient of 104850 M-1cm-1. ML1 concentrations were also quantified by sandwich ELISA, as describe elsewhere[38].Anti-ML-A-5F5 was used as trapping antibody while anti-ML-A-5H8-POD was used as detection antibody.

ML1 was fluorescently labeled with Alexa Fluor 647 (AF647) succinimidyl ester according to the manufacturer's protocol. In brief, 250 µL of 0.02 M bicarbonate buffer pH 8.3 was added to 2 mL of ML1 solution (5.6 mg/mL; 0.2 µmol). The diluted protein was reacted with AF647 dye (5:1 mol:mol: AF647:ML1) under stirring at room temperature for 1h and purified by dialysis (Slide-A-Lyzer 0.5-3 mL, MWCO 10000 Da). Purified AF647-ML1 was characterized by analytical size-exclusion chromatography on a BioSep 3000 column (20 min, PBS 1mL/min) and NanoDrop analysis of the collected fractions (AlexaFluor extinction coefficient 239000 M-1cm-1). The typical final AF647:ML1 ratio was 1:2 (mol/mol). Labelled ML1 was kept protected from

the light at 4 °C until further use.

2.2.2. Preparation of nanocarrier formulations

The preparation of USL involves several steps as depicted in the scheme below (**Figure 1**). Each of the steps is described in detail in the following sections.

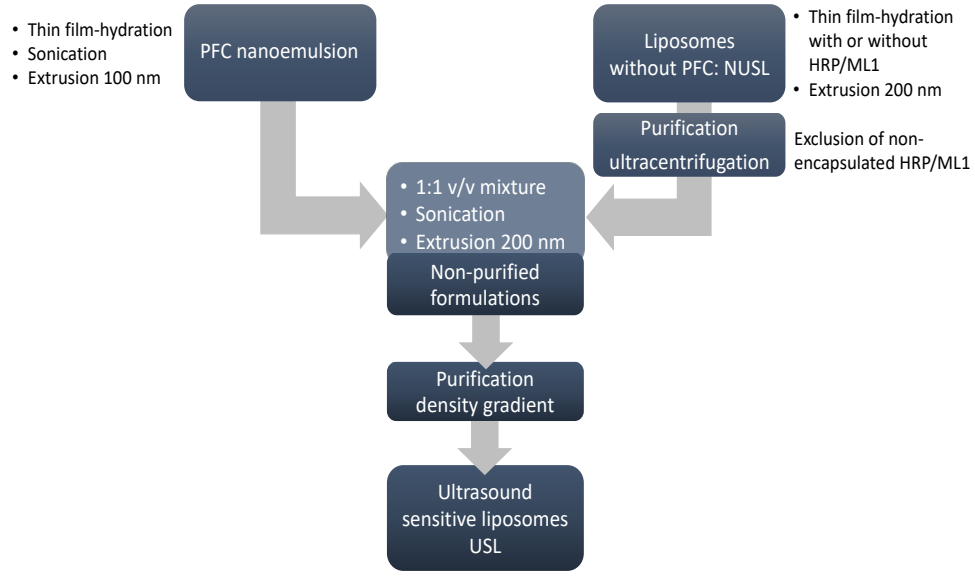

Figure 1 – Workflow for the preparation of USL. First, PFC nanoemulsions were prepared by thin film-hydration method using DPPC for the lipid monolayer. The resulting emulsion was downsized by sonication and extrusion through 100 nm pore size. In parallel, we prepared the liposomal formulations with or without cargo, by thin film-hydration method and extrusion through 200 nm extrusion membranes, and purified to remove non-encapsulated cargo. At this point the liposomes do not contain any PFC nanoemulsion and thus are non-ultrasound sensitive liposomes (NUSL). The last step consisted of mixing nanoemulsion and NUSL in the same volume ratio, and the incorporation of the PFC into the NUSL by sonication. The resulting mixture was extruded once more through 200 nm pore size membranes. All formulations were purified by sucrose density gradient to separate non-encapsulated drug, nanoemulsions and empty liposomes from the final USL.

2.2.2.1. Preparation of PFC nanoemulsions

PFC nanoemulsions were prepared by thin film-hydration method [19,26]. A lipid film containing 10 mg (15 μmol) of DPPC was prepared by evaporating the solvents from 0.5 mL of a DPPC solution (20 mg/mL in chloroform) using a rotavapor at 60 °C. The film was kept for 1h in a nitrogen stream at room temperature before it was hydrated with 2 ml HBS (10 mM HEPES buffer pH 7.4 containing 150 mM NaCl) thus yielding DPPC micelles with a final concentration of 7.5 mM; the resulting DPPC dispersion was cooled to 4°C on

an ice bath. Perfluoropentane (3.5 mmol; density 1.6 g/mL) was added to the DPPC dispersion and the mixture was sonicated (Branson Sonifier 20 kHz 13 mm) 3 times for 30 seconds on the lowest energy input (10% frequency, 1 amplitude), with 1 min interval between each sonication. The resulting emulsion was extruded ten times over 100 nm polycarbonate extrusion membranes (Whatman) to narrow the size and polydispersity of the nanodroplets, as was confirmed by dynamic light scattering (DLS) using a Zetasizer Nano-S (Malvern Instruments).

2.2.2.2. Preparation of liposomes

Liposomes with different lipid compositions were prepared by the lipid film and extrusion method. DPPC/Cholesterol/DSPE-PEG_{2000} lipid molar ratios before combination with PFC nanoemulsions (named NUSL, non-ultrasound sensitive liposomes) were 60/20/20 for NUSL20; 60/30/10 for NUSL10; 65/30/5 for NUSL5; control liposomes were prepared with DPPC/Cholesterol/DSPE-PEG_{2000} 65/30/5 mol ratio only. For fluorescently labeled liposomes, 0.5 mol% of DIO' was added when applicable. In brief, 80 μmol total lipid (TL) was dissolved in 4 mL 1:1 chloroform/methanol. Solvents were evaporated in a rotavapor for 20 min at 60 ºC. The formed lipid films were kept for 1h in a nitrogen stream and hydrated at 50 ºC with 1 mL HBS (in case of control liposomes) or HBS solutions of ML1 (1.5 mg/ml) or HRP (0.2 mg/ml). After reconstitution of liposomes, the final lipid concentration was 80 mM. Liposomes were extruded ten times over 400 and 200 nm pore-size polycarbonate filters at 45 ºC. Non-encapsulated ML1 and HRP were removed by ultracentrifugation of the liposomes (Beckmann ultracentrifuge, 2 cycles, 55000 rpm, 1 h, 4 ºC) and resuspension in 1 ml HBS.

2.2.2.3. Combination of PFC nanoemulsion and liposomes into USL

USL were formed by mixing the DPPC-PCF5 nanoemulsion and the different NUSL liposomes in 1:1 volume ratios. The resulting solutions were sonicated (Branson Sonifier 20 kHz 13 mm) 3 times for 30 seconds on the lowest energy input (10% frequency, 1 amplitude), with 1 min interval between each sonication, on ice bath. Finally, USL were extruded over 200 nm pore size polycarbonate membranes. The theoretical DPPC/Cholesterol/DSPE-PEG_{2000} lipid compositions of the final formulations (named USL, ultrasound sensitive liposomes) were USL20: 65/17/17; USL10: 63/30/7; USL5: 70/26/4. All USL formulations were purified by sucrose density gradient centrifugation to remove un-encapsulated drugs, nanoemulsions and empty liposomes. In brief, sucrose solutions (10, 15, 20, 25, 40 and 50 w/w%) were prepared by dissolv-

ing pure sucrose in deionized water. The sucrose solutions with different mass fractions were carefully added to 15-mL ultracentrifuge tubes (Beckmann) in different volumes (2, 2, 2, 1, 1, 1 mL, respectively). Unpurified USL dispersion (1 mL) was carefully added to the top of the gradient and centrifuged at 35000 rpm for 16 h and 4 °C (Beckmann ultracentrifuge). Non-encapsulated PFC nanoemulsion droplets have the highest density (1.6 g/ml) and settled at the bottom of the tube; free ML1 and emulsion-free NUSL had the lowest density and were collected in the upper sucrose layers. USL were recovered from the 20% sucrose layer. Isolated fractions were dialyzed against 2 L of HBS buffer for 24 h. USL and other fractions stored at 4°C until further studies.

2.3. Characterization of PFC nanoemulsions and liposomes

2.3.1. Size and polydispersity index

The hydrodynamic diameter and polydispersity index of all lipid formulations were measured by dynamic light scattering using a Zetasizer Nano-S (Malvern Instruments). Appropriate dilutions were made in HBS buffer.

2.3.2. Lipid recovery

The overall recovery of TL was determined by determination of phospholipids in 160 µl liposomal aliquots according to the method of Rouser et al [39]. Sodium biphosphate was used as a standard. The blue colored reaction product was detected at 797 nm spectrofotometrically. TL recovery was calculated by correcting for lipid compositions.

2.3.3. Recovery of payloads - HRP and ML1

An aliquot of 20 µL of liposome dispersion was diluted in 1000 µL of HBS, to which TritonX-100 0.1% v/v was added to destroy the liposomal bilayer. HRP was determined enzymatically by eHRP-TMB reaction. In brief, 100 µL of HRP was added to the wells of a 96-well plate. The substrate (TMB, 25 µL/well) was added, and the mixture was allowed to react for 2 min 30 sec, after which the reaction was stopped by addition of 25 µL/well 1 M sulfuric acid. The yellow colored reaction product was detected at 450 nm with the spectrometric plate reader. ML1 was determined by sandwich ELISA as described above. Loading contents (LC%) and encapsulation efficiencies (EE%) were calculated as follows:

$$LC\% = \frac{\mu g\ payload}{\mu mol\ total\ lipid} \times 100 \quad (1)$$

$$EE\% = \frac{payload_{end}}{payload_{start}} \times 100 \quad (2)$$

where, payloadend is payload of HRP or ML1 determined experimentally after formulation and purification, and payloadstart is the starting amount of payload. Concentrations are expressed in μg/ml.

2.4. Stability studies and release experiments

2.4.1 Storage stability

Storage stability of liposomes was studied at 4 °C and included colloidal stability (i.e. nanoparticle size and polydispersity) and drug retention capacity over a time period of 4 weeks. At each time point, small aliquots were diluted and analyzed by DLS or analyzed for released cargo (i.e. HRP) by enzymatic analysis. Drug retention capacity was calculated as follows:

$$Drug\ retention\ \% = \frac{payload_0 - leaked_t}{payload_0} \times 100 \quad (3)$$

where $payload_0$ is the amount of encapsulated HRP at the initial timepoint of the stability study and $leaked_t$ is the amount of HRP detected in the supernatant of the liposomes.

2.4.2. HIFU triggered release experiments

Ultrasound-triggered release of HRP and ML1 was measured using an in-house developed experimental setup [40] for HIFU triggered release in which the sample is suspended in a water bath at the focal point of the single-element focused US transducer (Imasonic, Besançon, France) operated at 1.3 MHz, duty cycle = 1%, pulse repetition period = 50 ms. The dimensions of the focal point were 1×1×3 mm (at −3 dB). Liposomal stock solutions (USL, NUSL), ML1 and HRP reference solutions and 1:1 v/v mixtures of PFC nanoemulsion plus NUSL were diluted 50-fold in HBS; 170 μl was transferred into the reaction vessel (170 μL PCR tubes; BioRad) and positioned in the HIFU setup. Samples were exposed to ultrasound (see exposure conditions below) and immediately thereafter transferred to an ice bath (4°C). Reference samples that had not been treated with ultrasound were kept at 4 °C and were used as background levels of ML1 and HRP. In all cases, not more than 2% of background release was observed. Samples treated with TritonX-100 (0.1% v/v) were used as reference in which full release had occurred. Release of HRP was analyzed without further processing of the sampled aliquots. In the case of ML1, samples were processed by Vivaspin ultrafiltration (300 kDa MWCO; Sartorius) after which the ultrafiltrate was analyzed for released ML1 by ELISA as described above. In all release experiments, the percent release of the compounds was quantified by using the equation:

$$Release\% = \frac{amount\ released}{total\ release\ by\ TritonX100} \times 100 \quad (4)$$

where *amount released* is the amount of HRP or ML1 at a certain time point or fixed temperature, and *total release by TritonX100* is the total mass found after liposomes were treated with Triton X-100.

HIFU Exposure conditions

HIFU exposure conditions were investigated by varying the acoustic pressure conditions at constant exposure time (1-50 MPa for 1 min at room temperature), or by varying the exposure time at constant acoustic pressures (2 or 25 MPa for 30 sec, 1 min, 2 min, 4 min, 8 min). The samples were immediately transferred to the ice bath until further analysis as described above. Acoustic pressures in the focal point were calibrated as a function of input voltage using a fiber-optic hydrophone (Precision Acoustics) in a tank filled with degassed water.

2.5. Bioactivity of free and formulated ML1

Bioactivity of ML1 that had been encapsulated in liposomes and released by HIFU was studied in two experimental settings that reflect either the uptake of ML1 in target cells (functionality of the A-chain of ML1) or that represent the biological activity of ML1 (cytotoxin activity). All experiments were conducted with murine CT26 colon carcinoma cells that has been obtained from American Type Culture Collection (ATCC). RPMI cell culture media, PBS and FBS were purchased from Sigma-Aldrich, and OptiMem was obtained from Gibco. CT26 cells were cultured in RPMI supplemented with 10 % FBS, at 37 °C in a 5% CO2 and humidified atmosphere. For all cell experiments, CT26 colon carcinoma cells were first seeded in 96-well plates (10000 cells/well) and allowed to adhere for 24 h prior to the experiment.

2.5.1. Uptake of released ML1

Uptake studies were conducted with HIFU treated DiO' labeled liposomes (NUSL, USL, control liposomes) that had been loaded with AF647-labeled ML1. Liposomes were diluted 1:10 in OptiMEM (final concentrations 2 μg/mL AF647-ML1 and 7 mM total lipid) and treated with HIFU as described above with the following acoustic settings: 2 MPa for 1 min exposure and 25 MPa for 1 min exposure. Samples were transferred to the ice bath and used for uptake studies without further processing. Before addition of the samples, nuclei of CT26 cells were pre-stained with Hoechst 33342. After replacement

of the culture medium with the HIFU-treated samples, 96-well µClear® black plates (Greiner) were transferred into a Yokogawa Cell Voyager CV7000s microscope (Tokyo, Japan). Live-cell confocal microscopy images were taken for 4 h at 37 °C and analyzed for uptake of liposomes (red), uptake of ML1 (green) and nuclei (blue). Uptake was semi-quantified with Columbus® image analysis software (PerkinElmer) using automated protocols for nuclei and cytoplasm detection and build-in functionalities for fluorescence intensity determination.

2.5.2. Cytotoxic activity of ML1

Cytotoxic activity of ML1 was indirectly measured by a mitochondrial activity assay that quantified the number of surviving cells. Non-fluorescently labeled ML1 and ML1-loaded liposomes (NUSL, USL, control liposomes) were diluted in RPMI+10%FBS (20 µL in 1000 µL); 170 µL of the diluted sample was then exposed to HIFU as described above with the acoustic settings of 2 MPa for 1 min exposure or 25 MPa for 1 min exposure. Samples were transferred to the ice bath and analyzed for cytotoxic activity after dilution of 50 µL of the samples with 80 µL of culture medium. The thus obtained samples were transferred onto the cells and incubated under culture conditions for 4h.

Final concentrations incubated with the cells were 80-800 ng/mL for ML1 and 0.4-8 mM TL. After refreshing the media with drug-free culture medium, cells were cultured for an additional 44 h in the incubator before determination of the number of surviving cells according to the supplier's instruction (CellTiter 96® AQueous One Solution Cell Proliferation Assay). Bioactivity IC50 values of each treatment were calculated by non-linear curve fitting using GraphPad Prism software. Appropriatre reference samples included free ML1, blanc liposomes and samples not treated with HIFU ultrasound.

2.6. Statistical analysis

Data are presented as average with standard deviation. Statistical differences between groups were computed using GraphPad Prism7 with 95% confidence one-way ANOVA and using Sidak multicomparison test.

3. Results

3.1. Characterization of PFC nanoemulsions and liposomes

The final size of PFC nanoemulsion was 118 ± 11 nm (PDI 0.26 ± 0.01) which is the expected size range after extrusion over 100 nm filters. Although PFC nanoemulsions were relatively stable, the size and PDI of PFC nanodroplets doubled upon storage at 4 °C in 48 h, and after 4 days the size had increased drastically (1120 nm, PDI 1.0). We therefore used freshly prepared PFC nanoemulsions to prepare USL.

The characteristics of NUSL and the corresponding USL are shown in **Table 1**. Before their loading with PFC nanodroplets NUSL10 and NUSL5 displayed sizes and PDI within the expected range (size 156-191 nm, PDI 0.11-0.09). NUSL20 showed sizes two times smaller than expected (i.e. 95 nm instead of ~200 nm), which may be related to the formation of DSPE-PEG2000 micelles due to very high concentrations of this lipid in the formulation [41–45]. Similar encapsulation efficiencies for HRP and ML1 were found for all NUSL formulations, i.e. no specific trend was observed towards the lipid composition.
After mixing the PFC nanoemulsion with the NUSL and sonication to enable the inclusion of PFC nanodroplets, the now-formed USL were extruded again. The average size remained unchanged but we observed an increase in PDI by ca. 2-fold (not shown), as anticipated by the fact that it is a mixture of two populations with different sizes.
USL were separated from non-encapsulated nanoemulsion and non-encapsulated HRP or ML1 by sugar density gradients. The top layer contained mainly non-encapsulated proteins, fraction 1 (10% sucrose) contained purified NUSL, fraction 2 (20 % sucrose) contained purified USL and the bottom fraction (50% sucrose) contained the nanoemulsion. Fraction 2 or USL was dialyzed to replace the external sugar solution by fresh HBS. The sizes and PDI of the final preparations were comparable to their corresponding NUSL formulation; representative size distributions are shown in **Supplementary Figure 1**. When comparing the PDI of purified USL with the PDI of the USL before sucrose gradient purification, the decrease in PDI suggests that we have removed the non-encapsulated PFC nanodroplets and that we obtained a monodispersed sample. The recovery of lipids (TL%) and encapsulated cargo (EE%) decreased substantially when NUSL were converted into USL, but the LC remained constant.
We attribute the numerical decrease to the USL formation process: to prepare USL, that is, to incorporate the PFC nanoemulsion in the liposomes, it is necessary to apply sonication to the NUSL already encapsulating the drug. This

step includes not only transient opening of the NUSL bilayer and thus loss of some of the encapsulated cargo, but also partial replacement of the internal volume by PFC nanoemulsion. Moreover, the purification over sugar density gradients also removed liposomal vesicles that had not been loaded with PFC, which was responsible for ~80% loss in recovery of both phospholipid and loaded drugs. Since LC were not affected largely, it can be inferred that the loss of drugs was primarily related to low inclusion of PFC and removal of NUSL, rather than leakage of HRP or ML1 during sonication and extrusion.

Table 1 - Physicochemical characteristics and loading results of NUSL and USL. Lipid molar ratio of DPPC/Cholesterol/DSPE-PEG2000 for (N)USL20: 60/20/20; for (N)USL10: 60/30/10; for (N)USL5: 65/30/5. TL%: total lipid yield; EE%: encapsulation efficiency; LC: loading content expressed as μg drug to μmol lipid ratio. Average ± standard deviation of 2 independent samples.

Step	Formulation	Size, nm	PDI	TL, %	EE%	LC, μg drug: μmol lipid
NUSL HRP	NUSL20	95 ± 1	0.12 ± 0.02	58 ± 1	29 ± 1	3.7 ± 0.2
	NUSL10	156 ± 2	0.11 ± 0.01	63 ± 2	40 ± 1	4.6 ± 0.3
	NUSL5	191 ± 4	0.09 ± 0.03	62 ± 2	25 ± 3	3.6 ± 0.1
USL HRP	USL 20	98 ± 2	0.17 ± 0.02	12 ± 1	3 ± 1	1.1 ± 0.3
	USL10	209 ± 13	0.15 ± 0.02	17 ± 1	7 ±1	2.0 ± 0.1
	USL5	181 ± 1	0.06 ± 0.05	11 ± 1	7 ± 1	3.2 ± 0.2
NUSL ML1	NUSL20	97 ± 2	0.11 ± 0.03	66 ± 2	21 ± 1	4.1 ± 0.1
	NUSL10	186 ± 4	0.12 ± 0.01	72 ± 1	23 ± 1	4.5 ± 0.1
	NUSL5	179 ± 5	0.07 ± 0.04	59 ± 2	21 ± 1	4.7 ± 0.2
USL ML1	USL 20	88 ± 8	0.16 ± 0.01	18 ± 1	2 ± 1	2.9 ± 0.4
	USL10	179 ± 1	0.15 ± 0.01	14 ± 2	4 ±1	6.7 ± 0.6
	USL5	201 ± 8	0.07 ± 0.03	15 ± 1	4 ± 1	6.5 ± 0.4

3.2 Stability studies and release experiments

3.2.1 Storage stability

Formulations containing 5 and 10 mol% DSPE-PEG2000 with and without PFC nanoemulsion, i.e. (N)USL5 and (N)USL10, were stable with respect to particle size (**Figure 2A**) as well as drug retention (**Figure 2B**) when stored at 4 °C for 1 month. On the contrary, (N)USL20 leaked 50% of the loaded HRP in the first week of storage, and also showed decreases in size revealing colloidal instability. This can be related to the amounts of 15-20% DSPE-PEG_{2000} in the (N)USL formulation. DSPE-$PEG2_{000}$ amounts above 12 mol% are known for the formation of micelles and increased instability of liposomal bilayers

[41–45]. Since both NUSL20 and USL20 showed similar leakage in the first week of storage, PFC nanoemulsion does not seem to play a role in the instability.

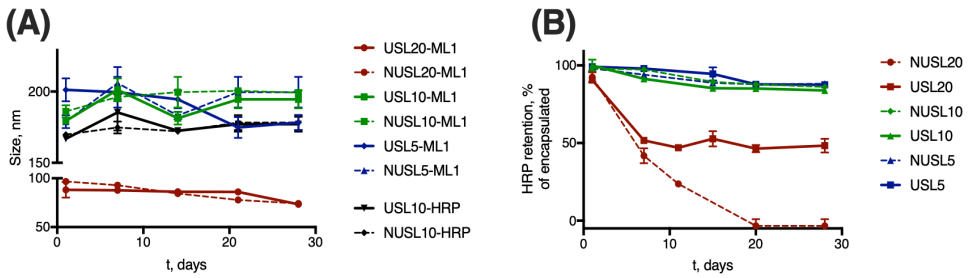

Figure 2 – Storage stability of USL at 4°C in HBS buffer. Panel (A) shows nanoparticles characteristics determined by DLS and panel (B) shows HRP retention. In both graphs, the colors of the lines correspond to the same lipid composition: the red line corresponds to liposomal formulations composed of initial 20 mol% DSPE-PEG_{2000} and containing (full line, USL20) or not (dashed line, NUSL20) PFC nanoemulsion; the green line corresponds to liposomal formulations composed of initial 10 mol% DSPE-PEG_{2000} and containing (full line, USL10) or not (dashed line, NUSL10) PFC nanoemulsion; the blue line corresponds to liposomal formulations composed of initial 5 mol% DSPE-PEG_{2000} and containing (full line, USL5) or not (dashed line, NUSL5) PFC nanoemulsion.

3.2.2 HIFU-triggered release experiments

To investigate HIFU-triggered release of macromolecular drugs from USL, we assessed acoustic pressure- and time-dependent release of HRP and ML1. **Figure 3** shows the release of HRP (panels A and B) and ML1 (panels C and D) from USL10. With both macromolecules as cargo, we obtained highest release for moderate-low HIFU conditions (2-25 MPa) and 1-2 min exposure time. At higher acoustic pressures or longer exposure times the percentage of HRP and of ML1 recovered decreased and we speculate that it is due to the cargo damage. We therefore continued our experiments using 1 min exposure time and 2MPa/25MPa acoustic pressures.

Remarkably, NUSLs also showed HIFU triggered release, although the released amounts were considerably lower than observed for USL. It has been previously observed that normal liposomes can respond to ultrasound fields [40,45]. Evjen et al. demonstrated that conventional liposomes can be triggered by ultrasound especially when DSPE has been included in the formulation [45].

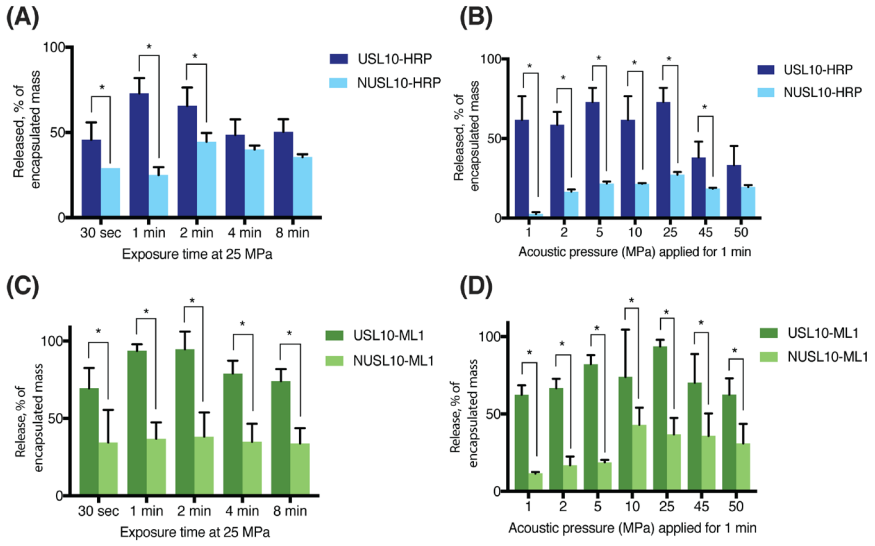

Figure 3 – HRP (A and B) and ML1 (C and D) release from USL10 at different intervals of time at constant acoustic pressure of 25 MPa (A and C) and a wide range of acoustic pressures for 1 min HIFU treatment (B and D), n=2.

The authors speculated that DSPE promotes the formation of membrane defects and polymorphic rafts, which may create larger membrane defects that allow release of drugs under ultrasound application. Doxorubicin was released from such so-called sonosensitive liposomes (DSPE:DSPE-PEG_{2000}:Chol 62:8:30 mol%) 7-fold more than from reference doxorubicin-loaded liposomes (HSPC:DSPE-PEG_{2000}:Chol 57:5:38 mol%) [45]. Our results show that also much larger macromolecules like HRP and ML1 can be released from DSPE-PEG2000 containing liposomes but the release extent can be significantly improved by incorporating the PFC nanoemulsion.

To investigate whether the HIFU-triggered release of USL really depended on the inclusion of PFC nanodroplets inside the liposomes, we evaluated the release of HRP from a physical mixture of NUSL and PFC nanoemulsions. Since we did not further treat the NUSL to promote encapsulation of the PFC nanodroplets, this formulation does not contain the merged nanoparticles in which PFC is encapsulated in the inner volume of USL. HRP release from such after different acoustic pressures (1-25 MPa) and fixed exposure time (1 min) is shown in **Figure 4**. The formulations containing emulsion only on the outside (NUSL*x*+PFC) showed an intermediate release performance (**Figure 4c**). This shows that the presence of the nanoemulsion is influencing drug

release also when it is not encapsulated in the liposomes, possibly by energy transfer to the lipid bilayer that can deform the bilayer from outside. However, the physical mixtures of PFC nanodroplets with NUSL were much less effective in releasing the loaded cargo than USL (**Figure 4b**). Moreover, the concentration of PFC in the physical mixture was relatively high in comparison with the USL formulation since these samples did not follow the sugar gradient purification step of the USL formulations. It therefore seems plausible that phase transition of PFC from liquid to gas and the resulting expansion from within the USL is the mechanism for payload release. USL20 and USL10 released the highest amounts of HRP while USL 5 released the least of the three formulations. However, USL20 showed the least storage stability, as noticed above. Overall USL10 stands out as the best formulation and we continued to use this formulation for cell-based studies.

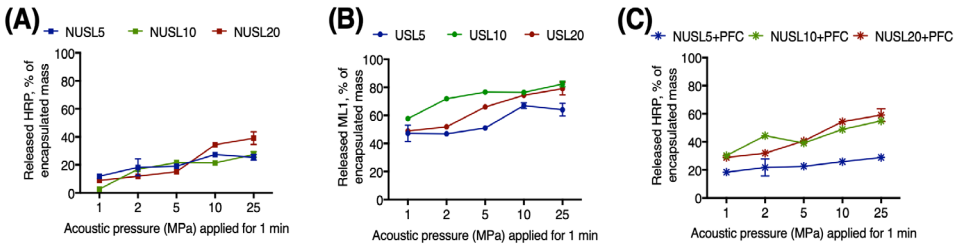

Figure 4 – HRP release profiles from (A) NUSL, (B) USL and (C) NUSL mixed with nanoemulsion. Samples were exposed to HIFU for low acoustic pressure range (1-25 MPa) for 1 min exposure (n=2). In all graphs, the colors of the lines correspond to the same lipid composition. Red line: liposomal formulations composed of initial 20% mol DSPE-PEG_{2000} (USL20); green line: liposomal formulations composed of initial 10% mol DSPE-PEG_{2000} (USL10); blue line: liposomal formulations composed of initial 5% mol DSPE-PEG_{2000} (USL5).

All three USL formulations containing ML1 were tested for HIFU-triggered release. Results of release experiments with different acoustic pressures are summarized in **Figure 5**. Similar to HRP-loaded USL formulations, USL5 released less ML1 than its counterparts USL20 and USL10. In conclusion, the formulations can be ordered according to their overall performance: USL20 < USL5< USL10.

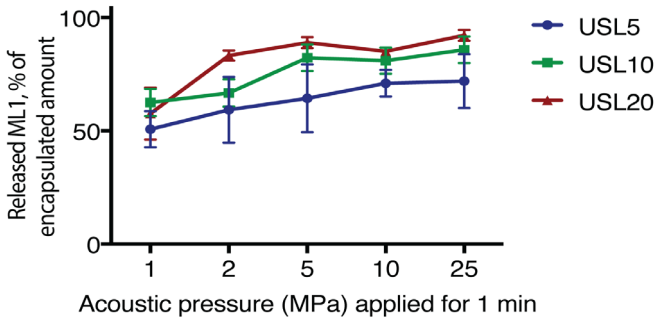

Figure 5 – ML1 release profiles from the USL formulations after exposure to HIFU for 1 min and variable acoustic pressure (1-25 MPa). The red line corresponds to liposomal formulations composed of initial 20% mol DSPE-PEG_{2000} containing PFC nanoemulsion (USL20); the green line corresponds to liposomal formulations composed of initial 10% mol DSPE-PEG_{2000} containing PFC nanoemulsion (USL10); the blue line corresponds to liposomal formulations composed of initial 5% mol DSPE-PEG_{2000} containing PFC nanoemulsion (USL5).

3.3 Bioactivity of free and formulated ML1

To investigate the overall bioactivity of the formulated ML1 we studied two phenomena related to the functionality of the protein. ML1 is composed of a cytotoxic A-chain linked to the lectin B-chain responsible for cellular binding and for mediating the protein uptake [46]; thus cytotoxic activity is ensured if the structure of the protein is conserved. Taking this in mind, we studied both uptake of ML1 in CT26 cells and its cytotoxic activity. Uptake of ML1 was visualized by live-cell confocal fluorescence microscopy, using fluorescently labeled ML1 loaded in fluorescently labeled liposomes. CT26 cells were incubated for 4h with HIFU-treated formulations, and the released ML1 induced cytotoxicity was measured 48 h later, as described before [17,37].

3.3.1 Uptake of released ML1

Figures 6 shows the live-cell confocal fluorescence microscopy pictures and semi-quantitative analysis of the uptake study. We detected cell-associated AF647-ML1 signal when the protein had been released from liposomes, or (in control experiments) added free AF647-ML1 to the cells. NUSL did not release ML1, either untreated or after HIFU treatment. USL10 on the other hand, showed some spontaneous release without HIFU treatment which was only detected by the image analysis software. After HIFU treatment and at both acoustic conditions, ML1 released from USL10 was internalized by CT26, resulting in a punctuated red pattern in the cells cytoplasm. In the latest timepoint, ML1 was also found co-localized with the cell nucleus.

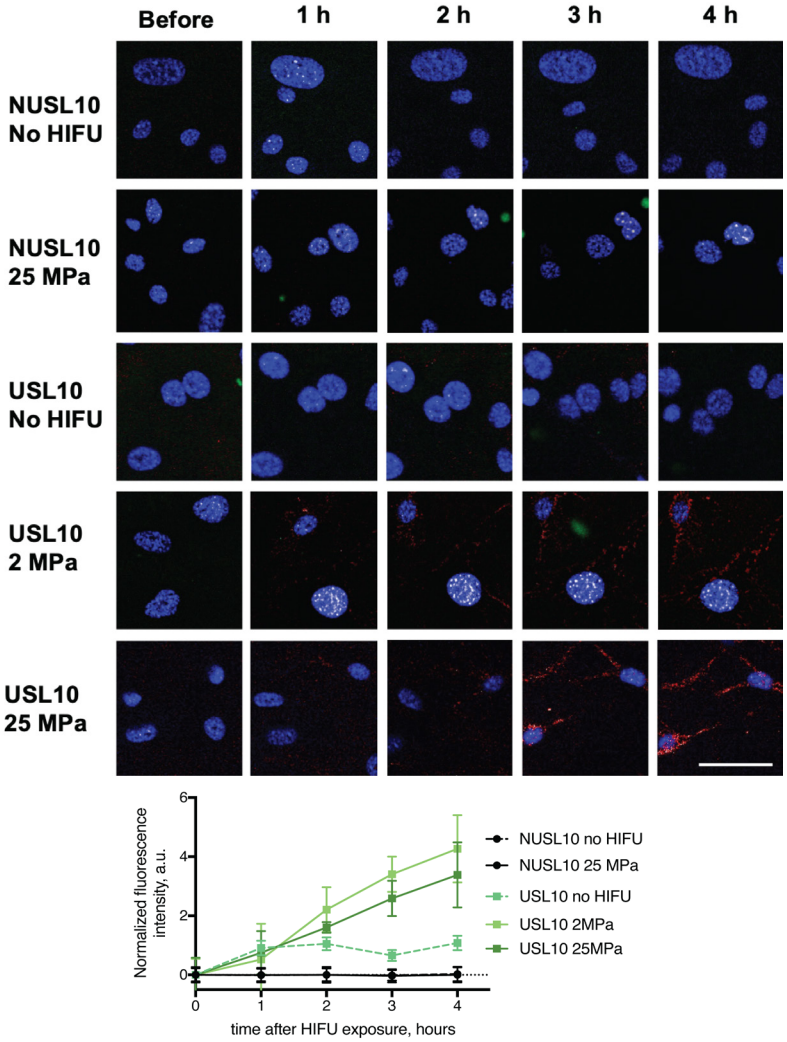

Figure 6 – Uptake of ML1 released from NUSL10 and USL10 after HIFU treatment. Liposomal formulations were diluted in cell culture media and transferred without further processing onto CT26 and cells were evaluated for 4 h uptake of ML1 by live cell imaging. For the uptake studies, liposomes were labeled with DiO' (green) while ML1 was labeled with AF647 (red). Nuclei of CT26 were stained with Hoechst 33342 (blue) prior to addition of the preconditioned culture media. Scale bar is 50 micron and is applicable to all images. Timepoint "Before" corresponds to the point immediately before adding the liposomes, i.e. cells not exposed yet to treatments. Semi-quantitative analysis of co-localization of the cell cytoplasm and AF647ML1 released from NUSL10 and USL10 is shown in the graph. In the graph, the black-full and black dashed lines correspond to NUSL10 composed with no HIFU treatment and after 25 MPa 1 min HIFU, respectively. The green lines correspond to USL10 with no treatment (dashed green line), USL10 after 2 MPa 1 min HIFU (light green full line) and USL10 after 25 MPa 1 min HIFU (dark green full line).

3.3.2 Cytotoxic activity of ML1

CT26 cells are sensitive to ML1 in the low ng/ml range as shown before by us using similar assays as studied in the current report [17,37]; since we planned to refresh media after 4h incubation with liposomes, we now evaluated the cell killing activity of ML1 after 4h exposure followed by incubation with fresh culture medium for 44 h. We also investigated whether the treatment with HIFU would affect its cytotoxicity, in view of reports that ultrasound can lead to local heating (> 40 °C) [47], which possibly may inactivate ML1. We exposed free ML1 to two different acoustic pressures (2 and 25 MPa) for 1 min and tested different concentrations of the thus-treated ML1 on CT26 cells. The cytotoxic profile is presented in **Figure 7** and resulted in quite similar dose-response curves and IC_{50} values of 280-350 ng/ml. We concluded that ML1 cytotoxicity is not influenced by the HIFU exposure at these experimental conditions, remaining constant around 300 ng/mL.

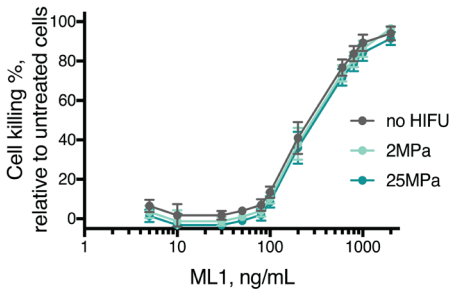

Figure 7 – Cytotoxicity of free ML1 after exposure to HIFU 1 min 2 MPa (light blue line) and 25 MPa (dark blue line). After HIFU treatment, ML1 was incubated with CT26 cells for 4h, following which the medium was replaced by toxin-free medium. The IC_{50} was measured indirectly by MTS after 48 h. Free ML1 without any HIFU treatment was used as reference (grey line) and incubated with cells using the same protocol. Untreated cells were used as 0% killing control (n=2). Untreated ML1 had an IC_{50} of 281 ng/mL, 2MPa treated ML1 an IC50 of 316 ng/mL and 25MPa ML1 an IC_{50} of 345 ng/mL.

As we demonstrated in the previous sections, only ML1-USL formulations were able to release ML1 when exposed to HIFU, while ML1-NUSL released the cytotoxic cargo to a much lower extent. This result was confirmed by the cytotoxicity evaluation of ML1 containing liposomes. Viability of CT26 after treatment with ML1-NUSL10 was only affected minimally, as only 10% cell killing was observed irrespective of HIFU had been applied (**Figure 8**). These results are in good agreement with the live-cell imaging studies in which no uptake was visualized from ML1-NUSL10 (see **Figure 6**). Since ML1 is such

a potent cytotoxin, the cell viability assay can detect the minor amount of release while the confocal fluorescence microscope was not sensitive enough to detect such low amounts of AF647ML1 (in the ng/ml range). When no HIFU was applied to ML1-USL10, there was 30% cell killing for the highest tested concentration. Extrapolation of the cell killing curve, indicates that it would require ca. 950 ng/mL of released ML1 to reach 50% cell killing. This is in line with the uptake quantification results (**Figure 6**) where the uptake difference was 4-fold different between the HIFU-exposed formulations and the non-treated formulation.
Regarding ML1-USL10, potent cytotoxic activity was observed, corresponding to IC_{50} values of 471 ng/ml and 408 ng/ml for 2 MPa and for 25 MPa, respectively.

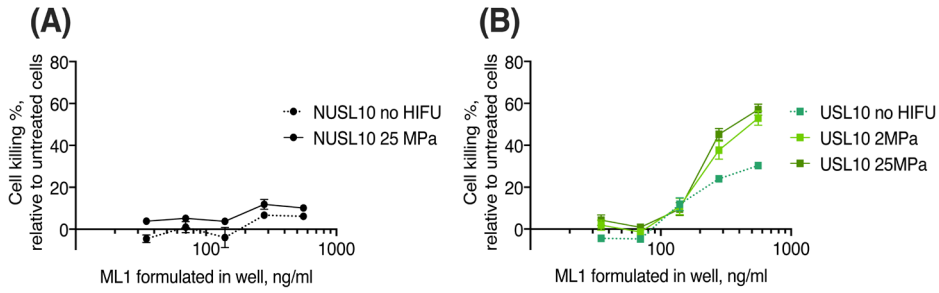

Figure 8 – Bioactivity of ML1- NUSL10 (A) and ML1-USL10 (B) were exposed to HIFU. The ML1-loaded formulations were in contact with cells for 4h to allow the uptake of released ML1, then the medium was replaced by fresh medium and the cytotoxicity was measured 44 h later. The black-full and black-dotted lines correspond to NUSL10 composed with no HIFU treatment and after 25 MPa 1 min HIFU, respectively. The green lines correspond to USL10 with no treatment (dashed green line), USL10 after 2 MPa 1 min HIFU (light green full line) and USL10 after 25 MPa 1 min HIFU (dark green full line).

We compared the amount of released ML1 as shown in **Figure 5** with cytotoxic data of **Figure 8**. Although similar outcomes are observed, small differences in experimental setup such as different media and different detection methods can be the cause for different quantitative outcome of both sets of experiments. Release experiments with ML1-ULS10 in which ML1 was quantified by ELISA (**Figure 5**) showed approx. 60-70% release for either HIFU condition. In comparison, ML1-ULS10 cytotoxicity experiments in CT26 (**Figure 8**) showed 67 and 84% ML1 release for 2 MPa and 25 MPa HIFU (as calculated from the relative IC_{50} values for free and liposomal ML1). Collectively, these results confirm that HIFU is capable of triggering ML1 release from USL.

Conclusion

We have demonstrated the loading of the high-molecular weight toxin ML1 in ultrasound sensitive liposomes is feasible. We tested three distinct formulations in terms of stability, release and in vitro bioactivity. Overall, two USL formulations, USL10 and USL5, complied with the requirements of stability, while USL10 stood out as the formulation that released the highest amounts of ML1. Our experiments with CT26 cells confirmed that ML1-USL10 was preventing target cells from its cytotoxicity, and that ML1 only acted as potent cytotoxin after HIFU treatment. We therefore conclude that the encapsulation of ML1 in ultrasound sensitive liposomes has successfully improved its activity and safety profile.

References

[1] A. L. Demain, P. Vaishnav, Microb. Biotechnol. 2011, 4, 687.
[2] A. Mukherjee, S. Basu, N. Sarkar, A. Ghosh, Curr. Med. Chem. 2001, 8, 1467.
[3] D. J. Newman, G. M. Cragg, J. Nat. Prod. 2016, 79, 629.
[4] L. M. Roberts, J. M. Lord, Curr. Opin. Biotechnol. 1992, 3, 422.
[5] M. Marvibaigi, E. Supriyanto, N. Amini, F. A. Abdul Majid, S. K. Jaganathan, Biomed Res. Int. 2014, 2014, 785479.
[6] P. Fritz, J. Dippon, T. Kierschke, I. Siegle, A. Möhring, A. Moisa, T. E. Mürdter, Anticancer Res. 2004, 24, 1187.
[7] K.-C. Kim, J.-H. Yook, J. Eisenbraun, B.-S. Kim, R. Huber, BMC Complement. Altern. Med. 2012, 12, 172.
[8] M. Horneber, G. Bueschel, R. Huber, K. Linde, M. Rostock, M. Horneber, G. Bueschel, R. Huber, K. Linde, M. Rostock, Cochrane Libr. 2010, 4.
[9] T. M. Allen, P. R. Cullis, Adv. Drug Deliv. Rev. 2013, 65, 36.
[10] M. van Elk, B. P. Murphy, T. Eufrásio-da-Silva, D. P. O'Reilly, T. Vermonden, W. E. Hennink, G. P. Duffy, E. Ruiz-Hernández, Int. J. Pharm. 2016, 515, 132.
[11] T. Stylianopoulos, R. K. Jain, Nanomedicine Nanotechnology, Biol. Med. 2015, 11, 1893.
[12] A. Wicki, D. Witzigmann, V. Balasubramanian, J. Huwyler, J. Control. Release 2015, 200, 138.
[13] Z. Al-Ahmady, K. Kostarelos, Chem. Rev. 2016, 116, 3883.
[14] V. Saxena, C. Gacchina Johnson, A. H. Negussie, K. V. Sharma, M. R. Dreher, B. J. Wood, Int. J. Hyperth. 2015, 31, 67.
[15] X. Huang, M. Li, R. Bruni, P. Messa, F. Cellesi, Int. J. Pharm. 2017, 524, 279.
[16] Y. Yuyama, M. Tsujimoto, Y. Fujimoto, N. Oku, Cancer Lett. 2000, 155, 71.
[17] M. B. C. de Matos, N. Beztsinna, C. Heyder, M. H. A. M. Fens, E. Mastrobattista, R. M. Schiffelers, G. Leneweit, R. J. Kok, Eur. J. Pharm. Biopharm. 2018, 132, 211.
[18] W. G. Pit, Ghaleb Husseini, Technique for Drug and Gene Delivery to the Cell Cytosol, n.d., US20110104258A1.
[19] M. Javadi, W. G. Pitt, D. M. Belnap, N. H. Tsosie, J. M. Hartley, Langmuir 2012, 28, 14720.
[20] J. R. Lattin, 2012.
[21] J. R. Lattin, W. G. Pitt, D. M. Belnap, G. A. Husseini, Ultrasound Med. Biol. 2012, 38, 2163.
[22] J. R. Lattin, D. M. Belnap, W. G. Pitt, Colloids Surfaces B Biointerfaces 2012, 89, 93.
[23] M. Javadi, W. G. Pitt, C. M. Tracy, J. R. Barrow, B. M. Willardson, J. M. Hartley, N. H. Tsosie, J. Control. Release 2013, 167, 92.
[24] J. R. Lattin, W. G. Pitt, J. Pharm. Sci. 2015, 104, 1373.
[25] C. Y. Lin, M. Javadi, D. M. Belnap, J. R. Barrow, W. G. Pitt, Nanomedicine Nanotechnology, Biol. Med. 2014, 10, 67.
[26] J. R. Lattin, M. Javadi, M. McRae, W. G. Pitt, J. Drug Target. 2015, 2330, 1.
[27] G. a. Husseini, W. G. Pitt, M. Javadi, Technol. Cancer Res. Treat. 2015, 14, 379.
[28] R. Suzuki, T. Takizawa, Y. Negishi, N. Utoguchi, K. Maruyama, Int. J. Pharm. 2008, 354, 49.
[29] R. Suzuki, E. Namai, Y. Oda, N. Nishiie, S. Otake, R. Koshima, K. Hirata, Y. Taira, N. Utoguchi, Y. Negishi, S. Nakagawa, K. Maruyama, J. Control. Release 2010, 142, 245.
[30] A. Bouakaz, M. Versluis, N. de Jong, Ultrasound Med. Biol. 2005, 31, 391.
[31] V. P. Torchilin, AAPS J. 2007, 9, E128.
[32] Y.-Z. Zhao, Y.-K. Luo, C.-T. Lu, J.-F. Xu, J. Tang, M. Zhang, Y. Zhang, H.-D. Liang, J. Drug Target. 2008, 16, 18.
[33] N. . Rapoport, D. . Christensen, H. . Fain, L. Barrows, Z. Gao, Ultrasonics 2004, 42, 943.
[34] W. G. Pitt, R. N. Singh, K. X. Perez, G. A. Husseini, D. R. Jack, Ultrason. Sonochem. 2014, 21, 879.
[35] P. S. Sheeran, S. H. Luois, L. B. Mullin, T. O. Matsunaga, P. A. Dayton, Biomaterials 2012, 33, 3262.
[36] P. S. Sheeran, N. Matsuura, M. A. Borden, R. Williams, T. O. Matsunaga, P. N. Burns, P. A. Dayton, IEEE Trans. Ultrason. Ferroelectr. Freq. Control 2017, 64, 252.
[37] N. Beztsinna, M. B. C. de Matos, J. Walther, C. Heyder, E. Hildebrandt, G. Leneweit, E. Mas-

trobattista, R. J. Kok, Sci. Rep. 2018, 8, 2768.
[38] R. Eifler, K. Pfuller, W. Gockeritz, U. Pfuller, in Lectins 9 Biol. Biochem. Clin. Biochem. (Eds: J. Basu, M. Kundu, P. Chakrabari, T. Bog-Hansen), Wiley Eastern Limited, New Delhi, 1993, pp. 1–5.
[39] G. Rouser, S. Fleischer, A. Yamamoto, Lipids 1970, 5, 494.
[40] C. Oerlemans, R. Deckers, G. Storm, W. E. Hennink, J. F. W. Nijsen, J. Control. Release 2013, 168, 327.
[41] M. C. Sandström, E. Johansson, K. Edwards, Biophys. Chem. 2008, 132, 97.
[42] E. Johansson, C. Engvall, M. Arfvidsson, P. Lundahl, K. Edwards, Biophys. Chem. 2005, 113, 183.
[43] K. Vainikka, K. Reijmar, G. Yohannes, J. Samuelsson, K. Edwards, M. Jussila, M.-L. Riekkola, Anal. Biochem. 2011, 414, 117.
[44] M. Johnsson, K. Edwards, Biophys. J. 2003, 85, 3839.
[45] T. J. Evjen, E. A. Nilssen, S. Rögnvaldsson, M. Brandl, S. L. Fossheim, Eur. J. Pharm. Biopharm. 2010, 75, 327.
[46] E. Pizzo, A. Di Maro, J. Biomed. Sci. 2016, 23, 54.
[47] K. Ng, Y. Liu, Med. Res. Rev. 2002, 22, 204.

Supplementary information

Encapsulation and ultrasound-triggered release of mistletoe lectin-1 from liposomes

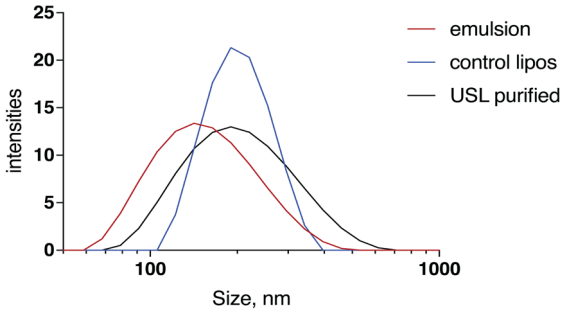

Supplementary Figure 1 – Typical size distributions of nanoparticles containing 10 mol% of DSPE-PEG_{2000} at the initial formulation. of the NUSL10. Blue line: NUSL10; red line: PFC nanoemulsion; black line: USL10. NUSL5 and USL5 had similar size distributions.

Part IV | New technologies for preparation of nanocarriers

Chapter 6 -Liposomes with asymmetric bilayers produced from inverse emulsions for nucleic acid delivery

Maria B. C. de Matos, Bárbara S. Miranda, Yudha Rizky Nuari, Gert Storm, Gero Leneweit, Raymond M. Schiffelers and Robbert J. Kok

Journal of Drug Targeting (2019)

DOI: 10.1080/1061186X.2019.1579819

Abstract

Asymmetrical lipid nanoparticles are interesting nanocarriers for charged molecules, like nucleic acids. They promise control over inner and outer charge. High charge density on the inside is favorable for efficient condensation and charge neutralization of highly charged biopharmaceuticals, while a neutral or slightly negative outer layer promotes biocompatibility. The main goal of this work was the development and characterization of asymmetric liposomes, prepared using water in oil (w/o) nanoemulsions of phospholipids and squalene in a centrifugal field. This method enables the control over the lipid composition of each monolayer.

Liposomes were prepared by passing phospholipid w/o nanoemulsions through an oil-water interface previously saturated with phospholipids. We used NBD-PE/PC as a fluorescent marker for either the inner or outer lipid layer and plasmid DNA as nucleic acid payload. The final liposomes had sizes below 200 nm and polydispersity indexes of 0.3 and had a bilayer asymmetry of 70%, thus shielding the charge of positive phospholipids in the inner bilayer leaflet. Final formulations were examined using negative staining transmission electron microscopy (TEM). Plasmid encapsulation efficiency of the method was 10-15%. Our results indicate that the w/o nanoemulsion-centrifugation method allows the successful production of liposomes with tailored features for encapsulation of nucleic acid therapeutics.

Keywords: Lipid bilayers; water-in-oil emulsification; phase transfer; asymmetric vesicles; pDNA encapsulation

1. Introduction

Nucleic acids therapeutics have been widely accepted as a cornerstone of future molecular medicine, aiming for precise and targeted intervention in diseases. The main limitation of using such molecules in a therapeutic setting is their inability to enter cells, which is related to their negative charge that impairs the passage over target cells' membranes. In addition, they tend to be rapidly degraded and cleared [1–4]. Biological and synthetic nanoparticles have been suggested as delivery vehicles for nucleic acids to overcome such problems. Viral vectors that include retroviruses, adeno-associated viruses and lentiviruses, are efficient vehicles. However, they may provoke mutagenesis and carcinogenesis and repeated administration can trigger immune responses that impair payload delivery. Therefore, non-viral vectors (e.g. lipoplexes) are an attractive alternative [5].

Nucleic acids can be efficiently entrapped into lipoplexes. Electrostatic interactions between positively charged lipids and negatively charged nucleic acids are a strong driving force for effective encapsulation. In addition, cationic lipids can play a role in destabilizing the endosomal membrane facilitating functional nucleic acid release. However, nanocarriers with a cationic surface charge are rapidly removed and cleared by RES in the primary organs, which constitutes the major obstacle for their therapeutic efficacy. In addition, aggregation with negatively charged blood components may occur and that can produce severe adverse effects such as clogging of capillaries in the lungs. The traditional way of circumventing this is by shielding the positive charge of the carrier with DSPE-PEG_{2000}. However, this shielding is often suboptimal as evidenced by the fact that cationic PEG-liposomes never reach circulatory half-lives encountered for neutral or negatively charged PEG-liposomes [4].

Asymmetric nanocarriers with a neutral or negatively charged surface may combine the best of both worlds: protection of the nucleic acid as well as improved biocompatibility [4]. A variety of procedures have been described for preparing formulations with asymmetric bilayers [6]. The choice of the appropriate method is dependent on the required size and characteristics of the nucleic acids during the production process of the nanocarrier, in relation to the composition of the nanocarrier [1].

An innovative method to prepare liposomes, which has attracted attention recently [7–11], is based on the inverted emulsion or phase transfer method. It involves the transfer of water-in-oil (w/o) emulsion droplets through an oil-water interface saturated with a phospholipid monolayer. The transfer process might occur either spontaneously [11–14], and/or use centrifugal force [7,15–

18] and/or use sugar gradients [7,13,17,18], as represented in the scheme in **Figure 1**.

In practice, an oil phase containing dispersed phospholipids is poured on top of an aqueous phase. The phospholipids diffuse towards the water/oil interface to form a monolayer, which will serve as the external layer of the liposome. Next, the inverted w/o emulsion can be created using several methods. This emulsion should have appropriate stability to avoid nucleic acid leakage and a suitable size to serve as the inner leaflet of a liposome. This emulsion is carefully placed onto the interface and either spontaneously or external force, the w/o droplets will cross the interface and pick up a second layer of lipids, forming liposomes [7,8,21,22,9–11,14,15,18–20].

Zhang and co-workers obtained 50-200 nm size liposomes with relatively high encapsulation efficiencies of 6-carboxyfluorescein [22]. Pautot et al have shown that this technique can yield unilamellar liposomes with sizes ranging from 100-1000 nm and encapsulation efficiencies of pyrene-labeled actin that corresponded to 98 % [15,16,20]. Later research using the phase transfer method focused mainly on the production of giant liposomes and the study of droplet-transfer phenomena through the oil-water interface [12,19], encapsulation of nucleic acids [8,23,24], actin reconstitution [17], and other uses as synthetic cell models [7,18]. The technology is also popular to address fundamental aspects in cell biology, since all biological membranes are asymmetric. Taken together, the inverted emulsion-centrifugation method is a versatile method that allows relatively high encapsulation of water-soluble compounds, allows the use of various buffer conditions, and the inner and outer leaflet compositions of the liposomes can be controlled independently. Despite these advantages, the method is not suitable for industrial applications. The slow equilibration of lipid monolayers at the oil-water interface limits replenishment and thus vesicle yield. This is essentially a diffusion-based process and it depends on several parameters, like the properties of the phospholipids, oil viscosity and density. In addition, the reported sizes are often in the micrometer range and thus not suitable for intravenous administration.

Our aim was to improve the inverted-emulsion centrifugation technique for the development of nanosized asymmetric liposomes for nucleic acid delivery. We started with nanoemulsions, prepared using phospholipids and Professor Patrick Couvreur's favorite molecule: squalene. It adds another avenue of exploration for this remarkable molecule that has been studied intensively as excipient and active ingredient in his laboratory. Initially, we investigated the stability of different w/o nanoemulsions as the initial nanodroplets which form the template for the liposomes. We studied different compositions and

emulsification processes on the overall properties and stability of the nanoemulsions. We then incorporated plasmid DNA as a model compound into the most stable nanoemulsions and used the centrifugation technique to prepare liposomes.

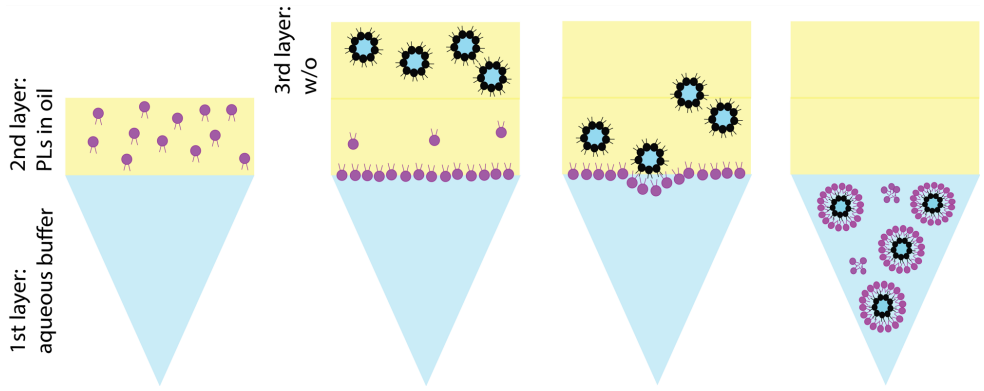

Figure 1 – Schematic representation of the inverted emulsion process. First, a phospholipid (PL) solution in oil is placed on top of the buffer phase and allowed to equilibrate to form the interface oil-water. After equilibration, the w/o emulsion is gently pipetted on top of the second layer and the system is centrifuged, allowing the w/o droplets to cross the interface. At the end of the process, liposomes are collected from the bottom of the tube.

2. Materials and Methods

2.1. Materials

Phospholipids (PL) DPPC (1,2-dipalmitoyl-sn-glycero-3-phosphocholine), DOTAP (1,2-dioleoyl-3-trimethylammonium-propane, chloride salt), DOPE (1,2-Dioleoyl-sn-glycero-3-phosphoethanolamine) and DSPE-PEG_{2000} were obtained from Lipoid (Ludwigshafen, Germany). NBD-PE (N-(7-Nitrobenz-2-Oxa-1,3-Diazol-4-yl)-1,2-Dihexadecanoyl-sn-Glycero-3-Phosphoethanolamine, Triethylammonium Salt) and NBD-PC (N-(7-Nitrobenz-2-Oxa-1,3-Diazol-4-yl)-1,2-Dihexadecanoyl-sn-Glycero-3- phosphocholine, Triethylammonium Salt) were obtained from Life technologies (Karlsruhe, Germany). HPTS (8-Hydroxypyrene-1,3,6-trisulfonic acid trisodium salt, >97%) and squalene (purity 98%) were purchased from Sigma-Aldrich (Deisenhofen, Germany).

2.2 Methods

2.2.1. Preparation of w/o nanoemulsions

Nano-emulsions (150 µL) were freshly prepared from a phospholipid (PL) solution in squalene (typically 1 mg PL/ mL squalene) [25,26]. In optimization studies we used different water fractions (1, 3, 5 and 10% w/o v/v) for a fixed

lipid composition (DPPC/DOTAP (1:1 mol:mol).
After optimization of the dispersed phase fraction, the lipid ratios and compositions were varied according to **Table 1**. The emulsions were prepared using three different emulsification instruments:

- The first method required the use of a high energy sonication (HES) method using the ultrasound sonotrode (Branson Sonifier S-450A) using 50 % power and 5 cycles. The emulsification time was varied from 1 min up to 10 min, as presented in the results section.
- The second method made use of low energy input ultrasound (LES). Samples were pre-sonicated on the sonotrode at 50% power and 5 cycles for 10 seconds, followed by emulsification in a water bath (Fisher Scientific FB15047) for 15 min.
- The last method for downsizing nanoemulsions was vortex-mixing of the nano-emulsion for 5 min followed by hand-extrusion through 400 nm and 200 nm pore size polycarbonate membranes.

Table 1 – Lipid composition and ratios used to screen 1% w/o emulsification conditions. All lipids were previously dissolved in squalene at the indicated concentrations.

Sample	Molar ratios			
	DOTAP (1.43 mM)	DOPE (1.34 mM)	DPPC (1.36 mM)	Span 80
A	1	-	5	-
B	1	5	-	-
C	1	3	3	-
D	1	-	5	0.5
E	1	5	-	0.5
F	1	2	2	0.5

2.2.2. Phospholipid equilibration at oil-water interface

The lipids used to serve as outer leaflet of the liposomes were dissolved in squalene. A 2 mL Eppendorf tube was first filled with 400 µL of HEPES buffered saline (HBS) (HEPES 10 mM, 0.9% NaCl, pH 7.4); then, 200 µL of squalene containing the outer leaflet lipids (DPPC/ DSPE-PEG2000 95:5 v/v , mol:mol ratio 72:1) was poured over the aqueous phase, and a "milky" layer formed between the oil-water interface.

2.2.3. Liposomes preparation

To finally obtain the liposomes, 150 µL of w/o nanoemulsion was added onto the intermediate phase that was previously equilibrated for approximately

2h with phospholipid monolayer. After this, samples were centrifuged for 30 minutes at 120×g to spin down all the droplets through the oil-water interface to form liposomes. Liposomes were collected from the aqueous phase and kept at room temperature until further analysis.

2.2.4. Characterization of nano-emulsions and liposomes

The hydrodynamic diameter and polydispersity index of all w/o emulsions (before centrifugation) and liposomes (after centrifugation) were measured by dynamic light scattering using a DLS Malvern Zetasizer Nano S (Malvern Instruments, Malvern, UK). The zeta-potential of the liposomes was measured using laser Doppler electrophoresis on a Zetasizer Nano Z (Malvern Instruments) with samples dispersed in 10 mM HEPES buffer pH 7.4 (with no additional salts added). Nanoemulsions were characterized in terms of stability over time. After emulsification, the nanoemulsions were monitored every 5 minutes for 1 hour, and the position of nanoemulsions was measured as a determinant for phase separation/stability as follows:

$$Phase\ stability, \% = \frac{H_t}{H_0} \times 100 \quad (1)$$

Where *Ht* is the height of the interface between the turbid nanoemulsion in the tube and the clear supernatant measured at time t, and *H0* represents the initial height.

Membrane asymmetry of liposomes was determined using a fluorescent quenching assay [27]. The liposomes were prepared by adding either NBD-PE lipid to the inner lipid layer or NBD-PC lipid to the outer lipid layer (1 mol%). The fluorescence of the resultant bilayer vesicles was measured before and after addition of a quenching agent (50µL of sodium hydrosulfite in 1M Tris at pH 10). Inner leaflet quenching was achieved by adding 50µl of Triton-X100 to lyse the bilayer vesicles, allowing access of sodium hydrosulfite and further reduction of fluorescent intensity. The measurement was done by setting the excitation wavelength at 470 nm and the emission wavelength at 550 nm in a Jasco FP8300 spectrofluorometer and calculating as follows:

$$Normalized\ Fluorescence\ Intensity, au = 100 - \left(\frac{Intensity_t}{Intensity_0} \times 100\right) \quad (2)$$

Where $Intensity_t$ is the fluorescence intensity at time t after quenching, and $Intensity_0$ represents the initial signal.

The overall lipid recovery (yield) was determined by determination of PL in the water phase according to the method of Rouser using sodium dihydro-

gen phosphate as a standard [28]. The total lipid was then derived from the amount of PL present in the formulation.

The structure of the final nanoparticles was visualized by negative staining transmission electron microscopy (TEM). In brief, the sample was placed on a carbon-coated copper grid (300 mesh; Plano GmbH, Germany) and allowed to settle for 2 min before being blotted away by filter paper. A 1% ammonium molybdate solution was added to the grid for 2 min before the solution was blotted away and the grid was allowed to dry. Images were recorded at 120 kV on a Philips CM12 transmission electron microscope coupled to a GATAN Multiscan 400HP camera.

2.3. Preparation and characterization of nucleic acid containing emulsions and liposomes

Nano-emulsions B, E and F containing 1 mg/ml PL and ca. 200 ng of pDNA (pCMV-Lacz plasmid DNA, 7164 bp, 2.56 mg/ml; 1% w/o v/v) were freshly prepared by LES emulsification as described above. 150 μL of w/o nanoemulsion was added onto 600 μL intermediate phase that was previously formed by equilibration of 400 μL water pahse with 200 μL PL/squalene phase (see section 2.2.2.). After this, samples were centrifuged for 30 minutes at 120×g and liposomes were collected from the aqueous phase and purified by ultracentrifugation (Beckmann ultracentrifuge, 55000 rpm, 55 min). The pellet was re-suspended in fresh HBS using the initial volume of water (400 μL).

Plasmid DNA encapsulation was determined by gel electrophoresis. Agarose (Roche) 1% w/v was dissolved in 1x Tris-acetate-EDTA buffer (Bio-Rad), and after complete dissolution, propidium iodide (Invitrogen, 16 μL/gel) was added to the agarose. Prior to the experiment, DNA-containing samples were treated with Triton X100 to expose the entrapped pDNA and 8 μL of loading solution (6x solution, Thermo Scientific) was added to 20 μL samples. Electrophoresis was carried out in a vertical slab gel apparatus. Fifteen sample-wells were made by use of a comb. The power source was a regulated high-voltage power supply, and electrophoresis was carried out at 100 V 1.5 h or until the dye neared the bottom of the gel. The gel was imaged in a Gel Doc XR imager (Bio-Rad) and quantified using ImaGel software. The amounts of pDNA detected in the samples were calculated against a standard curve of pDNA in the range of 8.3 to 132.5 ng, and normalized by the amount used to prepare the emulsions:

$$Encapsulation\ efficiency\ \% = \frac{mass\ pDNA\ found\ in\ liposomes}{initial\ mass\ pDNA\ in\ emulsions} \times 100 \qquad (3)$$

3. Results and discussion

3.1. Phospholipid equilibration at oil-water interface

One of the requirements to successfully produce liposomes using the inverted emulsions in a centrifugation field is to have a fully equilibrated oil-water interface. Amphiphilic molecules dissolved in the oil phase will diffuse to the water-oil interface and align there with the hydrophilic heads towards the water phase and hydrophobic tails in contact with the oil phase. In this way, the outer leaflet is ready to receive the inner leaflet.

Typically, waiting until a white thin layer is formed is recommended [15]. In the case of DPPC/DSPE-PEG_{2000} we found that it takes approximately two hours to obtain a visible white thin layer (**Figure 2**). However, we might also speculate that this "thin layer" can be composed of multiple layers mainly composed of DPPC, as demonstrated by tensiometric measurements at oil-water interfaces by [25,29].

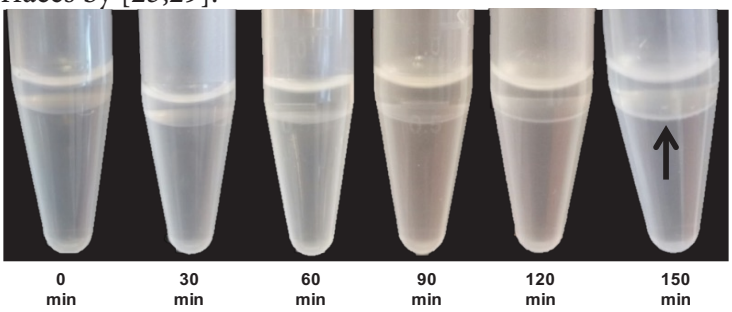

Figure 2 - Time series of oil-water interface equilibrium images. Each image was captured every 30 minutes for 2.5 hours to allow the interface to be lipid-rich. After 2.5 hours at room temperature, a milky thin layer, as pointed by the arrow, was finally formed showing that the interface has already been fully equilibrated.

3.2. Stability and phase separation in w/o nanoemulsions

We first evaluated the effect of varying the PL:water ratio on the stability of w/o nanoemulsions. We hypothesized that a higher PL:water ratio (i.e. less water) results in higher stability of the w/o nanodroplets [16]. The water fraction was varied between 1 and 10 % v/v. the total volume and lipid composition and emulsification method (HES) were kept constant (**Figure 3 A**).

Indeed, the emulsion containing 1% water showed the longest emulsion stability, up to 30 minutes after emulsification. Higher water contents showed emulsion sedimentation within 10 to 15 minutes after emulsification (**Figure 3 B**).

(A)

w/o emulsion, v/v %	Formulation, v/v % DOTAP (1.43 mM)	DPPC (1.36 mM)
10	15	75
5	15	80
3	15	82
1	15	84

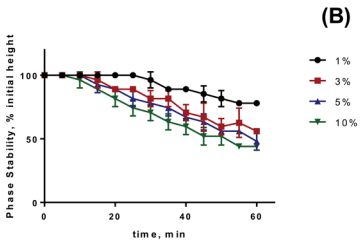

Figure 3 – Lipid composition and ratios used to screen the effect of water fraction in the emulsion stability. (A) composition of nanoemulsions. All lipids were previously dissolved in squalene at the indicated concentrations. (B) Phase stability of nanoemulsions prepared by variations of water content. The measurements were done by observing and measuring the height of phase separation for 60 minutes after preparation with 5-minutes interval per observation.

These results are in line with the results of Pautot et al [16] and confirm that the phase stability of inverted emulsions is improved by minimizing the amount of water in the composition. For this reason, formulations containing 1% water were used in the next experiments.

Additional functional lipids and surfactants were added to further improve the stability of the emulsions. [15], Span 80 has a hydrophilic-lipophilic balance (HLB as defined by Griffin) of 4.3 which is ideal for w/o emulsification and stabilization [15,30–33]. In addition, we introduced DOPE which has been used before for stabilization of w/o emulsions [34,35] and which is assumed to help in improving endosomal escape of nucleic acids.

Figure 4 shows that the use of both span 80 and DOPE/DPPC enhanced the stability the emulsions (formulations C and D). Surprisingly, formulations B, E and F showed complete stability even up to 3 h after emulsification. These results support the notion that DOPE is very important for emulsion stabilization and that it tolerates the additional inclusion of PC and Span80. The choice of DOPE as stabilizer phospholipid favors the negative curvature as this lipid has a relatively small polar head group [36,37].

Additionally, DOTAP was chosen as the cationic lipid, not only to increase the encapsulation efficiency of negatively charged payloads like siRNA, but also to stabilize the w/o emulsion in an unsaturated hydrocarbon like squalene. We hypothesized that the self-arrangement of the lipids would affect stability due to the presence of unsaturated bonds, headgroup size and electrostatic interactions. According to [25], there are large differences between, for example, POPC and DPPC at water-squalene interfaces. The disparities in area per molecule and critical aggregation concentration between different PCs were attributed to fatty acid saturation, where the presence of the double bond in oleoyl chain in POPC led to higher attractive (π-π) interactions between un-

saturated oil phase and unsaturated fatty acids of POPC, and less attractive interactions between saturated fatty acids chains of DPPC and squalene [25]. Emulsions containing a highly unsaturated hydrocarbon like squalene together with unsaturated (phospho)lipids are therefore more stable.
The three formulations with highest stability (B, E, F) were used for further optimization the emulsification method.

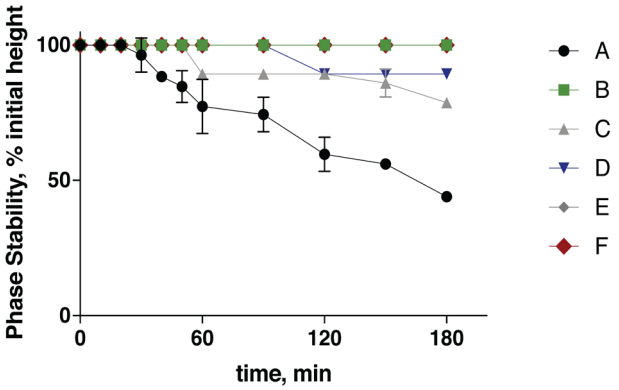

Figure 4 - Phase stability of w/o emulsions produced with different compositions as provided in Table 1. The measurements were done by observing and measuring the height of nanoemulsions for 180 minutes after preparation.

3.3. Comparison of emulsification methods

3.3.1. Hand extrusion

Emulsions corresponding to setups B, E and F were first vortexed for 5 minutes, followed by extrusion over 400 nm and 200 nm pore filters to reduce size and PDI of nanoemulsion droplets. Although extrusion is an excellent method for liposomes preparation, in the case of w/o nanoemulsions large variations were observed in both droplets size and PDI between batches, resulting in low reproducibility (**Table 2**). Thus, for squalene-based w/o emulsions, this method is not appropriate as the viscosity of the oil phase impairs the process. Stability results of hand-extruded nanoemulsions is shown in **Supplemental Figure 1**. The size of droplets increased from 150 nm to 300 nm during the first 15 minutes after extrusion; the droplets size even reached 600-700 nm 1 h after extrusion. The polydispersity index showed the same trend, increasing four-fold in 1 h. These findings suggest that hand-extruded emulsion had low stability. Whittenton et al [23] also reported the same phenomena; they suggested to measure and process the emulsion immediately after preparation [23].

Table 2 – Size and PDI of three different batches of formulations B, E and F. The results suggest high variability between batches.

Formulation	Size (nm)			PDI		
	Batch 1	Batch 2	Batch 3	Batch 1	Batch 2	Batch 3
B	346	161	412	0.24	0.15	0.29
E	103	270	434	0.11	0.25	0.32
F	290	118	402	0.29	0.19	0.40

3.3.2. High-energy sonication (HES)

The three potential formulations showed very high stability in section 3.2 (B, E and F) but displayed very poor reproducibility and stability when processed by hand-extrusion (section 3.3.1). Thus, a high energy input emulsification method was employed. Ultra-sound sonication offers ease of operation and it is not as time consuming as other techniques [36,37].

The optimal sonication time was investigated by varying the time from 1 min up to 10 min. longer emulsification times were not investigated because increasing energy input may lead to API degradation.

Figure 5 and **Table 3** show that the droplet size decreased to minimally 100 nm, PDI 0.2 with increasing sonication time. This size and PDI was reached after 5 min sonication. Prolonging sonication time to 10 min did not further reduce these parameters. These results are in agreement with the results of Delmas et al [37].

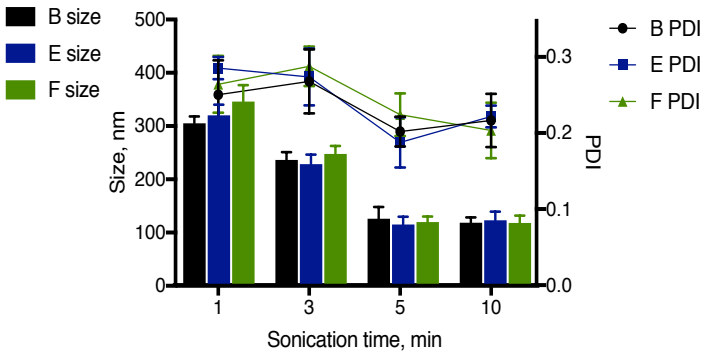

Figure 5 – Size (columns) and PDI (lines) of w/o emulsion produced from formulations B (black), E (blue) and F (green) obtained after 1 – 10 min of HES exposure. Samples were emulsified using the same energy settings.

All three nanoemulsions B, E and F were subjected to centrifugation to produce liposomes. We expected to obtain similar sizes and PDI for the final liposomes as observed for the respective nanoemulsions, as the w/o nanoemulsion serves as a template for the final vesicles which would only add a single lipid leaflet.
A comparison between the emulsion and final liposomes is shown in **Figure 6**. Astonishingly, the resulting liposomes were much bigger (mean diameter 400-500 nm) than the initial w/o nanoemulsions (mean diameter 130-160 nm). Potential problems that may have resulted in an increased size are fusion of nanoemulsion droplets at the squalene/water interface, or inclusion of squalene oil in the phospholid layer thus not forming a true phospholipid unilamellar bilayer of the liposomes. Similar observations were made previously [23]. Even emulsions stabilized by a surfactant, formulation B and E, resulted in much larger liposomes, indicating processes of either emulsion instability or aggregation during phase transfer.

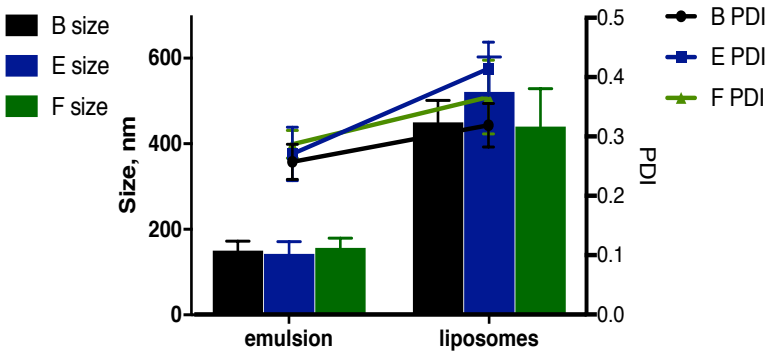

F**igure 6 –** Comparison between the w/o emulsions produced by HES and resulting liposomes, in terms of size (columns) and PDI (lines). Emulsions and corresponding liposomes were produced from formulations B (black), E (blue) and F (green).

3.3.3. Low-energy sonication (LES)

As an alternative to high energy sonication, the water bath sonicator is a milder technique in terms of mechanical stress, circumventing the possibility of denaturing sensitive APIs [38]. In a bath sonicator, the force is transferred indirectly through the medium so that the wave generated is milder, yet still able to downsize the particle with less destructive potential. Furthermore, a bath sonicator offers a more homogenous distribution of the wave resulting in the formation of more homogenous droplets sizes, whereas a probe tip soni-

cator relies mainly on the depth of the tip submerged which determines the distribution of the wave into the samples.
As shown in **Figure 7**, **Figure 8** and **Table 3**, we could obtain w/o nanoemulsions with a size below 150 nm after 15 min of ultrasound exposure. These were subjected to centrifugation to produce liposomes which had an acceptable size (below 200 nm) and PDI (PDI 0.2-0.3). Although subject to artifacts introduced by sample preparation, negative staining TEM images (**Figure 8**) suggest that the liposomes resemble the size measured by DLS. Moreover, it appears that addition of Span 80 or DPPC/Span 80 is not necessary. All three formulations where investigated for asymmetry and plasmid DNA encapsulation.

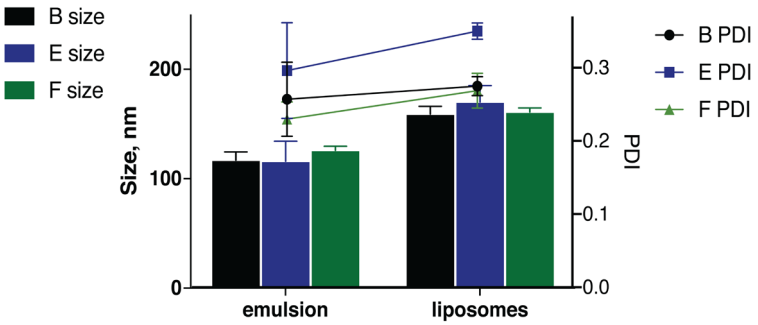

Figure 7 - Comparison between the w/o emulsions produced by LES and resulting liposomes, in terms of size (columns) and PDI (lines). Emulsions and corresponding liposomes were produced from formulations B (black), E (blue) and F (green).

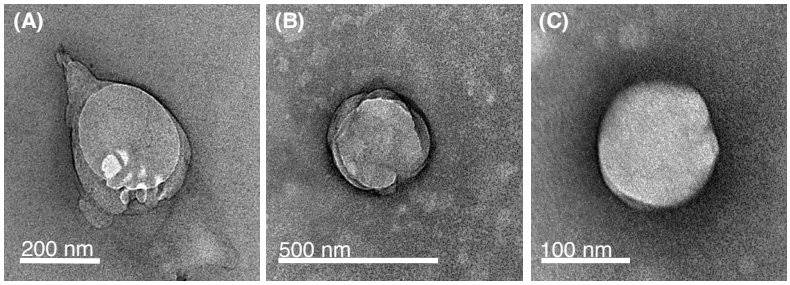

Figure 8 - TEM images of negatively stained liposomes produced from formulations B (panel A), E (panel B) and F (panel C) by low-energy sonication (LES).

Table 3 – Summary of the sizes and PDI of the 1% w/o emulsion provided by the three emulsification methods used in this study.

	Formulation, v/v %				Hand-extrusion		High energy ultrasound (HES)		Low energy ultrasound (LES)	
	DOTAP 1.43 mM	DOPE 1.34 mM	DPPC 1.36 mM	Span 80	Size, nm	PDI	Size, nm	PDI	Size, nm	PDI
B	15	84	-	-	306 ± 130	0.30 ± 0.07	126 ± 22	0.20 ± 0.02	159 ± 7	0.28 ± 0.01
E	15	79	-	5	269 ± 166	0.33 ± 0.11	115 ± 14	0.19 ± 0.03	170 ± 15	0.35 ± 0.01
F	15	39.5	39.5	5	270 ± 143	0.40 ± 0.11	120 ± 14	0.22 ± 0.03	161 ± 4	0.27 ± 0.02

3.4. Asymmetry of lipid bilayers of liposomes

For the bilayer asymmetry studies, 1 mol% of fluorescent NBD-PE was added to the nano-emulsions that formed the inner lipid leaflets, or 1 mol% of NBD-PC was added to the outer lipid composition that was used to saturate the oil-water interface. The addition of NBD-labeled lipids did not influence the size of the vesicles. Sodium hydrosulfite (1M $Na_2S_2O_4$ in Tris pH 10) was employed as a quencher. Since this molecule does not diffuse across lipid bilayers, it will only quench NBD in the outer lipid leaflet, thus allowing determination of the NBD residing in the inner lipid leaflet. Total quenching of the NBD signal was achieved after addition of Triton X-100 in order to lyse the bilayer, allowing excess sodium hydrosulfite to further quench NBD dye inside the vesicles.

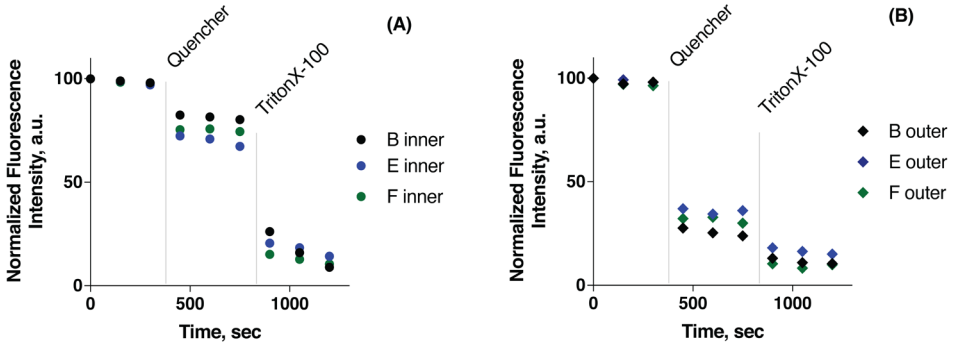

Figure 9 - Fluorescence quenching assay for determination of asymmetry degree of liposomes produced from the compositions B (black), E (blue) and F (green). A) NBD-PE was added to the inner layer; B) NBD-PC was added to the outer layer.

As shown in **Figure 9A**, when NBD-PE was incorporated in the inner leaflet, only about 20-30% of total fluorescence intensity decreased upon addition of quencher while the remaining fluorescence was only quenched after adding Triton X-100. This suggests that 80-70% of the lipid marker was located in

the inner leaflet of the bilayer. Similarly, when NBD-PC was added to outer leaflet, 65-75% of the fluorescence intensity was quenched immediately, i.e. once the quencher was offered to the outer lipid leaflet; the remaining signal was quenched after TritonX-100 was added to the cuvette (**Figure 9B**). Again, this trend was observed in the vesicles from all formulations. These results confirm that the produced bilayers from the three formulations (B, E and F) contain 70-80% asymmetry (**Table 4**).
The asymmetry assay showed uneven distributions for all the formulations. These results are in line with previous research [16] where the authors also reported negligible flip-flop over a 24 h period.

3.5. Characterization of pDNA-loaded asymmetric liposomes

Following the successful production of liposomes with a high asymmetry degree, the next step was to encapsulate plasmid DNA (pDNA) as a model biopharmaceutical drug. The purified liposomes were characterized for particle size, PDI, zeta potential, phospholipid recovery and pDNA encapsulation efficiency (see **Table 4**).

Table 4 – Main features of the liposomes produced from LES-nanoemulsions.

Formulation	Size (nm)	PDI	Zeta Potential (mV)	PL recovery, %	% Asymmetry	% Estimated Encapsulated pDNA
B	181 ± 4	0.24	-9.0 ± 1.3	47 ± 5	78 ± 5	14 ± 2
E	202 ± 2	0.29	-15.2 ± 0.3	44 ± 3	67 ± 4	8 ± 4
F	193 ± 5	0.25	-10.1 ± 0.7	44 ± 4	72 ± 5	11 ± 2

These results show pDNA loaded liposomes had similar size and PDI as empty liposomes prepared by LES method, as presented in **Figure 7**. Final size (<200 nm) and charge (slightly negative zeta-potential) of the liposomes is in good agreement with their intended application as nanocarrier for in vivo applications. Some authors have discussed that droplets with small sizes provide good transfer, contrary to the larger droplets that may cross the interface oil-water, but most of them break up and release the encapsulated APIs [10,19,20,23,39]. It has also been described that some of the droplets stay stationary at the interface while others may fuse with the interface [23] or most of the liposomes stay anchored to the interface [21]. Accordingly, a low transfer yield is obtained after centrifugation previously reported to be around 4% [40]. Consequently, the encapsulation of an API in the w/o is compromised during the droplets crossing the interface.

Our results set a turning point to these observations. We show that it is possible to obtain liposomes with narrow (nano)size distributions and accordingly the transfer of intact nanoemulsion droplets was ~10 15%, as can be deduced from recovery of encapsulated pDNA. Even higher phospholipid recoveries were found of ca. 45%, which can be related to transfer of empty nanoemulsion droplets besides pDNA filled nanoemulsion droplets. Since the zeta-potential of the pDNA-loaded lipid nanoparticles was negative for all three formulations, we concluded that the cationic DOTAP lipid had been retained within the inner lipid leaflet. The presence of pDNA thus did not perturbed the asymmetry of the liposomes.
It is worth to stress that, to the best of our knowledge, this is the first report in which the centrifugation technology is employed for production of nanosized liposomes that actually contain a payload like pDNA. Our results are encouraging and indicate that the positive charge of the inner leaflet is fully masked by 95 % (v/v) of zwitterionic lipids (DPPC) and 5% of anionic DSPE-PEG2000 in the outer leaflet of small liposomes.

4. Conclusions

The inverted emulsion technique is based on the premise that stable inverted emulsions cross the interface oil-water and are enwrapped by a second monolayer of phospholipids during transfer over the interface. We have improved protocols for preparation of w/o nanoemulsions and have collected liposomes from the water phase that are similar in size and dispersity as the initial nanoemulsions. The simplicity of the protocol, the opportunity to create asymmetric bilayers and the improvements in encapsulation efficiency make this technique attractive for the formulation of nucleic acids. Encouraged by these results, research is ongoing to improve lipid and drug recovery rates, liposome yield and encapsulation efficiency as well as to investigate the oil-lipid interactions, scale-up and the bioactivity of the encapsulated cargo.

References

[1] M.B. de Jesus, I.S. Zuhorn, Solid lipid nanoparticles as nucleic acid delivery system: Properties and molecular mechanisms, J. Control. Release. 201 (2015) 1–13. doi:10.1016/j.jconrel.2015.01.010.
[2] J. Wei, J. Jones, J. Kang, A. Card, M. Krimm, P. Hancock, Y. Pei, B. Ason, E. Payson, N. Dubinina, M. Cancilla, M. Stroh, J. Burchard, A.B. Sachs, J.H. Hochman, W.M. Flanagan, N.A. Kuklin, RNA-Induced Silencing Complex-Bound Small Interfering RNA Is a Determinant of RNA Interference-Mediated Gene Silencing in Mice, Mol. Pharmacol. 79 (2011) 953–963. doi:10.1124/mol.110.070409.
[3] T. Lobovkina, G.B. Jacobson, E. Gonzalez-Gonzalez, R.P. Hickerson, D. Leake, R.L. Kaspar, C.H. Contag, R.N. Zare, In Vivo Sustained Release of siRNA from Solid Lipid Nanoparticles, ACS Nano. 5 (2011) 9977–9983. doi:10.1021/nn203745n.
[4] A.A. Mokhtarieh, S. Cheong, S. Kim, B.H. Chung, M.K. Lee, Asymmetric liposome particles with highly efficient encapsulation of siRNA and without nonspecific cell penetration suitable for target-specific delivery, Biochim. Biophys. Acta - Biomembr. 1818 (2012) 1633–1641. doi:10.1016/j.bbamem.2012.03.016.
[5] F. Liu, L. Huang, Development of non-viral vectors for systemic gene delivery, J. Control. Release. 78 (2002) 259–266. doi:10.1016/S0168-3659(01)00494-1.
[6] W. Li, F.C. Szoka, Lipid-based Nanoparticles for Nucleic Acid Delivery, Pharm. Res. 24 (2007) 438–449. doi:10.1007/s11095-006-9180-5.
[7] M. Chiba, M. Miyazaki, S. Ishiwata, Quantitative analysis of the lamellarity of giant liposomes prepared by the inverted emulsion method, Biophys. J. 107 (2014) 346–354. doi:10.1016/j.bpj.2014.05.039.
[8] S. Fujii, T. Matsuura, T. Sunami, T. Nishikawa, Y. Kazuta, T. Yomo, Liposome display for in vitro selection and evolution of membrane proteins., Nat. Protoc. 9 (2014) 1578–91. doi:10.1038/nprot.2014.107.
[9] M. Hadorn, E. Boenzli, P. Eggenberger Hotz, M.M. Hanczyc, Hierarchical Unilamellar Vesicles of Controlled Compositional Heterogeneity, PLoS One. 7 (2012) 1–7. doi:10.1371/journal.pone.0050156.
[10] K. Nishimura, H. Suzuki, T. Toyota, T. Yomo, Size control of giant unilamellar vesicles prepared from inverted emulsion droplets, J. Colloid Interface Sci. 376 (2012) 119–125. doi:10.1016/j.jcis.2012.02.029.
[11] A. Saha, G. Mondal, A. Biswas, I. Chakraborty, B. Jana, S. Ghosh, In vitro reconstitution of a cell-like environment using liposomes for amyloid beta peptide aggregation and its propagation., Chem. Commun. (Camb). 49 (2013) 6119–21. doi:10.1039/c3cc41287c.
[12] A. Yamada, T. Yamanaka, T. Hamada, M. Hase, K. Yoshikawa, D. Baigl, Spontaneous transfer of phospholipid-coated oil-in-oil and water-in-oil micro-droplets through an oil/water interface, Langmuir. 22 (2006) 9824–9828. doi:10.1021/la062221+.
[13] T. Hamada, Y. Miura, Y. Komatsu, Y. Kishimoto, M. Vestergaard, M. Takagi, Construction of asymmetric cell-sized lipid vesicles from lipid-coated water-in-oil microdroplets, J. Phys. Chem. B. 112 (2008) 14678–14681. doi:10.1021/jp807784j.
[14] E.A. Kubatta, H. Rehage, Characterization of giant vesicles formed by phase transfer processes, Colloid Polym. Sci. 287 (2009) 1117–1122. doi:10.1007/s00396-009-2083-3.
[15] S. Pautot, B.J. Frisken, D. a. Weitz, Production of unilamellar vesicles using an inverted emulsion, Langmuir. 19 (2003) 2870–2879. doi:10.1021/la026100v.
[16] S. Pautot, B.J. Frisken, D. a Weitz, Engineering asymmetric vesicles., Proc. Natl. Acad. Sci. U. S. A. 100 (2003) 10718–10721. doi:10.1073/pnas.1931005100.
[17] L.L. Pontani, J. Van Der Gucht, G. Salbreux, J. Heuvingh, J.F. Joanny, C. Sykes, Reconstitution of an actin cortex inside a liposome, Biophys. J. 96 (2009) 192–198. doi:10.1016/j.bpj.2008.09.029.
[18] M. Yanagisawa, M. Iwamoto, A. Kato, K. Yoshikawa, S. Oiki, Oriented reconstitution of a membrane protein in a giant unilamellar vesicle: Experimental verification with the potassium channel KcsA, J. Am. Chem. Soc. 133 (2011) 11774–11779. doi:10.1021/ja2040859.

[19] M. Hase, A. Yamada, T. Hamada, K. Yoshikawa, Transport of a cell-sized phospholipid micro-container across water/oil interface, Chem. Phys. Lett. 426 (2006) 441–444. doi:10.1016/j.cplett.2006.06.016.
[20] S. Pautot, B.J. Frisken, J.X. Cheng, X.S. Xie, D. a Weitz, Spontaneous formation of lipid structures at oil/water lipid interfaces, Langmuir. 19 (2003) 10281–10287. doi:10.1021/la034532f.
[21] K. Takiguchi, M. Negishi, Y. Tanaka-Takiguchi, M. Homma, K. Yoshikawa, Transformation of ActoHMM assembly confined in cell-sized liposome, Langmuir. 27 (2011) 11528–11535. doi:10.1021/la2016287.
[22] L. Zhang, J. Hu, Z. Xiao, Z. Lu, Preparation of Liposomes by a Controlled Assembly Method, Mol. Cryst. Liq. Cryst. Sci. Technol. Sect. A. Mol. Cryst. Liq. Cryst. 295 (1997) 125–128. doi:10.1080/10587259708042812.
[23] J. Whittenton, S. Harendra, R. Pitchumani, K. Mohanty, C. Vipulanandan, S. Thevananther, Evaluation of asymmetric liposomal nanoparticles for encapsulation of polynucleotides, Langmuir. 24 (2008) 8533–8540. doi:10.1021/la801133j.
[24] V. Noireaux, A. Libchaber, A vesicle bioreactor as a step toward an artificial cell assembly., Proc. Natl. Acad. Sci. U. S. A. 101 (2004) 17669–17674. doi:10.1073/pnas.0408236101.
[25] E. Hildebrandt, A. Dessy, J.-H. Sommerling, G. Guthausen, H. Nirschl, G. Leneweit, Interactions between Phospholipids and Organic Phases: Insights into Lipoproteins and Nanoemulsions, Langmuir. 32 (2016) 5821–5829. doi:10.1021/acs.langmuir.6b00978.
[26] E. Hildebrandt, M. Vrânceanu, H. Nirschl, G. Leneweit, Phospholipids as emulsifiers for micro/nano droplets suitable for biotechnological systems integration, La Houille Blanche. (2013) 68–73. doi:10.1051/lhb/2013018.
[27] J.C. McIntyre, R.G. Sleight, Fluorescence assay for phospholipid membrane asymmetry., Biochemistry. 30 (1991) 11819–27. doi:10.1021/bi00115a012.
[28] G. Rouser, S. Fleischer, A. Yamamoto, Two dimensional thin layer chromatographic separation of polar lipids and determination of phospholipids by phosphorus analysis of spots, Lipids. 5 (1970) 494–496. doi:10.1007/BF02531316.
[29] E. Hildebrandt, C. Heyder, M.B.C. de Matos, N. Beztsinna, R.J. Kok, H. Nirschl, G. Leneweit, Liposomal formulations of mistletoe produced by centrifugal technologies and cell proliferation analysis of both mistletoe extracts and isolated mistletoe lectin I = Liposomale Formulierung von Mistelextrakten durch Zentrifugationsverfahren und Analyse de, Die Mistel Der Tumortherapie 4 AktuellerStand Der Forsch. Und Klin. Anwendung. Hrsg. R. Scheer. (2016).
[30] N. Politova, S. Tcholakova, N.D. Denkov, Factors affecting the stability of water-oil-water emulsion films, Colloids Surfaces A Physicochem. Eng. Asp. 522 (2017) 608–620. doi:10.1016/j.colsurfa.2017.03.055.
[31] A.S. Koneva, E.A. Safonova, P.S. Kondrakhina, M.A. Vovk, A.A. Lezov, Y.S. Chernyshev, N.A. Smirnova, Effect of water content on structural and phase behavior of water-in-oil (n-decane) microemulsion system stabilized by mixed nonionic surfactants SPAN 80/TWEEN 80, Colloids Surfaces A Physicochem. Eng. Asp. 518 (2017) 273–282. doi:10.1016/j.colsurfa.2017.01.020.
[32] M. Capdevila, A. Maestro, M. Porras, J.M. Gutiérrez, Preparation of Span 80/oil/water highly concentrated emulsions: Influence of composition and formation variables and scale-up, J. Colloid Interface Sci. 345 (2010) 27–33. doi:10.1016/j.jcis.2010.01.045.
[33] G. Lv, F. Wang, W. Cai, H. Li, X. Zhang, Influences of addition of hydrophilic surfactants on the W/O emulsions stabilized by lipophilic surfactants, Colloids Surfaces A Physicochem. Eng. Asp. 457 (2014) 441–448. doi:10.1016/j.colsurfa.2014.06.031.
[34] A. Knoth, I. Scherze, G. Muschiolik, Stability of water-in-oil-emulsions containing phosphatidylcholine-depleted lecithin, Food Hydrocoll. 19 (2005) 635–640. doi:10.1016/j.foodhyd.2004.10.024.
[35] F.Y. Ushikubo, R.L. Cunha, Stability mechanisms of liquid water-in-oil emulsions, Food Hydrocoll. 34 (2014) 145–153. doi:10.1016/j.foodhyd.2012.11.016.
[36] S. Mahdi Jafari, Y. He, B. Bhandari, Nano-Emulsion Production by Sonication and Microfluidization—A Comparison, Int. J. Food Prop. 9 (2006) 475–485. doi:10.1080/10942910600596464.

[37] T. Delmas, H. Piraux, A.-C. Couffin, I. Texier, F. Vinet, P. Poulin, M.E. Cates, J. Bibette, How To Prepare and Stabilize Very Small Nanoemulsions, Langmuir. 27 (2011) 1683–1692. doi:10.1021/la104221q.
[38] M.M. Lapinski, A. Castro-Forero, A.J. Greiner, R.Y. Ofoli, G.J. Blanchard, Comparison of Liposomes Formed by Sonication and Extrusion: Rotational and Translational Diffusion of an Embedded Chromophore, Langmuir. 23 (2007) 11677–11683. doi:10.1021/la7020963.
[39] P.C. Hu, N. Malmstadt, Microfluidic fabrication of giant lipid vesicles, ACS Appl Mater Interfaces. 3 (2012) 1434–1440. doi:10.1021/am101191d.Microfluidic.
[40] M. Abkarian, E. Loiseau, G. Massiera, Continuous droplet interface crossing encapsulation (cDICE) for high throughput monodisperse vesicle design, Soft Matter. 7 (2011) 4610. doi:10.1039/c1sm05239j.

Supplementary Information

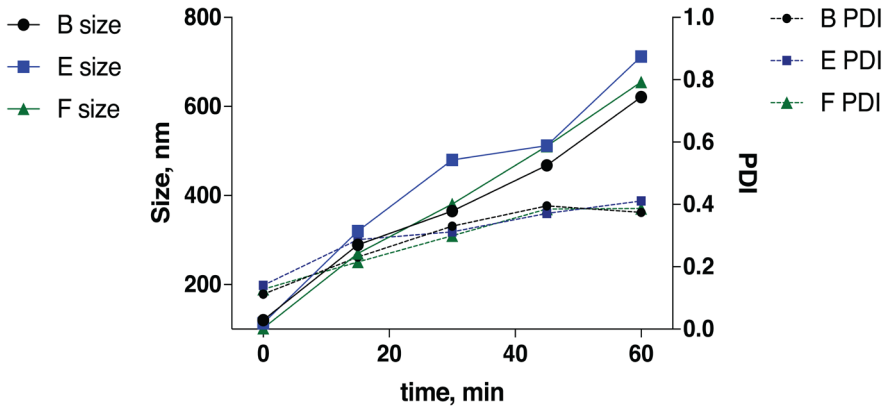

Supplemental Figure 1- Stability of hand-extrusion nanoemulsions. Stability of nanoemulsions was measured during 60 min after preparation by hand-extrusion method as described in the main manuscript. Size and polydispersity were determined by DLS. Full lines: mean diameter (left axis); dashed lines: polydispersity index (right axis). Black: formulation B; Blue: formulation E; Green: formulation F.

Part V | Summary and perspectives

Chapter 7 – General discussion

Development of triggered liposomal drug delivery systems

Liposomes are by far the most used pharmaceutical nanocarrier. They are versatile and robust systems and can encapsulate a wide range of drugs [1,2]. Liposomal encapsulation of cytotoxic anticancer drugs offers several advantages: 1) protection of the drugs against premature clearance and enzymatic degradation, 2) protection of healthy tissues against off-target effects and 3) passive accumulate into tumors by the enhanced permeation and retention (EPR) effect [3–7]. Although the extent of the EPR effect in human patients is debatable, it is a common concept for many preclinical proof-of-concept studies regarding anticancer nanomedicines. The underlying principle of EPR, i.e. the relative higher tumor uptake of nanoparticles due to vascular leakiness as compared to normal tissues has been proven repeatedly; whether such events can occur in all types of (clinical) tumors or only in certain subsets of rapidly growing cancers is however uncertain [6,8,9]. Another problem that is now recognized is the therapeutic availability of the released drug in the tumor. This is due to slow and uncontrolled release of the drug from classical liposomes.

Release is needed before the drug can effectively interact with its molecular target. As a consequence, cytotoxic concentrations of drugs in the tumors are often sub-optimal [10–13]. This is especially true for drugs, like doxorubicin and docetaxel, with a pharmacodynamic profile that is related to peak concentrations rather than prolonged exposure. In order to increase the therapeutic availability of free drug in the tumor, stimuli responsive liposomes are under investigation: such systems can release high peak concentrations and hence can more easily reach concentrations above the minimum effective levels. Temperature-sensitive liposomes are the most relevant and successful example of stimuli-responsive carriers. They are able to release their cargo upon exposure to mild hyperthermia (42 °C). Inclusion of lysolipids into the liposomal bilayer can confer such temperature sensitivity. Lysolipid-containing thermosensitive liposomes (LTSL) encapsulating doxorubicin (DOX) have shown improved antitumor efficacy in combination with mild hyperthermia treatment compared to free DOX and the non-temperature sensitive Doxil-like formulation in vivo [14,15]. This demonstrates proof-of-concept for this type of stimuli-responsive liposomes.

Besides development of better nanocarrier systems, it is important that the nanomedicine research field changes its focus from classical anticancer drugs to payloads with more attractive antitumor efficacy profiles. The presently studied plant-derived cytotoxins may have such qualities as they are also cytotoxic after only a short peak exposure. Formulation of such high molecular weight drugs has yet been ill- addressed in nanomedicine research. The majority of cytotoxic anticancer drugs, like doxorubicin, were discovered well over 50 years ago. Current oncology research is devoted to molecular targeted drugs and biotechnology-based macromolecular drugs such as therapeutic proteins [16–19]. Avoidance of toxicity sensitive tissues and protection against degradation by site-specific (triggered) delivery can also be critical for therapeutic effects for cytotoxic macromolecules. In addition to the delivery/release method, efficient methods to encapsulate these proteinaceous macromolecules are required. Standard protocols yield low encapsulation as they are based on passive encapsulation. Some of these molecules may lose activity or be damaged during processing. Improving the encapsulation efficiency can lead to major advances. Hence, for these novel classes of drugs, proper drug delivery systems and proper encapsulation techniques are required to maximize the therapeutic benefit.

Motivated by the challenges of site-specific delivery of macromolecules and their encapsulation in nanomedicines, the European Project decentAID was initiated. It aimed for the "development of novel drug delivery system produced by centrifugal technologies, composed to minimize adverse immune reactions and designed for optimised therapeutic effects". A macromolecular protein-type drug, mistletoe lectin-1 (ML1), was used as a model compound. ML1 is one of the active components in mistletoe extracts which are being used in alternative medicine treatment of cancer [20–23]. Mistletoe is a semi-parasitic plant that grows on a different types of host trees such as pine, apple and oak. The exact composition of mistletoe extracts is not known in detail and may vary depending on its natural origin and processing of the extract, and various parameters such as time of harvesting and growing conditions that affect both host and mistletoe plant. Existing literature on mistletoe extracts is not consistent on the mode of action, which involves both immunomodulatory effects and direct anticancer activity of mistletoe lectins [24–31]. Nevertheless, mechanistic studies with isolated or recombinantly prepared mistletoe lectins have shown direct cytotoxic activity of ML1 in cancer cells [32–34]. The research described in chapter 3 of this thesis was performed to further support evidence for the pharmacological potency of ML1, while the other

experimental chapters focus on the encapsulation of ML1 in nanocarriers and the functional evaluation of the developed formulations. Collectively, this thesis makes a first step in the development of ML1-loaded lipid-based nanomedicines that can be used for improved tumor delivery of such plant derived cytotoxins.

Chapter 1 presents a general introduction to the topics addressed and an outline of the thesis. We identify the hurdles in cancer treatment, describe liposomal delivery systems, emphasize the relevance of cytotoxins as anticancer biotherapeutics and the obstacles for their formulation in nanocarrier systems. In **Chapter 2** we provide an in-depth reflection of nanoparticulate drug delivery systems and the challenges behind their clinical translation. Such aspects are dynamically entangled in nanomedicines development and need to be carefully considered upon.

Cytotoxic proteins: how much do we know about them?

Following introductory considerations, we proceeded with the in-depth study of ML1 in **Chapter 3**. Although similar in structure to other RIP-II toxins, the particular cell binding properties, endocytosis pathway(s), subcellular processing and apoptosis activation of ML1 were not well studied when this PhD project started. As stressed in **Chapter 2**, detailed knowledge on the pharmacological mode of action is of utmost importance for the clinical translation of nanomedicines. Knowledge of the molecular activity and other activities of ML1 allows to predict its potential side effects or toxicity profile when administered as free drug to animals or human subjects. Such activities do not only concern the free drug itself, but also the activities of ML1 once it has been released from the nanocarrier.

For this purpose, we used state-of-the-art imaging equipment and automated image analysis algorithms to study the binding and uptake of ML1 with tumor cells. ML1 displayed very fast uptake by CT26 murine colon carcinoma cells. ML1 endocytosis involved both clathrin-dependent and clathrin-independent pathways. Once inside the cell, ML1 is transported from early endocytic vesicles to the Golgi network. The pro-apoptotic and anti-proliferative activity of ML1 against CT26 cells was also visualized and quantified. Cytotoxicity was additionally evaluated against a multidrug resistant tumor cell line (4T1). Interestingly, ML1 was very effective against the doxorubicin resistant cancer cells. This opens new perspectives and opportunities for the use of ML1 as an alternative cancer therapeutic.

We can still expand our knowledge on ML1 and increase our chances of reaching a safer and more effective formulation in the future. For example, we observed that there was only little co-localization of ML1 and lysosomal markers. This indicates that ML1 does not follow the normal endosomal-lysosomal pathway leading to protein degradation, but instead is routed to a retrograde pathway from endosomes to Golgi and endoplasmic reticulum. The exact endosomal escape mechanism remained unclear but may involve a membrane destabilization step due to structural changes in the transport chain of ML1, which is also shown for ricin toxin[35]. Other escape mechanisms described for plant toxins are pore formation and membrane fusion [36]. The escape domains of ML1 or its possible fusogenic properties may help in circumventing a common problem observed the intracellular delivery of macromolecules by nanocarrier systems. Although nanocarriers can enter cells by receptor-mediated endocytosis, their common end-station is the lysosomal compartment which is often not the designated site-of action of the encapsulate payloads. Since transfer into the cytosol and sometimes even further into the nucleus is required for therapeutic activity, endosomal or lysosomal escape is an important hurdle in the design of viable nanomedicines. The intrinsic capability of ML1 to escape from endocytic vesicles is therefore an important asset. Moreover, it is worthwhile to investigate other macromolecular drugs that possess similar escape mechanisms from endosomes or lysosomes.

In **Chapter 3**, all the experiments were performed using murine-derived cell lines; since ML1 is a sugar-binding protein which binds to O-glycans, i.e. complex glycosidic groups attached to sidechains of O-containing amino-acids (e.g. serine, threonine) in membrane proteins. Binding sites for ML1 and related plant derived lectins vary not only between cell types but also according to the species [37]. It is therefore warranted that more experiments should be done using human-derived cell lines and organoids to determine the specific interaction of ML1 with target cells in a more complex setting. Some preliminary experimental work in **Figure 1** indicates that there is substantial variability in sensitivity of several cell lines towards ML1 but the species does not seem to be a decisive parameter for interaction with target cells.

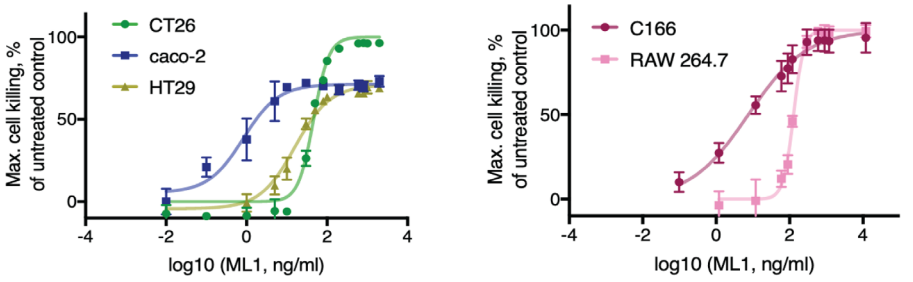

	Colon carcinoma	Colorectal adenocarcinoma		Endothelial	Macrophages
	CT26 Murine fibroblast	**Caco-2** Human epithelial	**HT29** Human epithelial	**C166** Murine Endothelial	**RAW264.7** Murine leukemia virus-transformed
EC_{50}, ng/ml	46	1	16	9	129

Figure 1 - Variability in sensitivity to of several cell lines towards ML1. Cells were seeded in 96-well plates and 24h later they were incubated with several concentrations of ML1. Following 48 h incubation, the remaining number of metabolically active cells was determined by MTS cell viability assay.

The collective results of **Chapter 3** confirm that ML1 is a potent cytotoxin. Its rapid uptake in tumor cells makes it feasible to be delivered extracellularly to tumor cells, avoiding the need for targeting ligand-decorated liposomal formulations which may only increase the complexity of the carrier system. Aiming for extracellular release, we investigated two triggered systems: heat-triggered release and ultrasound-triggered release.

Liposomal formulations for triggered release of macromolecules

Lyso-lipid containing thermosensitive liposomes

In **Chapter 4** we describe the findings on lysolipid-containing thermosensitive liposomes (LTSL) for encapsulation of macromolecules. Specifically, we intended to use ML1 as the bioactive agent and we envisioned a formulation with triggered release properties after tumor accumulation by EPR effect, that is, intratumoral extracellular release. After its release, ML1 will interact with the surface of the tumor cells to be internalized and exert its cytotoxic activity. Taking doxorubicin as an example, it has been suggested that intravascular release is the preferred approach of LTSL [38]. Doxorubicin is able to penetrate deep into the tumor tissue upon its intravascular release in the tumor blood vessels. On the other hand, in the intratumoral release scenario the permeation is mainly dictated by the local distribution of the liposomes within the tumor. The intravascular drug release model may therefore not be the preferred

choice for all compounds, as ML1 will bind cell to glycosylated surface receptors that are abundantly present on erythrocytes [39–41]. This will certainly limit the uptake of ML1 into tumors upon its intravascular release. It thus, seems logical to pursue intratumoral release of ML1 rather than intravascular. Hence, we designated our liposomal carrier systems for an EPR-based accumulation, followed by local tumor-restricted release of ML1 from the lipid-based capsules.
In a broader sense, the site of release really depends on the timing between intravascular administration and local triggered release of LTSL. Only when the triggered release is effectuated shortly after intravenous administration, one can assume intravascular release. Inversely, a deliberate waiting time of several hours can promote the accumulation of nanoparticles intratumorally and hence extravascular intratumoral release.

In agreement with previous hypotheses of pore formation or bilayer defects upon heating, our results indicate that the magnitude of release after heat treatment depends on the size of the molecule. Surprisingly, at storage conditions ($T<T_m$) and for all formulations, we found considerable spontaneous leakage for all types of macromolecules in **Chapter 4a** (dextrans and proteins). At these conditions, size analysis confirmed colloidal stability. We therefore did not anticipate any pore formation and low membrane permeability events. In view of the correlation to lipid composition of LTSL, we attributed the loss of payload retention to membrane instability of the thermosensitive liposomes, i.e. to a loss of liposomal integrity due to inclusion of the lysolipids. This assumption is merely speculative and not in line with common models for the behavior of liposomal bilayers below T_m, and also not in line with the colloidal stability data. Thus, it is important to address this in future research.
The heat triggered release difference between the smallest molecule tested (dextran of 4 kDa) and the larger one (BSA of 67 kDa) was about 5-6 fold. The two molecules with similar sizes (BSA and ML1) showed similar release profiles. Thus, it appears likely that it is possible to modulate and design LTSL for the release of macromolecules. Interestingly, with all the molecules tested, LTSL reached a release plateau after 15 min of heat treatment. It could be worthwhile to study this mechanism systematically and propose a release-predictive model, in which lipid composition, drug molecular weight and heat-exposure time are comprehensively considered.
Released ML1 was still effective against CT26 tumor cells. Although only about 10% of the encapsulated ML1 was released, it was taken up by the cells and effectively induced cell killing.

Other strategies can be used in future projects to improve the encapsulation and release of ML1 or other pertinent drugs. One of these strategies is to use cationic thermosensitive liposomes as proposed by Dicheva et al [42,43]. Cationic liposomes can readily bind proteins with an isoelectric point below 7 due to electrostatic charge interactions and this could substantially boost encapsulation efficiency. Yet, cationic liposomes are notorious for their toxicity profile as they tend to bind to all negatively charged cell surfaces. Although cationic particles achieve high transfection efficiency in cell culture, upon intravenous administration positively charged nanoparticles interact with the negatively charged serum proteins forming clots or aggregates that accumulate mainly in the lungs, liver, and spleen. Often these clots stay entrapped in the endothelial capillary bed or are taken up by the RES, inducing pulmonary toxicity associated with complement activation and inflammation [44–46]. Keeping in mind the possibility of unfavorable in vivo toxicity, we can develop asymmetric liposomes as done in the last research chapter (**Chapter 6**) of this thesis. But to take the first steps and explore these systems, we performed preliminary work regarding conventionally prepared cationic thermosensitive liposomes using BSA as a model compound for encapsulation and release studies (*Additional study* **Chapter 4b**). Thermal analysis indicated that the introduction of cationic lipid combined with lysolipid did not interfere with the transition temperature, making these systems suitable for heat-triggered release. In the presence of serum there is a substantial decrease in the enthalpy, suggesting release impairment. This behavior is important to address in future studies.
Although we raised even more research questions, overall, these preliminary results underline the potential of using cationic thermosensitive liposomes and make them attractive candidates for future studies.
A different thermosensitive liposome composition that shows promising results is composed of DPPC, DSPC, and 1,2-dipalmitoyl-sn-glycero-3-phosphodiglycerol ($DPPG_2$), and was reported for the first time in 2004 [15]. Incorporation of $DPPG_2$, a synthetic phospholipid, led to a prolonged circulation time of thermosensitive formulations [15,47]. The transition temperature of $DPPG_2$-TSL is narrow and around 42 °C, similar to Lysolipid-TSL. $DPPG_2$-TSL showed improved in vitro stability in complete serum when compared with LTSL. The presence of serum components at 37 °C stabilized the formulation over time, whereas the opposite was found for LTSL [48]. Overall, $DPPG_2$-TSL is considered the only thermosensitive formulation that fulfills all the criteria for heat-triggered intravascular drug release. Hence, it would be very interesting to study this lipid composition for the delivery of macromolecular drugs and for intratumoral release applications.

Ultrasound-sensitive liposomes

The reports on LTSL and our own unpublished results often showed incomplete and rather longer release times are necessary for macromolecules. Encouraged by this and aiming for better and faster release systems, we studied the ultrasound release system described on **Chapter 5**. Ultrasound sensitive liposomes (USL) are stealth liposomes that have been loaded with liquid perfluorocarbon (PFC) emulsion nanodroplets. When heated or triggered with ultrasound, liquid PFCs can undergo phase transition from liquid into gas. As a result, the external lipid bilayer of the USL will be permeabilized, thus allowing release of the cargo payload. Hence, the release mechanism of USL is based on disruption of the lipid bilayers promoted by the PFC phase transition, rather than on pore formation supported by lysolipids as for thermosensitive systems. In addition, ultrasound can also affect the integrity of cell membranes of target cells and in this manner, improve cellular drug uptake. Together, these two processes may result in more effective delivery and cellular uptake of macromolecules delivered from USL, and this increased cell killing as compared to LTSL based nanocarriers as presented in **Chapter 4a**.

Three USL formulations, differing in the amount of DSPE-PEG_{2000}, were studied. One of the formulations contained 20% mol of DSPE-PEG_{2000} (USL20 and NUSL20) while the other systems contained lower amounts of this amphiphilic molecule. Compositions with high amounts of DSPE-PEG_{2000} are known to form structures other than liposomes, such as DSPE-PEG micelles, affecting long term stability. It was not surprising that 5 days after preparation the USL20 and NUSL20 had leaked payload. This motivated the additional investigation of formulations with 5% (USL5, NUSL5) and 10% (USL10, NUSL10) DSPE-PEG_{2000}.

Our results indicate that the magnitude of release depends on the encapsulation of the nanoemulsion inside the liposomes. Although the control formulations without nanoemulsion droplets also responded to the ultrasound trigger, the observed release was not to the same extent as the ones containing nanoemulsions. Plain liposomes and micelles also responded to ultrasound fields although the exact mechanism is not clear yet. Several hypotheses have been raised in literature including thermal effects and cavitation phenomena [49] but it is unclear whether these apply to the systems tested here. When the nanoemulsion was added to the outside of the liposomal NUSL suspension the payload release was smaller than for the USL formulations with the nanoemulsion on the inside. In all cases, the release was greatly improved in comparison with the LTSL system.

Bioactivity of released ML1 was tested against CT26 tumor cells and the cytotoxicity studies provide strong evidence that the released ML1 effectively induced cell killing, reaching 80% of cell death at the highest concentration tested. The IC_{50} of the USL was 2 times lower than the one showed for LTSL, supporting the previous observations of better release, although the overall yields may be the cause for such small difference.

These nanoemulsion-loaded liposomes, although very promising, still have a long way to go before they become a clinical reality. In **Chapter 2**, we specified that one of the essential requirements for clinical translation of nanomedicines is a preparation method that allows 1) production of large scalable quantities, 2) manufacturing consistency and high quality and 3) batch-to-batch reproducibility. The purification protocol for USLs suggested in literature was the so-called "pillow gradient"; although theoretically very simple, this method was difficult to reproduce. To overcome the lack of inter-lab reproducibility, we applied a more conventional density-separation method, widely used in molecular biology to separate components based on their buoyant density. However, this resulted in very low yields (lipids and drug). It would require tremendous amounts of materials and drug to obtain a formulation with sufficient amounts for intravenous administration, thus increasing the production costs. Thus, the purification process improvement can bring remarkable benefits for production and ultimately can improve the therapeutic value, marking a clearer line when compared with the LTSLs. Finally, we were unable to precisely determine the amount of nanoemulsion that is effectively entrapped in the liposomes. This makes reproducibility an issue and would require an in-depth study combining Cryo-TEM, F-NMR and elemental analysis to shed light on this issue.

We are yet unaware of the effect that plasma proteins may have on the release and stability of USL and to the best of our knowledge there are no in vivo experiments done with such liposomes. Previous experiments with plain liposomes can provide some indication, but this is clearly an important matter to be addressed in the future. Earlier research focused on the efficiency of LFUS (20 kHz)- and HFUS (1 and 3 MHz)- triggered release of Doxil™, and demonstrated that the release of doxorubicin sharply decreased with increasing medium complexity and with increasing frequency. It was hypothesized that release was due to cavitation, which would explain the reduced release with increasing frequency. The differences between the release in saline and human plasma can be explained by the fact that plasma proteins absorb some

of the acoustic energy, thus reducing the number of cavitation events [50]. The combined effect of temperature and serum proteins and USL has, to our knowledge, never been studied. It is possible that the complexity of the in vivo environment can prompt a whole new set of parameters and promote unintentional release.
In light of these results and although our USL5 and USL10 formulations showed remarkable storage stability and release profiles, the limited knowledge on the behavior of these liposomes in more complex environments makes testing in a simple PK/PD study in small animals still premature.
Other ultrasound sensitive and PFC loaded structures are interesting and may offer new opportunities in the macromolecular drug delivery field. Kagan et al demonstrated that PFCs can be used to directly deliver the payload deeply into tissues in vivo. These authors used PFC nanodroplets and loaded them into conically shaped micron-sized structures, that can be used as ultrasound-triggered propulsion system. The ultrasound mediated vaporization is described to cause linearly directed propulsion at high velocities (>6 m/s) [51]. This method could be useful in a wide variety of applications, especially those that require payloads to be delivered beyond the vasculature.

It has been demonstrated that ultrasound can enhance the release of drugs from liposomes, although the predominant underlying mechanism of drug release is not completely understood. Possibly, several mechanisms are at play and the dominant mechanism may depend on a particular ultrasound parameter or on the chemical composition of the liposomes. And these mechanisms may not be completely independent [52].
When combining hyperthermia and HIFU, the mechanisms for drug release include cavitation, thermal effects and acoustic streaming [53]. Conventional liposomal carriers like Doxil™ were not designed for triggered release. However, we can take advantage of the increased permeability of the LTSL already described in this thesis. For example, in 2007 Dromi et al used pulsed high-intensity focused ultrasound (HIFU) local DOX delivery by TTSL [54]. Many other examples can be found in literature, especially in the increased toxicity of hydrophobic drugs[53]. These studies indicate that local ultrasound-induced hypothermia can be an effective method for controlling drug release.

New possibilities for preparation of liposomes with high degree of bilayer asymmetry

The last research chapter of this thesis, **Chapter 6**, explored the use of a technique named the "inverted-emulsion method" for the production of asym-

metrical liposomes. The idea of controlling the composition of the outer and inner leaflets of the lipid bilayer has fascinated researchers. The encapsulation of certain compounds can greatly benefit from the independent control over both lipid layers. As mentioned earlier in this general discussion, macromolecular payloads with low isoelectric points can be bound to cationic nanocarriers by electrostatic interactions. However, such systems suffer from side effects due to the interaction of cationic lipids with the negatively charged cell membrane.
The first step in this chapter was to investigate emulsification procedures and downsize the w/o nanoemulsion, as well as improve reproducibility. Once satisfactory nanosized particles were obtained, we investigated the asymmetry degree and the encapsulation of a model plasmid DNA. We obtained 70-80% asymmetry and encapsulation efficiencies of around 15%. The results set a turning point on the negative observations previously made in literature and we hope our findings encourage future research.
Several questions still remain unaddressed in this chapter. The quaternary interaction between squalene-water-lipids-drug has not been fully elucidated. It is often observed that the accumulation of lipid material and API at the oil-water interface occurs, especially visible when the components were fluorescently labelled. Interestingly, this accumulation seemed to increase as the weight% of the drug was increased (unpublished results). Potential future directions for research can consider the use of different oil phases and the more profound study of solubility, interfacial tension and equilibrium and the interactions between oil and lipid combinations.

Using different chemical components may potentiate the use of this technology
Although this thesis is about lipid-based nanocarriers, different materials might offer attractive properties to circumvent part of the issues with (natural) lipids. Due to the weak effectiveness of emulsification by phospholipids in squalene, an alternative could be the use of amphiliphilic block copolymers as emulsifiers to form polymersomes [55].

One of the ideas for the consortium was to replace the DSPE-PEG_{2000} shielding by heparin, as liposomes entering the circulation may trigger an undesirable response of the immune system. Opsonized liposomes are phagocytosed by macrophages, monocytes or neutrophils which results in rapid clearance of non-coated liposomes from the circulation. The most common strategy to prevent rapid clearance by the mononuclear phagocyte system is to shield the liposomal surface with DSPE-PEG_{2000}. However, it is well known that

PEGylated liposomes stimulate the acquired immune system and trigger the accelerated blood clearance (ABC) phenomenon upon repeated injection.
Inspired by these facts and using their knowledge on innate immunity, complement activation and interaction of heparin with tissues and biomaterials, the authors of a recent publication [56] aimed for liposomes with an improved "stealth effect": non-activating liposomes with enhanced long-circulation. For this purpose, they used a novel heparin complex (CHC).
Heparin is a highly sulfated glycosaminoglycan, known for its anticoagulant, anti-inflammatory and immunomodulatory properties [57]. Other reports indicate increased liposome stability, reduced drug leakage, improved hemocompatibility [58–60] and showed high performance of heparin as PEG substitute in liposomes for the delivery of doxorubicin in an experimental melanoma lung metastasis [61]. Thus, CHC could easily bind to positively charged lipids by electrostatic interactions, neutralizing the surface charge of liposomes. Simultaneously, by replacing PEG, this glycosaminoglycan would shield the liposomes from interaction with blood components and avoid ABC-effect.
Their findings were obtained by preparation of cationic liposomes by conventional thin-film hydration and extrusion methods, and post-insertion of CHC onto the cationic liposomes. The separation method used to exclude unbound CHC was ultrafiltration using 300 kDa Vivaspins. Excited by the immunological studies, we proceeded to in vivo characterization of these NIR-dye labelled CHC coated liposomes and compared them against conventional PEGylated long-circulating liposomes (LCL).
The main features of these liposomes are presented in the figure below. The zeta potential indicates that CHC is present, as it is several times more negative than the control PEGylated stealth long circulating liposomes. However, the remaining features are substantially different from what can be expected for intravenous applications (size > 200 nm, PDI> 0.2). The lipid yield was also considerably low (~14% for CHC coated vs ~74% for LCL) which we attribute to the purification protocol. When comparing coated and non-coated liposomes (i.e., initial cationic liposomes) we could understand that the presence of CHC was the reason behind the increased size. The CHC molecule contains 70 molecules of heparin covalently bound to a polyamine backbone chain, and each heparin arm has a molecular weight of 13000 g/mol. If we have several "CHCs per liposome", then is logical that the size of the final vesicles is increased. Another hypothesis is that electrostatic interactions can promote the formation of aggregates or fusion between nanoparticles in close proximity. As an example, during coating we cannot control the number of

"CHCs per liposome"; hence, the same CHC can be indeed coating two distinct liposomes, thus increasing the overall size.

(A)

Sample	Size, nm	PDI	Z-potential, mV
CHC-coated	536 ± 18	0.29 ± 0.08	-36 ± 2
LCL	126 ± 2	0.06 ± 0.01	-9 ± 1

(B)

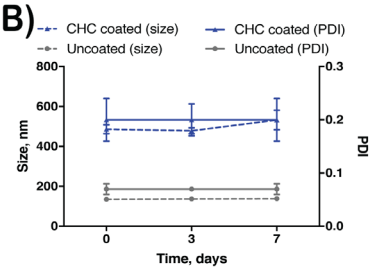

Figure 2 – Comparison between CHC-coated liposomes and PEGylated liposomes (LCL) used as control (A) and comparison between size/PDI time stability of CHC-coated and non-coated liposomes (B).

The in vitro testing for cytotoxicity revealed no toxicity induced by CHC-coated, initial cationic or LCL formulations after a 24- and a 48- h incubation with cells, for a wide range of lipid concentrations (40 up to 1000 μM). The plasma circulation time of these formulations was investigated in healthy female Balb/c mice after tail vein administration according to the schedule and procedure depicted below.

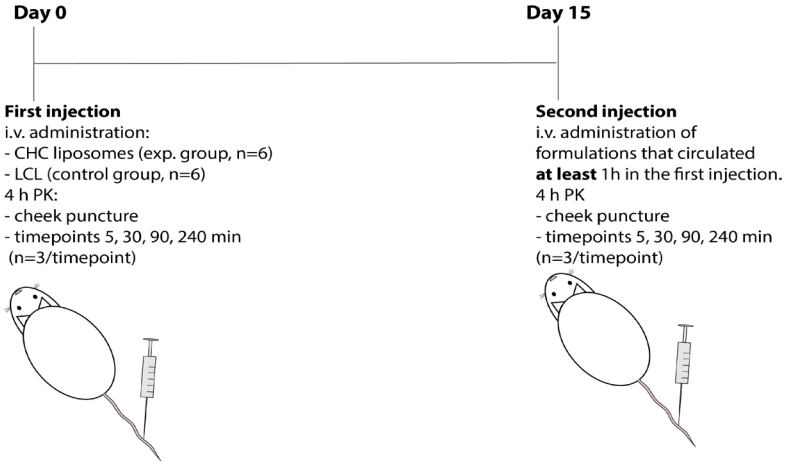

Figure 3 – Schedule for intravenous administration of CHC-coated liposomes and PEGylated liposomes (LCL).

The fluorescence of circulating liposomes (**Figure 4**) was quantified by blood spots. It was here confirmed that CHC liposomes are not appropriate for i.v. administration as they are cleared within the first 30 min after injection. We

speculate that the size of these liposomes is the main reason for such a rapid clearance.

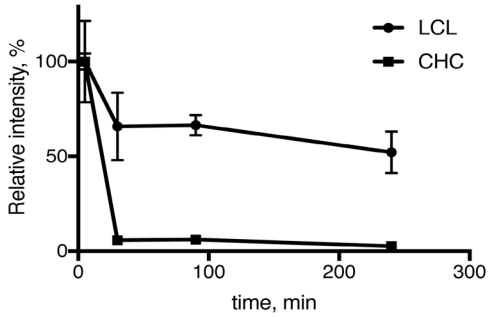

Figure 4 – Kinetic study of the CHC vs LCL liposomes. Blood aliquots of ca 50 µL were taken by cheek puncture after pre-determined intervals of time and the whole-blood was analyzed by blood spots. Isolated plasma analysis retrieved similar kinetic profile.

Improvements can be envisioned for this CHC system, as the CHC molecule itself is too large, as mentioned above. Assuming that the proposed coating model [56] is correct, the size of the final vesicles is unacceptably increased. Thus, shorter heparin molecules might be used instead that have a reduced propensity to induce aggregation or fusion with neighboring nanoparticles.
In addition to a shorter heparin, the insertion of heparin in the liposomes can be improved as well as the purifying steps which contribute significantly to material losses. In **Chapter 6** we showed the potential of the inverted nanoemulsion technique to control the inner and outer leaflets compositions and thus assemble asymmetric bilayers. Hence it can be adapted to this new coating: 1) producing a cationic w/o emulsion containing a negatively drug agent and 2) replacing the interface containing DSPE-PEG_{2000} by an interface containing heparin, could bring additional value to the method and potentially bring new nanomedicine products.

Conclusions and future perspectives

This thesis emphasizes the importance of delivery technology to unlock the potential of biotherapeutic macromolecules. It describes advanced nanomedicines that benefit from a variety of front-end technological innovations to improve delivery efficacies of proteinaceous macromolecules. The chosen macromolecular cargo (ML1) has promising cytotoxic properties, and nanomedicine encapsulation can be expected to improve translation into safer therapeutics. The LTSLs are effective and a relatively easy and safe choice – from a regulatory perspective - as their use is substantiated with clinical trial success stories. The USL systems, on the other hand, seem to be in a premature

stage of development stage to be assigned as a feasible delivery method. Yet, the remarkable in vitro release and tumor cell killing efficacy makes them an example of the versatility and robustness of lipid/ultrasound technology. Finally, for the production of asymmetric liposomes we took the first steps towards successful implementation of such technologies and it shows promise towards scale-up.

As highlighted throughout this thesis, the field of nanoparticle-based drug delivery is expanding beyond conventional strategies, materials and drugs. This addresses the need to rationally design constructs specifically tailored to overcome multiple biological barriers. And although the obstacles that hinder adequate delivery of (bio)therapeutics to tumors are complex, they are certainly not insurmountable.
Such innovative design implementations - such as the use of triggered release strategies or the re-evaluation of production methods - have shown distinct advantages over preexisting conventional nanocarriers formulations. But the necessity to transition towards more complex and progressive delivery approaches, will inevitably delay or hinder clinical translation. The additional complexities associated with these nanocarriers, biotherapeutics and technologies will directly affect scale-up, production and significantly increase the associated costs. Moreover, regulatory approvals regarding quality control, reproducibility and toxicity may present additional hurdles.
Despite these difficulties, innovations in materials science technology will continue to deliver better and more refined nanomedicines, capable of trading these obstacles for efficacious, site-specific drug delivery. This will not only result in successful translation of novel nanotherapeutics but will also bring the nanomedicines field from purely innovative promises to a viable and common strategy for cancer treatment.

References

[1] T. M. Allen, P. R. Cullis, Adv. Drug Deliv. Rev. 2013, 65, 36.
[2] V. P. Torchilin, Nat. Rev. Drug Discov. 2005, 4, 145.
[3] L. Li, T. L. M. ten Hagen, D. Schipper, T. M. Wijnberg, G. C. van Rhoon, A. M. M. Eggermont, L. H. Lindner, G. A. Koning, J. Control. Release 2010, 143, 274.
[4] H. Maeda, J. Control. Release 2012, 164, 138.
[5] H. Maeda, H. Nakamura, J. Fang, Adv. Drug Deliv. Rev. 2013, 65, 71.
[6] Y. H. Bae, K. Park, J Control Release 2012, 153, 198.
[7] T. Lammers, F. Kiessling, W. E. Hennink, G. Storm, J. Control. Release 2012, 161, 175.
[8] J. W. Nichols, Y. H. Bae, J. Control. Release 2014, 190, 451.
[9] S. Wilhelm, A. J. Tavares, Q. Dai, S. Ohta, J. Audet, H. F. Dvorak, W. C. W. Chan, Nat. Rev. Mater. 2016, 1, 1.
[10] S. Hua, M. B. C. de Matos, J. M. Metselaar, G. Storm, Front. Pharmacol. 2018, 9, DOI 10.3389/fphar.2018.00790.
[11] M. E. R. O'Brien, Ann. Oncol. 2004, 15, 440.
[12] T. Stylianopoulos, R. K. Jain, Nanomedicine Nanotechnology, Biol. Med. 2015, 11, 1893.
[13] S. Wilhelm, A. J. Tavares, Q. Dai, S. Ohta, J. Audet, H. F. Dvorak, W. C. W. Chan, Nat. Rev. Mater. 2016, 1, 16014.
[14] D. Needham, G. Anyarambhatla, G. Kong, 2000, 1197.
[15] L. H. Lindner, M. E. Eichhorn, H. Eibl, N. Teichert, M. Schmitt-Sody, R. D. Issels, M. Dellian, Clin. Cancer Res. 2004, 10, 2168.
[16] J. Swaminathan, C. Ehrhardt, Expert Opin. Drug Deliv. 2012, 9, 1489.
[17] D. S. Pisal, M. P. Kosloski, S. V. Balu-Iyler, NIH Public Access 2011, 99, 1.
[18] C. He, Z. Tang, H. Tian, X. Chen, Adv. Drug Deliv. Rev. 2016, 98, 64.
[19] S. Mitragotri, P. A. Burke, R. Langer, Nat. Rev. Drug Discov. 2014, 13, 655.
[20] M. Marvibaigi, E. Supriyanto, N. Amini, F. A. Abdul Majid, S. K. Jaganathan, Biomed Res. Int. 2014, 2014, 785479.
[21] M. Horneber, G. Bueschel, R. Huber, K. Linde, M. Rostock, M. Horneber, G. Bueschel, R. Huber, K. Linde, M. Rostock, Cochrane Libr. 2010, 4.
[22] P. Fritz, J. Dippon, T. Kierschke, I. Siegle, A. Möhring, A. Moisa, T. E. Mürdter, Anticancer Res. 2004, 24, 1187.
[23] K.-C. Kim, J.-H. Yook, J. Eisenbraun, B.-S. Kim, R. Huber, BMC Complement. Altern. Med. 2012, 12, 172.
[24] M. L. Jung, S. Baudino, G. Ribéreau-Gayon, J. P. Beck, Cancer Lett. 1990, 51, 103.
[25] E. Kovacs, J. Altern. Complement. Med. 2004, 10, 241.
[26] S. Y. Lyu, S. H. Choi, W. B. Park, Arch. Pharm. Res. 2002, 25, 93.
[27] G. Schaller, K. Urech, M. Giannattasio, Phyther. Res. 1996, 10, 473.
[28] W. B. Park, S. Y. Lyu, J. H. Kim, S. H. Choi, H. K. Chung, S. H. Ahn, S. Y. Hong, T. J. Yoon, M. J. Choi, Cancer Biother. Radiopharm. 2001, 16, 439.
[29] G. M. Stein, H. Meink, J. Durst, P. a. Berg, Eur. J. Clin. Pharmacol. 1996, 51, 247.
[30] T. J. Yoon, Y. C. Yoo, T. B. Kang, E. Her, S. H. Kim, K. Kim, I. Azuma, J. B. Kim, Int. Immunopharmacol. 2001, 1, 881.
[31] J. Y. Lee, J. Y. Kim, Y. G. Lee, S. E. Byeon, B. H. Kim, M. H. Rhee, A. Lee, M. Kwon, S. Hong, J. Y. Cho, Biol. Pharm. Bull. 2007, 30, 2043.
[32] J. Müthing, M. Burg, B. Möckel, M. Langer, W. Metelmann-Strupat, A. Werner, U. Neumann, J. Peter-Katalinic, J. Eck, Glycobiology 2002, 12, 485.
[33] C. E. Hong, A. K. Park, S. Y. Lyu, Mol. Cell. Biochem. 2014, 394, 225.
[34] A. L. Z. Lee, Y. Wang, W. H. Ye, H. S. Yoon, S. Y. Chan, Y. Y. Yang, Biomaterials 2008, 29, 1224.
[35] D. Vercauteren, R. E. Vandenbroucke, A. T. Jones, J. Rejman, J. Demeester, S. C. De Smedt, N. N. Sanders, K. Braeckmans, Mol. Ther. 2010, 18, 561.
[36] A. K. Varkouhi, M. Scholte, G. Storm, H. J. Haisma, J. Control. Release 2011, 151, 220.

[37] G. Poiroux, A. Barre, E. J. M. van Damme, H. Benoist, P. Rougé, Int. J. Mol. Sci. 2017, 18, DOI 10.3390/ijms18061232.
[38] K. Park, J. Control. Release 2014, 174, 219.
[39] K. Sano, H. Ogawa, in Lectins Methods Protoc. (Ed: J. Hirabayashi), Springer New York, New York, NY, 2014, pp. 47–52.
[40] M. Jungery, G. Pasvol, C. I. Newbold, D. J. Weatherall, Proc Natl Acad Sci U S A 1983, 80, 1018.
[41] G. Wu, M. Nagala, P. R. Crocker, Glycobiology 2017, 27, 800.
[42] B. M. Dicheva, T. L. M. Ten Hagen, L. Li, D. Schipper, A. L. B. Seynhaeve, G. C. Van Rhoon, A. M. M. Eggermont, L. H. Lindner, G. A. Koning, Nano Lett. 2013, 13, 2324.
[43] B. M. Dicheva, G. A. Koning, Expert Opin. Drug Deliv. 2014, 11, 83.
[44] J. Guo, L. Bourre, D. M. Soden, G. C. O. Sullivan, C. O. Driscoll, Biotechnol. Adv. 2011, 29, 402.
[45] M. Kapoor, D. J. Burgess, S. D. Patil, Int. J. Pharm. 2012, 427, 35.
[46] R. M. Schiffelers, G. Storm, Int. J. Pharm. 2008, 364, 258.
[47] S. Limmer, J. Hahn, R. Schmidt, K. Wachholz, A. Zengerle, K. Lechner, H. Eibl, R. D. Issels, M. Hossann, L. H. Lindner, Pharm. Res. 2014, 31, 2276.
[48] M. Hossann, Z. Syunyaeva, R. Schmidt, A. Zengerle, H. Eibl, R. D. Issels, L. H. Lindner, J. Control. Release 2012, 162, 400.
[49] S. E. Ahmed, A. M. Martins, G. a Husseini, J. Drug Target. 2015, 23, 1.
[50] A. Schroeder, Y. Avnir, S. Weisman, Y. Najajreh, A. Gabizon, Y. Talmon, J. Kost, Y. Barenholz, Langmuir 2007, 23, 4019.
[51] D. Kagan, M. J. Benchimol, J. C. Claussen, E. Chuluun-Erdene, S. Esener, J. Wang, Angew. Chemie Int. Ed. 2012, 51, 7519.
[52] S. R. Sirsi, M. A. Borden, Adv. Drug Deliv. Rev. 2014, 72, 3.
[53] K. Ng, Y. Liu, Med. Res. Rev. 2002, 22, 204.
[54] S. Dromi, V. Frenkel, A. Luk, B. Traughber, M. Angstadt, M. Bur, J. Poff, J. Xie, S. K. Libutti, K. C. P. Li, B. J. Wood, Clin. Cancer Res. 2007, 13, 2722.
[55] E. Mabrouk, D. Cuvelier, L.-L. Pontani, B. Xu, D. Lévy, P. Keller, F. Brochard-Wyart, P. Nassoy, M.-H. Li, Soft Matter 2009, 5, 1870.
[56] C. Duehrkop, G. Leneweit, C. Heyder, K. Fromell, K. Edwards, K. N. Ekdahl, B. Nilsson, Colloids Surfaces B Biointerfaces 2016, 141, 576.
[57] S. Mousavi, M. Moradi, T. Khorshidahmad, M. Motamedi, Adv. Pharmacol. Sci. 2015, 2015, 1.
[58] A. Sahli, M. Cansell, J. Tapon-Bretaudière, D. Letourneur, J. Jozefonvicz, A. . Fischer, Colloids Surfaces B Biointerfaces 1998, 10, 205.
[59] G. T. Köse, M. Y. Arica, V. Hasirci, Drug Deliv. 1998, 5, 257.
[60] H. Han, A. Lee, C. Song, T. Hwang, H. Seong, C. Lee, B. Shin, Int. J. Pharm. 2006, 313, 181
[61] Y. Chen, J. Peng, M. Han, M. Omar, D. Hu, X. Ke, N. Lu, J. Drug Target. 2015, 23, 335.

Part VI | Appendices

Nederlandse samenvatting

Verbeterde medicijnen zijn nodig voor de behandeling van kanker.

Normaal gesproken worden kankerpatiënten behandeld met chemotherapeutische geneesmiddelen, radiotherapie, chirurgische resectie of een combinatie hiervan. Het grootste probleem bij het gebruik van chemotherapeutica zijn de zeer ernstige bijwerkingen die hoofdzakelijk verband houden met het gebruikte doseringsregime: chemotherapeutische geneesmiddelen worden gewoonlijk hoog gedoseerd (in de maximaal getolereerde dosis) en bij deze hoge dosering worden vaak gezonde weefsels beschadigd.

Wanneer we daarentegen geneesmiddelen in *nanocarriers* insluiten, kunnen we het therapeutisch potentieel van kankerbestrijdende geneesmiddelen verbeteren door een verhoging van de therapeutische index: efficiëntere toediening op de doelplaats (meer geneesmiddel in het tumorweefsel zal leiden tot een verbeterd therapeutisch effect) en verminderde distributie naar andere weefsels (en dus een verminderde *off-target* toxiciteit).

Tot dusverre zijn liposomen de meest gebruikte *nanocarriers*. Liposomen zijn unilamellaire of multilamellaire blaasjes die voornamelijk bestaan uit fosfolipiden en die een compartiment van water omsluiten. In dit compartiment kunnen medicijnen opgelost zijn die zich met het liposoom door de bloedbaan verplaatsen. Conventionele liposomen zijn ontworpen om een hoge stabiliteit in de bloedbaan te hebben, waardoor voortijdige afgifte van het medicijn vóór aankomst op de tumorlocatie wordt voorkomen. Deze hoge stabiliteit voorkomt echter de snelle afgifte van het geneesmiddel na aankomst in het tumorweefsel, wat resulteert in een relatief lage vrije geneesmiddelconcentratie in de tumor. Op dit gebied bieden nanocarriers die op stimuli reageren goede mogelijkheden om de effectiviteit van nanomedicijnen te verbeteren: ze zijn ontworpen om het geneesmiddel onder invloed van endogene of exogene stimuli vrij te geven in de tumorcellen of hun lokale micro-omgeving. Tot dusver is lokale verwarming of hyperthermie, de meest intensief bestudeerde externe trigger voor dit soort gereguleerde afgifte uit liposomen. Het nanomedicijn ThermoDox® is daarvan het beste voorbeeld; dit product is in meerdere landen onder klinische evaluatie.

De opkomst van biotherapeutica

Het gebruik van biofarmaceutische geneesmiddelen is in de afgelopen decennia sterk toegenomen. De geneesmiddelklasse van biotherapeutica is breed en omvat therapeutische peptiden en eiwitten, nucleïnezuren, enzymen

en antilichamen.
De inherente complexiteit van dit soort moleculen maakt het formuleren en de gestuurde afgifte van biotherapeutische geneesmiddelen echter ook een extra grote uitdaging. Om klinisch toepasbaar te zijn, zijn de stabiliteit, de houdbaarheid, immunogeniciteit, werkzaamheid en toxiciteit belangrijke beoordelingscriteria. Vanuit het perspectief van de geneesmiddelformulering kunnen macromoleculaire biotherapeutica zelfs worden beschouwd als de minst aantrekkelijke kandidaten voor geneesmiddelontwikkeling.
De nadelen van biotherapeutica worden echter gecompenseerd door andere kwaliteiten zoals hun hoge potentie (dat wil zeggen: werkzaamheid per molecuul) en de mogelijkheid om ziektebeelden op een nieuwe manier aan te pakken. In dit proefschrift is het cytotoxische eiwit *mistletoe lectin-1* (ML1) onderzocht. Cytotoxinen zijn erg potente en daarom zeer aantrekkelijke geneesmiddelkandidaten bij kankertherapie. Een interessant kenmerk van ML1 en vergelijkbare cytotoxische eiwitten die behoren tot dezelfde klasse, is hun vermogen om te binden aan het celmembraan, opgenomen te worden door de cellen en effectief celdood te induceren. De toepassing hiervan in veilige therapeutica is echter moeilijk omdat ze slecht in staat zijn het onderscheid tussen gezonde cellen en tumorcellen te maken.
Zelfs in dit geval, waar de internalisering van het therapeuticum niet langer een beperking vormt voor efficiënte cellulaire aflevering, zijn de uitdagingen voor ML1-medicijnafgifte complex. De ontwikkeling van *nanocarriers* die reageren op externe stimuli zou aanzienlijke voordelen kunnen opleveren, omdat het cytotoxische geneesmiddel dan enkel lokaal, in de tumoromgeving, afgegeven kan worden.

Doel en overzicht van dit proefschrift
Het doel van dit proefschrift was om nieuwe tumor-gerichte *nanocarriers* en technologieën te onderzoeken voor de ontwikkeling van nanomedicijnen met biotherapeutica. Daarbij is voornamelijk gericht op de ontwikkeling van liposomen voor geoptimaliseerde afgifte van cytotoxische eiwitten.

Hoofdstuk 1 is een korte inleiding van het proefschrift en wordt gevolgd door **Hoofdstuk 2**, waarin een uitgebreider literatuur-overzicht wordt gegeven over nanogeneesmiddelen en hun klinische studies. Hierin hebben we een beschrijving van de algemene ontwerpkenmerken van liposomen opgenomen. Verder worden de overwegingen op het gebied van grootschalige productie, biocompatibiliteit en veiligheid, intellectueel eigendom, overheidsvoorschriften en algehele kosteneffectiviteit besproken.

Hoofdstuk 3 richt zich op de biologische karakterisering van het cytotoxische eiwit ML1. De opnameroute van ML1 in tumorcellen en de cytotoxische werking van het eiwit zijn bestudeerd met microscopiestudies in levende cellen,
Hoodstuk 4 beschrijft de ontwikkeling van warmtegevoelige liposomen voor ML1, en voor biotherapeutische macromoleculen in het algemeen. De *Aanvullende Studie* (**Hoofdstuk 4b**) verwijst naar complementaire experimentele studies waarin kationische lipiden werden gebruikt om de inlsuiting van biotherapeutische macromoleculen in de liposomen te verhogen.
Hoofdstuk 5 richt zich op stimulus-gevoelige liposomen die reageren op hoge intensiteit-gefocusseerde echografie (*High Intensity Focused Ultrasound, HIFU*). Hierbij werd gebruik gemaakt van nanodruppels van een ultrasound-gevoelige vloeistof. De meest geschikte formulering werd beladen met ML1.
Hoofdstuk 6 beschrijft een innovatieve methode voor de bereiding van asymmetrische liposomen, d.w.z. liposomen met een andere samenstelling van de binnenste en buitenste lipide-dubbellaag. Asymmetrische liposomen zijn aantrekkelijke *nanocarriers* omdat de binnenste lipiden kan worden geoptimaliseerd voor het complexeren van het geneesmiddel, terwijl de buitenste lipiden zo zijn gekozen dat het nanodeeltje lang blijft circuleren in de bloedbaan. We hebben onderzocht of de water-in-olie centrifugatie methode toepasbaar is voor het laden van macromoleculaire biotherapeutica in asymmetrische op lipide gebaseerde *nanocarriers*.
Tenslotte vat **Hoofdstuk 7** dit proefschrift samen en bespreekt de toekomstperspectieven.

Resumo em Português

São necessários medicamentos mais eficazes para o tratamento de cancro.
Pacientes diagnosticados com cancro são convencionalmente tratados com quimioterapia, radioterapia, ressecção cirúrgica ou combinação destes. Quimioterapia é o tratamento mais utilizado sendo o principal obstáculo os efeitos secundários graves. Estes surgem principalmente devido ao regime de administração comumente utilizado: para atingir o efeito desejado, é administrada uma dose elevada (dentro da dose máxima tolerada), e os tecidos saudáveis podem ser atingidos e danificados colateralmente.
Pelo contrário, a incorporação de fármacos em nanopartículas, pode melhorar substancialmente o potencial terapêutico do fármaco através do aumento do índice terapêutico: entrega mais eficaz do fármaco no local-alvo (mais fármaco no tumor resulta num efeito terapêutico melhorado) e redução da distribuição do fármaco em outros tecidos (por conseguinte, menos efeitos secundários).
De momento, lipossomas são as nanopartículas mais frequentemente utilizadas na realidade hospitalar. Lipossomas são vesículas unilamelares ou multilamelares, maioritariamente constituídas por fosfolípidos que rodeiam um núcleo aquoso. Os lipossomas convencionais (*stealth liposomes*) apresentam alta estabilidade na corrente sanguínea, impedindo que o fármaco seja libertado antes da chegada ao local de interesse (tumor). A alta estabilidade, no entanto, impede a libertação rápida do fármaco após a chegada ao tecido tumoral, resultando numa concentração de fármaco livre (isto é, em contacto com o tumor) relativamente baixa. Neste contexto, o desenvolvimento de nanopartículas "inteligentes" responsivas a estímulos (*stimuli-responsive drug delivery systems*) para libertação rápida de fármacos oferece grandes oportunidades para a melhoria da eficácia terapêutica. Estes sistemas de libertação são idealizados para libertar localmente a sua carga (fármaco) após a influência de estímulos endógenos ou exógenos no tumor ou no seu microambiente. O estímulo externo mais estudado para libertação rápida de fármacos em lipossomas é temperatura, sendo o ThermoDox® o melhor exemplo destes sistemas e está em sob avaliação clínica vários países.

O surgimento de biofármacos
O uso de biofármacos aumentou significativamente nas últimas décadas. A classe "biofármacos" é ampla e inclui bio-macromoléculas como péptidos e proteínas terapêuticas, ácidos nucleicos, enzimas e anticorpos.
No entanto, a complexidade inerente a este tipo de biomoléculas, impõem grandes desafios na sua formulação em nanopartículas e na entrega no

tumor. Para que estes fármacos sejam clinicamente viáveis, critérios como a estabilidade, a imunogenicidade, a eficácia e a toxicidade, devem ser escrupulosamente avaliados. Do ponto de vista da formulação, biofármacos podem ser considerados candidatos pouco atrativos.
Os obstáculos apresentados pelos biofármacos são compensados por outras qualidades, como sua alta potência (isto é, atividade por molécula). Nesta tese, foi investigada a proteína citotóxica *Mistletoe Lectin-1* (ML1). Uma particularidade da ML1 e proteínas citotóxicas semelhantes e pertencentes à mesma classe, é a sua capacidade para se ligar a recetores nas membranas celulares, de ser internalizada induzindo eficazmente morte celular. No entanto, a validação da ML1 enquanto fármaco seguro é difícil devido à sua baixa especificidade para células tumorais.
Mesmo neste caso, onde a internalização do fármaco não constitui uma limitação, os desafios para a entrega da ML1 são complexos. O desenvolvimento de nanopartículas responsivas a certos estímulos pode gerar benefícios significativos devido à liberação local do fármaco citotóxico no ambiente tumoral.

Objetivos da tese
O objetivo desta tese foi desenvolver novas nanopartículas e tecnologias para a fabricação de nano-medicamentos incorporando biofármacos. O foco esteve no desenvolvimento de lipossomas para uma entrega otimizada de proteínas citotóxicas.

O **Capítulo 1** constitui uma breve introdução da tese e é seguido pelo **Capítulo 2**, no qual é apresentada uma revisão da literatura sobre nano-medicina e os seus estudos clínicos. Foi incluída uma descrição das características gerais de design de lipossomas; foram também discutidos aspetos relacionados com produção em grande escala, biocompatibilidade e biossegurança, propriedade intelectual, regulamentos governamentais e relação custo-eficácia.
O **Capítulo 3** centra-se na caracterização biológica da proteína citotóxica ML1. A internalização da ML1 em células tumorais e o seu efeito citotóxico foram estudados com recurso a microscopia em células vivas.
O **Capítulo 4** descreve o desenvolvimento de lipossomas responsivos a temperatura para libertar ML1, e de forma geral para libertar biomacromoléculas. O *Estudo Adicional* (**capítulo 4b**) refere-se a estudos complementares em que foram utilizados lípidos catiónicos para aumentar o carregamento de biomacromoléculas nos lipossomas
O **Capítulo 5** foca-se no desenvolvimento de lipossomas responsivos a ultra-

som (*High Intensity Focused Ultrasound, HIFU*) como estímulo externo para libertar macromoléculas. Neste capítulo utilizaram-se nanoemulsões contendo um líquido sensível a HIFU.

O **Capítulo 6** descreve um método inovador para a preparação de lipossomas assimétricos, isto é, lipossomas com uma composição diferente nas camadas lipídicas interna e externa. Os lipossomas assimétricos são nanopartículas interessantes uma vez que os lípidos internos podem ser utilizados para complexar o fármaco aumentando o carregamento, enquanto os lipídios externos são escolhidos para aumentar ou favorecer a circulação das nanopartículas na corrente sanguínea. O processo de centrifugação de emulsões água-em-óleo foi investigado no que toca à potencial viabilidade para carregar biofármacos em nanopartículas assimétricas.

Finalmente, no **capítulo 7** é apresentado o resumo da tese, conclusões e perspetivas.

Curriculum Vitae and list of publications

Maria was born on 9th may 1984 in Coimbra, Portugal. After high school she decided to do a bachelor in Psychology (2003-2007) before pursuing Biomedical Engineering (2007-2012) in University of Coimbra. She followed the Biomaterials and Medical Instrumentation specialization master track, and joined Prof. dr. Hermínio C. de Sousa and Dr. Mara E.M. Braga in Chemical Engineering department of University of Coimbra as research intern and master thesis student. During her master, she also concluded an industrial internship at FeyeCon R&D in the Netherlands, supervised by Dr. Madalina Natu Tavares and Dr. Frank van de Manakker. During 2013 she was supported by CYTED-RIMADEL to continue her research in Pharmaceutical Technologies department in University of Santiago de Compostela under supervision of Prof. dr. Carmen Alvarez-Lourenzo and Prof. dr. Angel Concheiro. She began her PhD project in 2014 under the IAPP European Project decentAID. She started this project in ABNOBA GmbH under the supervision of Dr. Gero Leneweit and later she joined Deptarment of Biopharmaceutics and was supervised by Prof. dr. Raymond Schiffelers and Dr. Robbert Jan Kok. The results of the project are presented in this thesis.

Publications during her PhD

- Maria B.C. de Matos, Barbara S. Miranda, Yudha Rizky Nuari, Gert Storm, Gero Leneweit, Raymond Schiffelers, Robbert J. Kok. Liposomes with asymmetric bilayers produced from inverse emulsions for nucleic acid delivery. Journal of Drug Targeting. 2019. DOI: 10.1080/1061186X.2019.1579819
- Nataliia Beztsinna, Maria B.C. de Matos, Johana Walther, Christoph Heyder, Ellen Hildebrandt, Gero Leneweit, Enrico Mastrobattista, Robbert J. Kok. Quantitative analysis of receptor-mediated uptake and pro-apoptotic activity of mistletoe lectin-1 by high content imaging. Scientific Reports. 2018. DOI: 10.1038/s41598-018-20915-y.
- Susan Hua, Maria B.C. de Matos, Josbert M. Metselaar, Gert Storm. Current Trends and Challenges in the Clinical Translation of Nanoparticulate Nanomedicines: Pathways for Translational Development and Commercialization. Front Pharmacol. 2018. DOI: 10.3389/fphar.2018.00790

- Maria B.C. de Matos, Nataliia Beztsinna, Christoph Heyder, Marcel H.A.M Fens, Enrico Mastrobattista, Raymond Schiffelers, Gero Leneweit, Robbert J. Kok. Thermosensitive liposomes for triggered release of cytotoxic proteins. Eur J Pharm Biopharm. 2018. DOI: 10.1016/j.ejpb.2018.09.010.
- Jan-Hendrik Sommerling, Maria B.C. de Matos, Ellen Hildebrandt, Alberto Dessy, Robbert J. Kok, Herman Nirschl, Gero Leneweit. Instability Mechanisms of Water-in-Oil Nanoemulsions with Phospholipids: Temporal and Morphological Structures. Langmuir. 2018. DOI: 10.1021/acs.langmuir.7b02852.
- Gero Leneweit, Yvonne Klapper, Maria B. C. de Matos, Ellen Hildebrandt, Jan-Hendrik Sommerling, Claudia Duehrkop, Alberto Dessy, Illya Fedotenko, Hermann Nirschl, Robbert Jan Kok, Kristina Nilsson Ekdahl, Bo Nilsson, Christoph Heyder. Liposomal formulations of mistletoe produced by centrifugal technologies suitable for cancer therapy. Phytomedicine. DOI: 10.1016/j.phymed.2015.05.017

Previous Publications

- Mara E.M.Braga, Maria B.C. de Matos, Ana M.A. Dias, Herminio C. de Sousa, Desenvolvimento de aplicações farmacêuticas e biomédicas através de métodos de impregnação/deposição com fluidos supercríticos. In book: Biomateriales aplicados al diseño de sistemas terapéuticos avanzados Chapter: 8. Publisher: Imprensa da Universidade de Coimbra. 2015. DOI: 10.14195/978-989-26-0881-5_8
- Maria B.C. de Matos, Ana M. Puga, Carmen Alvarez-Lorenzo, Angel Concheiro, Mara E.M. Braga, Herminio C. de Sousa. Osteogenic poly(ε-caprolactone)/poloxamine homogeneous blends prepared by supercritical foaming. Int J Pharm. 2015. DOI: 10.1016/j.ijpharm.2014.12.041.
- Maria B.C. de Matos, Ana P. Piedade, Carmen Alvarez-Lorenzo, Angel Concheiro, Mara E.M. Braga, Herminio C. de Sousa. Dexamethasone-loaded poly(ε-caprolactone)/silica nanoparticles composites prepared by supercritical CO2 foaming/mixing and deposition. Int J Pharm. 2013. DOI: 10.1016/j.ijpharm.2013.08.042.
- Rita. B. Chim, Maria B. C. de Matos, Mara E. M. Braga, Ana M. A. Dias, H.erminio C. de Sousa. Solubility of Dexamethasone in Supercritical Carbon Dioxide. J. Chem. Eng. Data. 2012. DOI: 10.1021/je301065f

Acknowledgements

No one achieves anything alone and I am no exception.
I will not use a lot of words to express my gratitude, but I mean what I say.

I would like to thank my Promotor and Co-promotor for all the support, patience and the extra miles. Without you this thesis wouldn't have been possible.

I must thank our technicians for their advices and colleagues from Biofarmacie and ABNOBA GmbH with whom I did research, brainstormed, shared thoughts and coffee over the last years.
A special thank you note to the two beautiful creatures standing next to me on my promotion day: my paranymphs and dear friends Karina and Gui(lherme).

Thank you to my many families.
My partner in life and in crime. My family. His family. My forever and since ever friends, *a família que escolhemos*. All of you had something to add. It might have been small, but it sure made all the difference. I therefore thank you.